universität wien

DIPLOMARBEIT

Titel der Diplomarbeit

Investigation of ACTH response
to various stress conditions of mouse AtT-20 pituitaries *in vitro*
by means of Fluorescence Correlation Spectroscopy

angestrebter akademischer Grad

Magister der Naturwissenschaften (Mag. rer. nat.)

Verfasser:	Martin Gerald Puchinger
Matrikel-Nummer:	0406425
Studienrichtung (lt. Studienblatt):	Diplomstudium Molekulare Biologie (A490)
Betreuer:	Ao. Univ.-Prof. Dr. Gottfried Köhler

Wien, am 04. Jänner 2010

Dedicated to my family

Acknowledgement

I am very grateful to ao. Univ.-Prof. Dr. Gottfried Köhler for supervising my work in a very helpful and friendly way and for giving me the opportunity to work in his group at the Institute of Structural and Computational Biology, Max F. Perutz Laboratories, University of Vienna, Campus Vienna Biocenter 5, A-1030 Vienna, Austria.

Further my thanks go to the whole team of Prof. Köhler for the good working atmosphere and their suggestions and practical hints that helped me performing my tasks:

I want to thank Dr. Michael Edetsberger and Dr. Martin Knapp, who helped me to learn and perform Fluorescence Correlation Spectroscopy (FCS).

Further I thank our MTA Julia Schindelar for providing me most of the cell lines and culture medium.

Special thanks go to Mag. Erwin Gaubitzer for his great help in all computational questions and for providing me a software programmed by himself, that has helped me a lot in data analysis.

Furthermore I want to thank Dipl.-Ing. Clemens Zarzer (Johann Radon Institute of Computational and Applied Mathematics, Austrian Academy of Sciences, Linz, Austria) for the good collaboration in this project and Dr. Christina Maier (Institute of Endocrinology, Medical University of Vienna, Austria) and Dr. Aamir Shahzad for their help in medical questions.

Great thanks go to my family – to my brother Markus, who has given me the necessary diversion from study by collective sporting activities, to my parents and grandparents, who supported me and enabled the education at the university.

Finally I wanted to thank all my friends and colleagues for their consideration during my study.

The project was funded by the Vienna Science and Technology Fund (WWTF).

Index of Contents

1 Introduction

1.1 HPA axis

In 1922 the American scientist Philip E. Smith was one of the first, who described the beneficial clinical effects of adrenocortical extracts in animal models of adrenal insufficiency [32]. In the following years, scientists across the globe tried to understand the mechanism of action of adrenal hormones and other substances chemically very closely related to them.

Hypothalamic-hypophysiotropic factors were originally proposed by Geoffrey W. Harris in the 1940s. Since then substantial achievements, which were highlighted with a Nobel Prize 10 years later, confirmed that these factors do indeed exist [26].

In 1950 the Karolinska Institutet in Stockholm decided to award the Nobel Prize in Physiology or Medicine jointly to Dr. Philip S. Hench (1896-1965), Professor Edward C. Kendall (1886-1972) and Professor Tadeus Reichstein (1897-1996) 'for their discoveries regarding the hormones of the adrenal cortex, their structure, and biological effects' [21].

Their outstanding achievements through their work on the effect of pituitary adrenocorticotropic hormone (ACTH) and cortisol has contributed to open the door to new therapeutically concepts for the control of a wide variety of diseases, ranging from rheumatoid arthritis to some of the more perplexing cardiovascular and dermatological disorders [22].

Nowadays it should come as no surprise that the hypothalamus is centrally involved in orchestrating the appropriate humoral, visceromotor, and somatic motor responses. The humoral response is mediated by the hypothalamic-pituitary-adrenal (HPA) axis, which plays an important role in maintaining the homeostasis of an organism against stressful stimuli [61]. The HPA axis is the major part of the neuroendocrine system and its main role is to subserve the body's response to a stressor, physical or emotional, that disrupts the homeostatic balance of the organism [11].

The pituitary is composed of a thin intermediate portion (pars intermedia), the anterior lobe (adenohypophysis), and a posterior lobe (neurohypophysis). Each has its own characteristic endocrine functions.

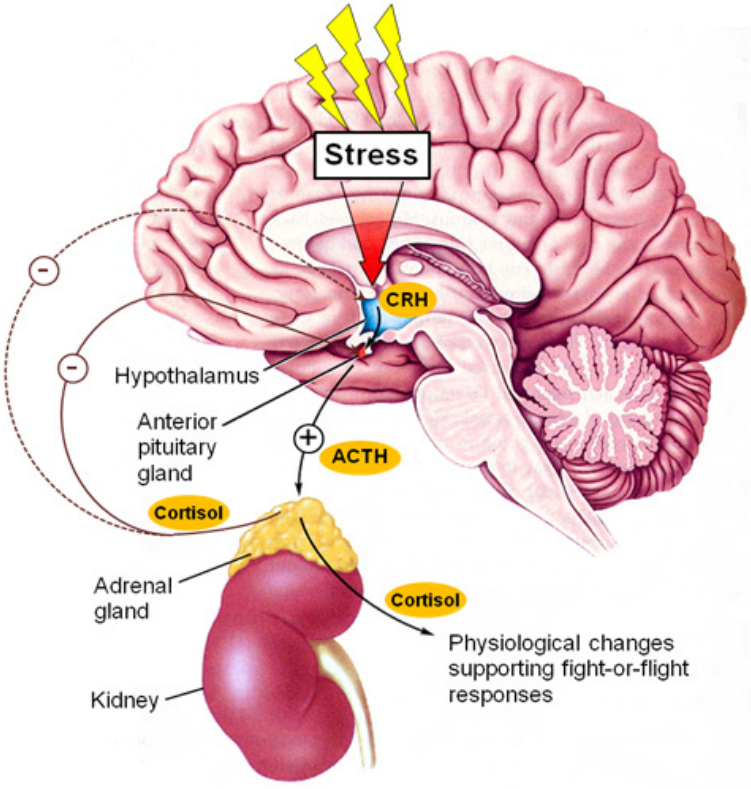

Fig. 1.1: The Hypothalamic-Pituitary-Adrenal Axis (modified from [61])

In response to a wide variety of stresses corticotropin releasing hormone (CRH) is released from the hypothalamus and stimulates the anterior pituitary to secrete ACTH, which in turn stimulates the adrenal cortex to secrete cortisol (Fig. 1.1). The sensitivity of the HPA-axis to incoming stimuli is modulated by two negative feedback mechanisms of cortisol targeted to the hypothalamus and the anterior pituitary gland. Therefore the sequential release of CRH and ACTH is suppressed by the glucocorticoids themselves and the magnitude of the HPA stress response depends upon the pre-existing glucocorticoid tone [5].

The interactions and feedback mechanisms among the involved cell types are highly complex and yield central topics of current research in the biomedical field [7][13][18][23] as well as in system biology for developing suitable models [55][56][57][58][59].

1.1.1 Anterior pituitary gland cell

Unlike the posterior lobe, which really is a part of the brain, the anterior lobe of the pituitary is an actual gland synthesising and secreting a wide range of hormones that regulate secretions from other glands throughout the body [61]. The pituitary hormones

act on different target organs of the endocrine system: on the gonads, the thyroid glands, the adrenal glands, and the mammary glands (Tab.1.1).

Hormone	Target	Action
Follicle-stimulating hormone (FSH)	Gonads	Ovulation, spermatogenesis
Luteinizing hormone (LH)	Gonads	Ovarian, sperm maturation
Thyroid-stimulating hormone (TSH, thyrotropin)	Thyroid	Thyroxin secretion (increases metabolic rate)
Adenocorticotropic hormone (ACTH, corticotropin)	Adrenal cortex	Cortisol secretion
Growth hormone (GH, somatotropin)	All cells	Stimulation of protein synthesis
Prolactin	Mammary glands	Growth and milk secretion

Tab.1.1: Hormones of the Anterior Pituitary (modified from [61])

It should be emphasized that perhaps all of the anterior pituitary hormones are secreted by cells elsewhere in the body and may have functions quite different from those in the HPA-axis. For example, ACTH is an important neurotransmitter in several brain areas [67].

1.1.2 AtT-20 cell line as model system

An adherent ACTH-producing cell line (AtT-20) derived from a pituitary tumor from an irradiated LAF_1 mouse [41] was chosen as a model secretory system for investigating ACTH response to different stress conditions as these cells retain many important biochemical and physiological properties similar to human pituitary corticotrophs.

However, *in vitro* cell cultures of AtT-20 pituitaries are very sensitive to any kind of stress. Already a little divergence in standard temperature (37°C), in vibrations, in lack of space to each other, or a pH change as well as too long exposure to light (see Tab.1.2) will induce additional ('unwanted') stress in AtT-20 cells and thus will have an effect on the basal ACTH levels and the significance of the result.

Since most of these stress factors, such as temperature change, vibrations or exposure to light, arise from human mistakes during experimental procedure, lots of unwanted stress

can be prevented by gently handling the *in vitro* culture and by choosing the right cell line. The additional risk of vibrations by clashing with other – mostly apoptotic – cells in solution is enhanced in AtT-20 suspension cell cultures. Therefore the adherent AtT-20 cell line was used for all measurements to diminish unwanted influence of this stress stimulus to the basal ACTH production during in-vitro analysis.

Stress stimulus	Action
Temperature	Optimal growing conditions are guaranteed in an incubator at 37°C. Removing cells from the incubator for analysis, e.g. for adding stress stimuli or for morphological studies, result in a temperature change and thus in a stress response.
vibrations	Vibrations due to human mistakes in handling result in mechanical shear force or clashing with apoptotic cells detached from the layer.
Space	An increasing cell number in a closed *in vitro* system leads to a lack of space for all cells adhered on the layer. As a consequence of the high cell density cells release signal molecules into the extracellular space and act locally on neighbouring cells causing stress, growth arrest and maybe apoptosis in the end.
pH-value	Cell growing goes along with increasing degradation products which cells accumulate during incubation. Without any medium change these waste materials lead to an acidic environment for the cells after 4-5 days and thus induce stress and apoptosis.
Light	As the pituitary gland lies in a pocket of the sphenoid bone at the base of the brain, cells remain in the dark all the time *in vivo* and thus a too long exposure to light in an *in vitro* system can result in a stress response.

Tab.1.2: Additional stress factors for adherent AtT-20 during in-vitro analysis

Moreover a good experimental setup with fix working steps for each sample preparation and measurement minimizes these sources of error and, thus, give rise to a statistically relevant basal level of ACTH stimulated by all additional stress factors. Any deviation to the basal ACTH level is noticed as a response to any stress factor derived from the HPA axis, such as CRH from the hypothalamus or cortisol from the adrenal glands.

Nevertheless it has to be pointed out that stress stimuli induced by a lack of space for the cells or a pH-change in the medium illustrate the limitation of a closed *in vitro* system after a long incubation period. Both are side effects of the cell growth: As cells undergo metabolic processes, acid is produced and the pH decreases. The buffer range of the medium is limited, meaning that too acidic levels will result in a dramatic pH decrease in the medium monitored as a colour change of the indicator from red to yellow. Secreted molecules may act as local mediators, affecting cells in the immediate environment of the adhered signalling cells.

1.1.3 Associated diseases

Recent research showed evidence that the so-called network diseases, which cannot be linked to a single indicator, like Alzheimer‘s disease [34], anxiety disorders [15][38] or Cushing‘s syndrome [9] are strongly linked to an abnormal function of the HPA axis.

Obstructive sleep apnea (OSA) is a common condition with significant cardiovascular and metabolic comorbidity and is associated with marked disturbances in ACTH and cortisol secretory dynamics, resulting in prolonged tissue exposure to disordered, elevated hormone levels [13].

There is evidence that the HPA-axis is centrally involved in the linkage between the nervous and immune systems [33].

Catecholamines, glucocorticoids, ACTH and other stress hormones can modulate the activity of multiple components of the tumour microenvironment such as the promotion of tumour-cell growth or the stimulation of angiogenesis by inducing production of pro-angiogenic cytokines [1]. Stress hormones can also activate oncogenic viruses and alter several aspects of immune function including antibody production, cytokine production profiles (e.g. interleukin-6) and cell trafficking [1].

Furthermore the HPA-axis effects and triggers a broad spectrum of diseases, but discussing all of them would go beyond the scope of this work.

1.2 ACTH

Adrenocorticotropic hormon (ACTH) – often simply referred as corticotrophin or adrenocorticotropin in literature – is a 4.5 kDa straight-chain peptide hormone consisting of 39 amino acids (Fig. 1.2). It is often produced in response to biological stress –

especially under the regulation of CRH from the hypothalamus – by a specialized subgroup of pituitary cells, the corticotrophs, which are located in clusters in the pars distalis of the pea-sized pituitary gland at the base of the brain.

Ac – Ser Tyr Ser Met Glu His Phe Arg Trp Gly Lys Pro Val Gly Lys Lys Arg Arg Pro Val Lys Val Tyr Pro Asn Gly Ala Glu Asp Glu Ser Ala Glu Ala Phe Pro Leu Glu Phe – NH_2

Fig. 1.2: ACTH sequence of mouse AtT-20 pituitary gland cells (three-letter-code)

The properties of ACTH were first investigated in the 1930s by the research groups of James Collip, Herbert Evans and Bernardo Houssay using pituitary extracts to stimulate the adrenal cortex, but not distinguishing between substances, which are chemically very closely related to ACTH, in these extracts.

1.2.1 Cellular synthesis

These results suggest that non-genomic and genomic mechanisms are involved in the glucocorticoid negative regulation of ACTH expression, and a pertussis toxin-sensitive GTP-binding protein might, at least partly, participate in the non-genomic effect [14].

A variety of hormons like ACTH, β-, γ-lipotropin, α-, β-, γ-melanotropin (MSH), β-endorpin, corticotrophin-like intermediary peptide (CLIP) and Met-enkephalin (Fig. 1.3) are all synthesized by post-translational cleavage of a large precursor molecule of about 31kDa, called proopiomelanocortin (POMC), in the secretory granules of endocrine cells.

The POMC gene encodes a polypeptide hormone precursor that undergoes extensive, tissue-specific, post-translational processing via cleavage by subtilisin-like enzymes known as prohormone convertases. Different cell types produce different concentrations of individual processing enzymes, so that depending on tissue type and the available convertases, processing may yield as many as ten biologically active peptides involved in diverse cellular functions. There are eight potential cleavage sites within the polypeptide precursor (Fig. 1.3). All these proteases cut next to pairs of positively charged amino acids (Lys-Arg, Lys-Lys, Arg-Lys, or Arg-Arg pairs) [65].

Proopiomelanocortin contains an N-terminal signal sequence which is suggested to be necessary for peptide expression [27] and is removed after synthesis.

In the anterior lobe of the pituitary the major secretory products are ACTH and β-lipotropin cleaved on the Lys-Arg pairs of adjacent basic residues by the prohormone convertase 1 [3]. Whereas the cleavage of all the other peptide hormones occurs in cells other than corticotroph cells of the anterior pituitary. In the intermediate lobe the ACTH is then cleaved by prohormone convertase 2 at the Lys-Lys and Arg-Arg pairs to form α-MSH and CLIP as the predominant products [8]. Beta lipotropin is degraded rapidly by the same proteolytic enzyme in the intermediate lobe and more slowly in the anterior lobe to γ-lipotropin and β-endorphin. Further cleavage these two peptides generates β-MSH and Met-enkephalin.

Nevertheless, the POMC gene is also expressed in a variety of other tissues, such as the CNS, placenta, or the immune system, where tissue-specific differential post-translational processing may give rise to a different spectrum of peptides with a diversity of actions [16].

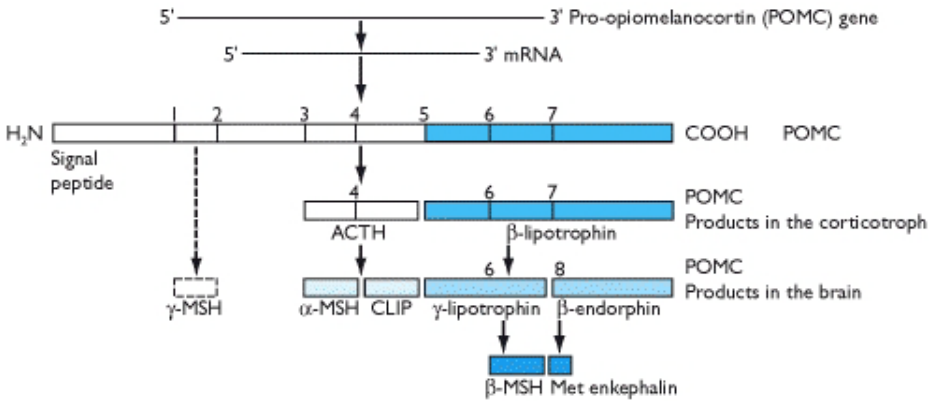

Fig. 1.3: Alternative processing pathways for the prohormone POMC (modified from [66])

Preliminary structural work on corticotropin isolated from acetone dehydrated human pituitaries indicated that it is similar to corticotropin from other species [17].

5' – S^{124}YSMEHFRWGKPVGKKRRPVKVYPN**V**AE**N**ESAEAFPLEF – 3' mus musculus

5' – S^{138}YSMEHFRWGKPVGKKRRPVKVYPN**G**AE**D**ESAEAFPLEF – 3' homo sapiens

Fig. 1.4: Amino acid sequence (one-letter-code) of ACTH in mouse and human

ACTH is a highly conserved part of the prohormone POMC since only the amino acids at position 26 and 29 vary between mouse and humans (Fig. 1.4). Only its position in the POMC protein is different and the amino acid serine is found at position 124 in mouse

and at position 138 in humans. The biological activity of the ACTH molecule depends on the first 24 N-terminal amino acids

The behaviour and the nature of ACTH is the very same in both individuals and illustrates that the AtT-20 cell line is a good model system for human ACTH studies.

1.2.2 Biological activity

The mechanism of ACTH action follows the classical rules of peptide hormones. ACTH travels through the blood stream to its target cells, the adrenal glands located on the kidneys, where it binds to its receptors on the adrenal cell membranes and results in cortisol secretion or physiological changes supporting fight-or-flight responses [61] in humans (Fig. 1.1).

The primary role of adrenocorticotropin is to increase the synthesis and the release of cortisol by the adrenal cortex [35], to regulate the secretion of adrenal androgens [28], to increase adrenal blood flow [6], and to regulate its own release via a short-loop negative feedback mechanism [5], etc.

1.3 CRH

Corticotropin-releasing hormone (CRH or CRF), which is synthesized in the hypothalamus, plays a crucial role in the endocrine response to stress [10][29].

CRH is a 41-amino acid peptide hormone first isolated in 1981 by Vale et al. [37] that is derived from a 196-amino acid preprohormone by prohormone convertases 1 and 2. The chromosomal locus of the human corticotropin-releasing hormone (hCRH) gene is localized to band 8q13 on the long arm of chromosome 8 [2].

In response to stress CRH is secreted in minute quantities *in vivo* by the paraventricular nucleus of the hypothalamus into the portal vein, travels directly to the pituitary via the blood stream where it promotes ACTH secretion and synthesis. This action was simulated *in vitro* on the AtT-20 pituitary cell line in a simplified manner by adding low quantities of CRH as an extracellular stress stimulus and monitoring its real time ACTH response.

CRH as well as cortisol activate genomic mechanisms via G-protein coupled receptors [14][48]. CRH binding to a CRH-receptor complex on the cell surface stimulates POMC expression in the nucleus via signalling cascades and the ACTH synthesis in the rough ER

and Golgi apparatus in the end. However, there is evidence of a non-genomic signalling pathway beside the genomic mechanism. CRH-binding to the same CRH-receptor complex or another receptor may induce the secretion of a reservoir of ACTH vesicles beneath the cell membrane via a fast-activating mechanism, but these mechanisms are still poorly understood.

For the sake of completeness, beside its production in the hypothalamus, CRH is also synthesized in peripheral tissues, such as in T-lymphocytes or in the placenta.

1.4 anti-ACTH IgG antibody

1.4.1 Antibody structure

Antibodies or Immunoglobulins are a family of structurally related glycoproteins synthesized in membrane-bound or secreted form by B-lymphocytes [60]. All antibodies have a common symmetric core structure of two identical disulfide-linked heavy chains and two identical light chains, each linked to one of the heavy chains (Fig. 1.5).

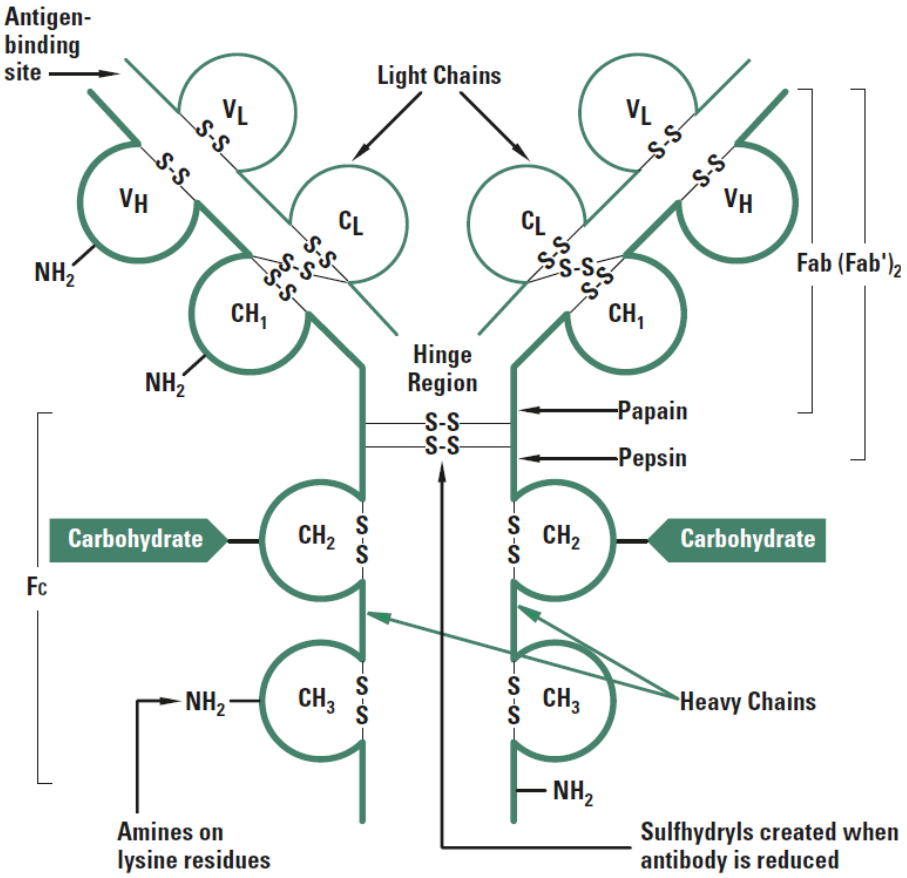

Fig. 1.5: Structure and functional groups of an IgG antibody for labelling (from Thermo Scientific)

Each heavy chain of IgG is composed of a variable (V_H) and three constant (C_H) immunoglobulin domains of about 110 amino acids containing conserved sequences and intrachain disulfide bonds. Each light chain consists of one variable (V_L) and one constant (C_L) immunoglobulin domain. The N-terminal variable region of the heavy (V_H) or light (V_L) chain of IgG is responsible for the specificity of an antigen and thus for recognizing the ACTH molecule. As each antibody consists of two heavy chains with a single molecular weight of about 50 kDa and two light chains of about 25 kDa each the resulting total immunoglobulin molecular weight is approximately 150 kDa.

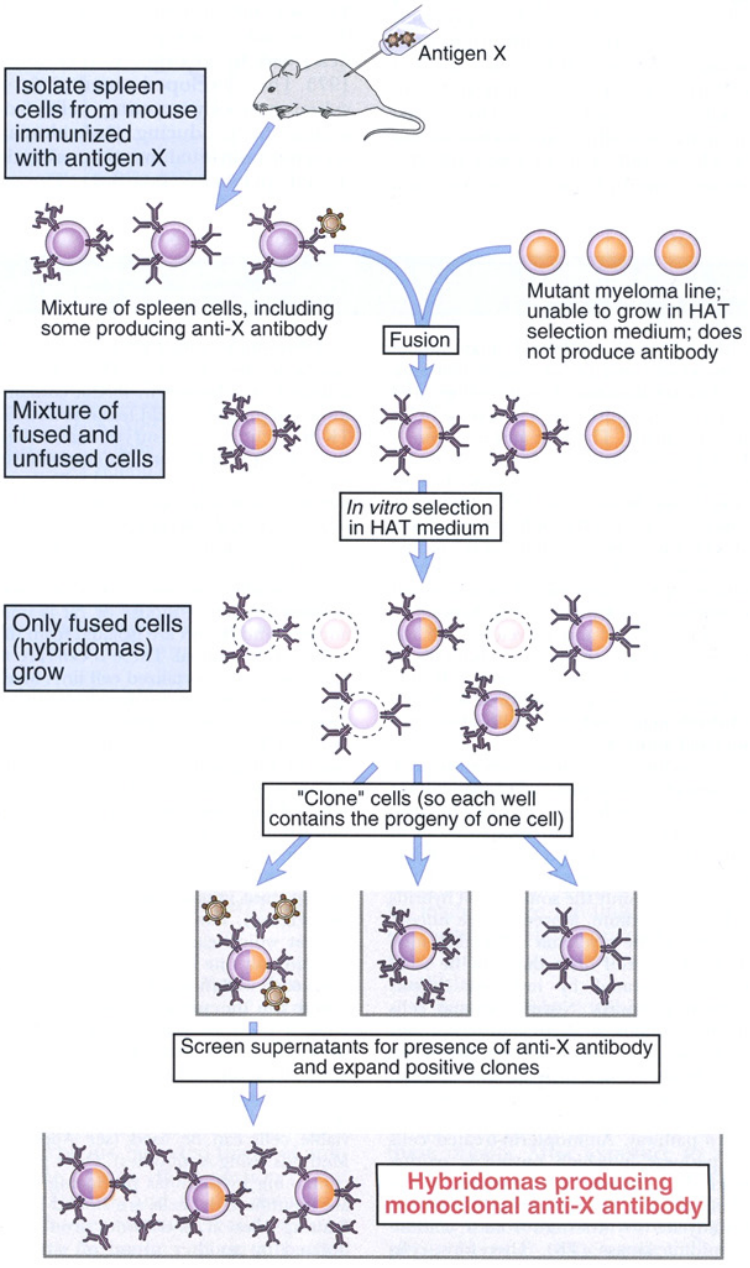

Fig. 1.6: Production of monoclonal antibodies (from [60])

1.4.2 Monoclonal mouse anti-ACTH antibody

For performing a precise FCS measurement it was important to label monoclonal antibodies which are identical antibody molecules specific for a particular region of the ACTH antigen. Labelled monoclonal antibodies are especially useful as capture antibodies in FCS-Immunoassays that require single-epitope specificity and an unchanging supply over many measurement cycles.

The first and now generally used method for producing monoclonal antibodies of known specificity was described by Köhler and Milstein in 1975 (Fig. 1.6).

These monoclonal antibodies are produced by B cell hybridomas which are cell lines derived by the fusion of a single normal murine B cell manufacturing anti-ACTH antibodies and an immortal B cell tumour line with no antibody production.

A purified monoclonal mouse anti-ACTH antibody specific for the N-terminal region of the ACTH molecule (Fitzgerald Industries, Massachusetts, USA) was used binding specific to the amino acids 1-24 of the ACTH molecule.

1.4.3 Functional groups for labelling

A couple of functional groups are available on an IgG antibody for labelling (Fig. 1.5):

- **Primary amines ($-NH_2$)** are localized on lysine residues and the N-terminus and are distributed over the entire antibody. Since primary amines are abundant on an IgG antibody the labelling reaction occurs with the utmost probability. Therefore, this was the method of choice for labelling an antibody.

- **Sulfhydryl groups (–SH)** on cysteine residues are generally involved in structural integrity of an antibody by forming disulfide bonds. Free sulfhydryls, which will react with the dyes, can be formed by selectively reducing disulfide bonds. However, only the reduction of one disulfide bond in the hinge region of the antibody won't lead to a conformational change and thus to a change in specificity and functionality of the antibody. The probability that the dye reacts with these two free sulfhydryls is lower and the risk of creating a non-functional antibody is too high compared to that of primary amines.

- **Carbohydrate residues** containing cis-diols are localized to the Fc region on antibodies and can be oxidized (–CHO) to create active aldehydes. Since carbohydrate residues are more abundant on polyclonal antibodies this option was dropped out.

1.5 Fluorescence

In condensed systems, e.g. solutions, there are more pathways available to the excited molecule for dissipation of excitational energy. Some of these photophysical processes are intrinsic properties of the molecule and are unimolecular whereas others depend on external perturbations and may involve bimolecular collisions like quenching or electronic energy transfer [68]. Nevertheless a more careful consideration is ignored in this way because it would go too far, but, anyway, all these photophysical processes must occur in a time period less than the natural radiative lifetime of the molecule and priorities are established by their relative rate constants [68].

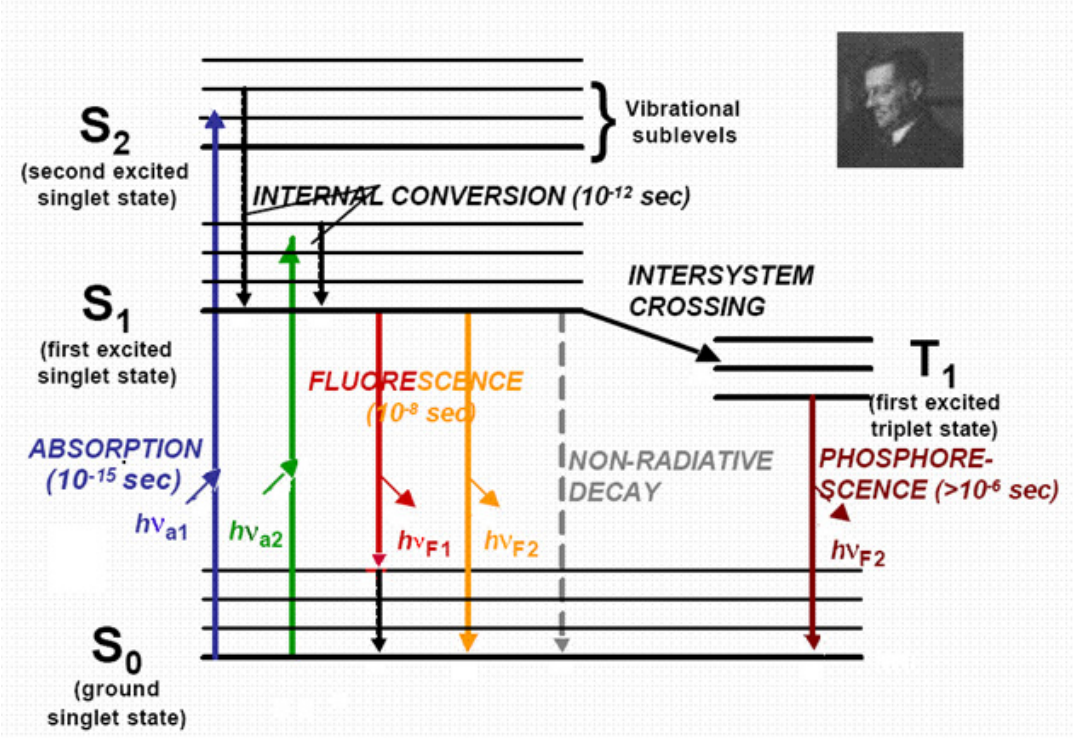

Fig. 1.7: Simplified Jablonski diagram showing quantum yields and lifetimes (modified from [64])

The fundamental absorption and emission properties of dyes are often represented in an energy level diagram that shows the various electronic and vibrational energy levels that may exist in a molecule, together with the pathways that exist between these various distinct states (the 'Jablonski' diagram) [62]. A simplified Jablonski diagram that does not include effects due to solvent quenching, intermolecular quenching or FRET is shown in Fig. 1.7. The Jablonski diagram, named after the Polish physicist Aleksander Jablonski (his portrait is shown in Fig. 1.7 on the upper right side), elegantly depicts molecular

electronic and vibrational energy levels illustrating the phenomenon of light absorption and emission [62].

Tab.1.3 shows the unimolecular processes, which are represented in the simplified Jablonski diagram above as arrows, in more detail. At equilibrium, a fluorophore is likely to exist in the lowest vibrational energy level of the molecular ground state (S_0). Upon absorption of a photon, whose energy closely matches an electronic transition in the fluorophore (under consideration of only a single-photon absorption), the fluorophore is excited to a high vibrational energy level in the first or second electronic singlet states (S_1 or S_2), a process which occurs essentially instantaneously (10^{-15} s). Rapid relaxation (~10^{-12} s) then occurs to the lowest vibrational energy level of the first singlet state (S_1) and is known as internal conversion.

Photophysical process	Transition	Reaction
Absorption	$S_0 \rightarrow S_n$	$A + h\nu \rightarrow A'^*$
Internal conversion	$S_n \rightarrow S_1$	$A'^* \rightarrow A^* + \text{heat}$
Fluorescence emission	$S_1 \rightarrow S_0$	$A^* \rightarrow A + h\nu_f$
Intersystem crossing	$S_1 \rightarrow T_1$	$A^* \rightarrow A^3 + \text{heat}$
Phosphorescence emission	$T_1 \rightarrow S_0$	$A^3 \rightarrow A + h\nu_p$
Internal conversion	$S_1 \rightarrow S_0$	$A^* \rightarrow A + \text{heat}$
Reverse intersystem crossing	$T_1 \rightarrow S_0$	$A^3 \rightarrow A + \text{heat}$

Tab.1.3: Various photophysical unimolecular processes occurring in a molecule (modified from [68])

A	molecules in ground state
A*	molecules in first excited singlet state
A'*	molecules with excess vibrational energy in S_1 state or excited to higher singlet states S_2, S_3, etc.
A^3	molecules in triplet state
h	Planck constant (= 6.626 x 10^{-34} J s)
v	electromagnetic wave

In a simplified view molecules in this equilibrated excited state can then lose energy through two primary mechanisms:

- **Fluorescence** involving the immediate relaxation of the photon to the ground state (10^{-8} s), as well as **delayed fluorescence**: Energy may also be transferred back from the triplet state to S_1 and result in delayed fluorescence with relaxation to S_0 (not shown in Fig. 1.7).

- **Phosphorescence** (>10^{-6} s) is termed as a transition after a circuitous route from the first triple state (T_1) to S_0, which is much slower than a fluorescence relaxation transition from S_1 to S_0. Thereby energy of a molecule is first transferred from the first singlet state (S_1) to the first triplet state (T_1) by inter system crossing (ISC) or an ISC to a higher triplet level occurs followed by internal conversion to T_1 (not shown in Fig. 1.7).

Both mechanisms have in common that excitation energy is dissipated in form of light energy and thus can be monitored with even ultrasensitive detectors whereas in radiationless processes such as internal conversion and inter system crossing the excess of energy is lost to the environment as thermal energy and thus remains undetected.

The fluorescent dye used for FCS should have a very low probability for a 'spinflip' from the S_1 to the long-lasting triplet state, where no fluorescence occurs.

Furthermore a fluorescent dye should have a high extinction coefficient at the laser wavelength of 488 nm, a bright fluorescence, an excellent photo and buffer stability and instrument compatibility.

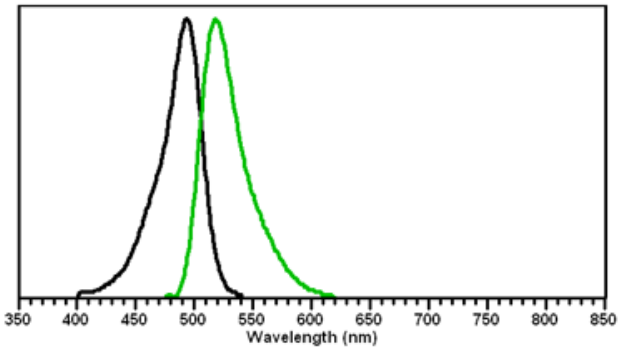

Fig. 1.8: Absoption and emission spectra of DyLight 488 fluorophor (from Pierce Biotechnology)

Moreover it should display emission spectrally distinct from the excitation wavelength. For our approach we used a fluorophore (DyLight, Pierce Biotechnology) with an excitation wavelength of 488 nm (black absorption curve in Fig. 1.8) and an emission maximum of 518 nm (green emission curve in Fig. 1.8) which highlights with bright fluorescence, excellent photostability, buffer stability and instrument compatibility. The DyLight 488 dye is spectrally similar to other commercial available dyes from other companies, such as Alexa Flour 488, fluorescein or FITC.

1.6 Fluorescence Correlation Spectroscopy

1.6.1 Principle

Fluorescence Correlation Spectroscopy (FCS) was introduced in the early 1970s by Madge, Elson and Webb [47]. This pioneering study was then followed by a number of successful FCS applications with impressive results in the last decades [46][45][50][52][54]. FCS has become a powerful tool especially in life sciences for studying supramolecular associations [42][48][49], DNA hybridization reactions [44][51], etc.

FCS is a spectroscopic technique for studying molecular interactions in solution. It monitors the random motion of fluorescently labelled molecules inside a defined volume element irradiated by a focused laser beam.

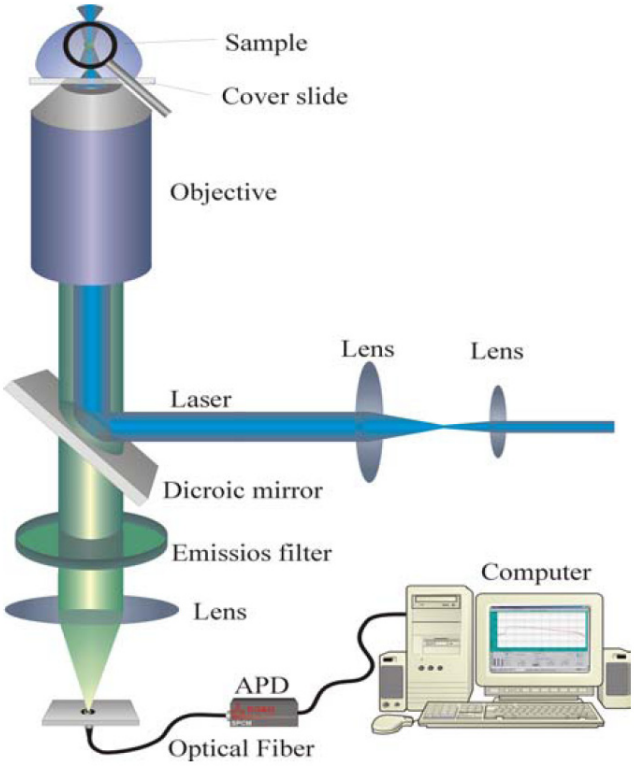

Fig. 1.9: Schematical drawing of an FCS setup (from [53])

The confocal FCS setup is illustrated schematically in Fig. 1.9. All measurements were performed on a laboratory-built FCS system consisting of a Confocor spectrofluorimeter (Carl Zeiss-Evotec, Jena, Germany) with the same equipment as previously published [48][49]. Intensity fluctuations were recorded by an avalanche photodiode (SPCM-CD 3017) and autocorrelated with a hardware correlator (ALV 5000, ALV, Langen, Germany) based on a two components fitting procedure. The obtained results showed that FCS can be

used for computationally eliminate diffusion times and particle numbers of two different fractions within a solution.

The advantage of this technique lies in its simplicity and rapidity. However the time over which a single molecule-antibody complex can be observed is limited to its diffusion time across the observation volume which is typically less than one millisecond.

In fact analyses of spontaneous, non-coordinated fluctuations due to Brownian motion can only be monitored, if the particle's number is low enough so that each contributes substantially to the measured signal [53]. Thus FCS can even detect sample volumes of about 10-30 µl.

1.6.2 FCS Immunoassay vs. ELISA

An enzyme-linked immunosorbent assay (ELISA) is a very sensitive method for the quantitative detection of peptides, proteins, pharmaceuticals etc. in solution. A big palette of different ELISA techniques with anti-ACTH detection antibodies for measuring ACTH peptide concentrations is available on the market ranging from indirect to direct and sandwich ELISAs.

A

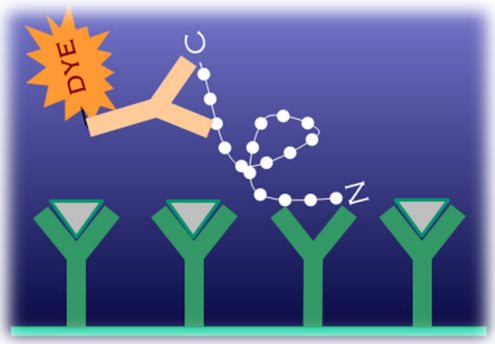

B

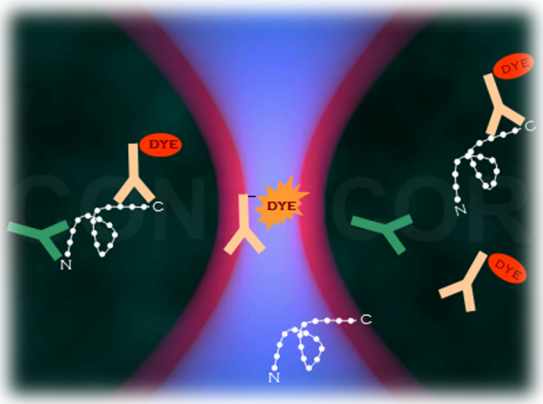

Fig. 1.10: The principle of a 'sandwich'-ELISA (A) vs. that of FCS-Immunoassay (B)

A fluorescent ELISA is a very sensitive technique for detecting even smallest amounts of molecules but it is a very expensive and time-consuming procedure and thus may have affects on the conformation and reactivity of molecules.

The washing steps during each ELISA-procedure which should remove unbound material to diminish background signals are the "bottleneck" of this technique and, thus, are very

time-consuming. The disadvantage of an ELISA is that it is expensive and laborious for measurements in high quantities.

	FCS-Immunoassay	fluorescent ELISA
Sensitivity	micro- to sub-nanomolar	nano- to sub-nanomolar
concentration range	High	Low
Sample volume	~ 20 – 30 µl	100 µl
Durability	~ 25 min	~ 2 h
Protein complex	in solution	on the surface
washing steps	None	3
Costs	low (≈2000 measurements)	high (96 measurements per kit)

Tab.1.4: FCS-Immunoassay compared with fluorescent ELISA

Therefore, a novel method – the FCS-Immunoassay – was developed, which allowed fast and precise determination of the concentration of ACTH in the extracellular space of the cell culture. Values were measured nearly continuously in small aliquots of the supernatant. Only a single drop (20 µl) of the sample was necessary for measuring any protein concentration whereas about 100 µl sample had to be applied for an ELISA in a 96-well plate. Furthermore additional incubation steps with e.g. blocking solutions or secondary antibodies were omitted because in contrast to ELISA no washing steps were necessary and molecules were directly detected by both antibodies in solution without any complicated construct on the layer of a well-plate. The main advantages of FCS-Immunoassay are listed in Tab.1.4.

1.6.3 FCS Immunoassay

The first goal in establishing a new detection method was to get rid of the 'mass problem' of different particles diffusing through the focus meaning that the diffusion time of a molecule is proportional to the third root of its molecular weight and thus only significant changes in particle's mass result in sufficiently different diffusion times, particle numbers and concentrations of the ACTH molecule.

$$\tau_D \approx \sqrt[3]{M_r}$$

In principle two detection methods can be used for monitoring protein concentrations by means of FCS. Nevertheless for quantifying ACTH molecules in solution only the second method is sufficient as mentioned below.

Method #1: ACTH detection with one anti-ACTH antibody

There is no possibility to distinguish the ACTH-bound antibody fraction from the free unbound one as the molecular weight of the ACTH peptide hormone (4541 g/mol) is too low for significantly changes in particle's mass.

Method #2: ACTH detection with two anti-ACTH antibodies

According to the 'sandwich'-ELISA principle the ACTH molecule is captured by a labelled and an unlabelled monoclonal anti-ACTH IgG antibody each binding specific to a well defined region on the peptide hormone resulting in a complex with highly increased mass (~300kDa) and significantly changed diffusion properties compared to the free fluorescent one (~150kDa).

For this method it is of indispensable importance that no crossreactivity of antibodies occurs. Otherwise we are confronted with the problem of method #1 and cannot distinguish between two crossreacted antibodies and two ACTH-bound antibodies!

Tab.1.5 shows a variety of ACTH interactions theoretically occurring to both antibodies but only the formation of an antibody(unlabelled)–ACTH–antibody(labelled) complex was sufficient for this purpose. A high potential binding of both antibodies to the peptide hormone was achieved by the right setup (see chapter 4.4) and ensured an exact quantification of ACTH molecules along with a correction factor obtained by the labelling reaction (see chapter 4.1). Only in this way it was possible to computationally 'scrape out' the labelled unbound antibody fraction from the desired ACTH-bound form via 2-component fitting. How experimental autocorrelation functions were evaluated by using a 2-component fit is discussed in detail in chapter 4.4.2.

possible complexes	detectable molecular masses	diffusion time τ_D
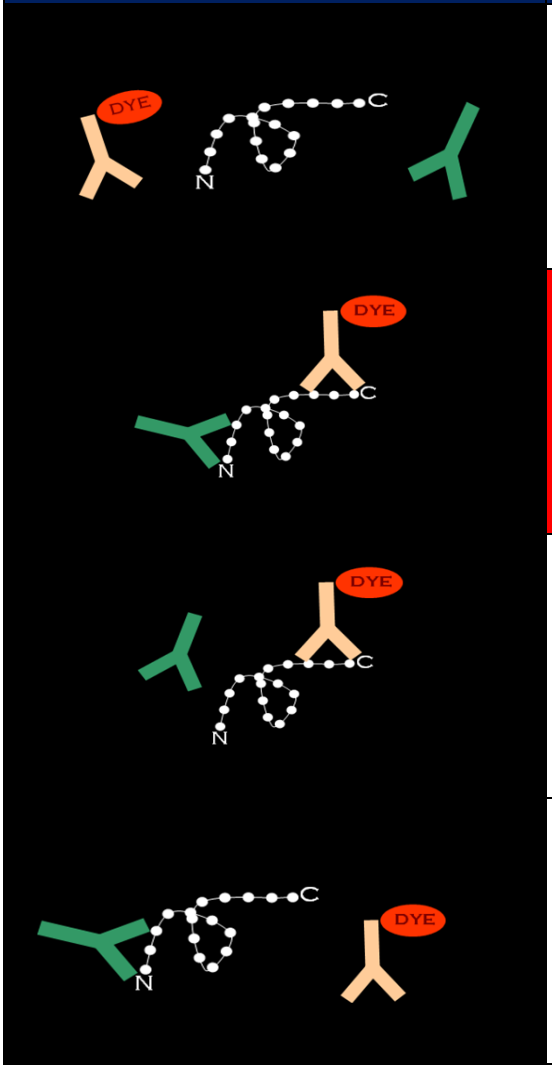	~ 150 kDa	~ 230 µs
	~ 300 kDa	**~ 1000 µs**
	~ 154 kDa	~ 230 µs
	~ 154 kDa	~ 230 µs

Tab.1.5: Possible ACTH/antibody formations in FCS-Immunoassay and its distinguishability

2 Aims

The aim of our study was the *in vitro* quantification of a protein – appearing in one of the central systems in the human body – with one of the most upcoming detection techniques in the last years.

Through important instrumental improvements in the last decades Fluorescence Correlation Spectroscopy (FCS) has become a powerful tool for kinetic measurements and binding studies. However, monitoring and quantifying the real time release of a protein in a cellular reaction network opens a fundamentally new application of FCS.

2.1 Specific aim #1

Optimizing Fluorescence Correlation Spectroscopy by establishing a novel solution-based technique as a counterpart to common used fluorescent ELISAs was the primary goal of study and obtaining highly resolved data in the period of interest for specific mathematical analysis in the future.

2.2 Specific aim #2

Employing this new assay to measure and quantify proteins of interest in an *in vitro* system represented the scientific application. For this purpose the HPA axis network, which plays a key role in the endocrine system of humans as well as in lots of diseases, was chosen as a model for our studies. The main focus of the work was the investigation of the real-time ACTH response of mouse AtT-20 pituitaries through different stress conditions.

The obtained results will yield an optimal basis for mathematicians (Johann Radon Institute of Computational and Applied Mathematics, Austrian Academy of Sciences, Linz, Austria), which were involved in this project in collaboration with us, for quantifying the developed model and testing the impact of the considered mechanisms on the overall dynamics using methods from the field of inverse problems (Inverse Bifurcation Analysis, Inverse Eigenvalue Analysis and Parameter Identification) [55][56][57][58][59].

3 Material

3.1 Equipment

3.1.1 Sample preparation

Equipment	Type	Company/supplier
Centrifuge	MIKRO 22R	Andreas Hettich GmbH&Co.KG, Tuttlingen, Germany
Gloves	Handsafe®	HPC Healthline Ltd., Morden, UK
Incubator	HERAcell®	Thermo Fisher Scientific Inc., Waltham, USA
Laminar flow	TWO 30	Faster Srl., Cornaredo, Italy
Microplate	24-well	IWAKI Glass Co., Funahashi, Japan
Pasteur Pipettes		VWR International GmbH, Wien, Austria
Pipette	PIPETMAN® P10	Gilson Inc., Middleton, USA
Pipette	PIPETMAN® P20	Gilson Inc., Middleton, USA
Pipette	PIPETMAN® P200	Gilson Inc., Middleton, USA
Pipette	PIPETMAN® P1000	Gilson Inc., Middleton, USA
Pipette (one-way)	1ml	Sterilin Ltd., Aberbargoed, UK
Pipette (one-way)	5ml	Sterilin Ltd., Aberbargoed, UK
Pipette (one-way)	25ml	Sterilin Ltd., Aberbargoed, UK
Pipette controller	accu-jet® pro	Brand GmbH&Co.KG, Wertheim, Germany
Pipette tips (micro)	0.5-10µl	Greiner Bio-One GmbH, Frickenhausen, Germany
Pipette tips	10-200µl	Greiner Bio-One GmbH, Frickenhausen, Germany
Pipette tips	200-1000µl	Greiner Bio-One GmbH, Frickenhausen, Germany
Rotor	1159	Andreas Hettich GmbH&Co.KG, Tuttlingen, Germany
Suction pump	LABOPORT®	KNF Neuberger Inc., Trenton, USA
Tube	50ml conical tube	Sterilin Ltd., Aberbargoed, UK
Tube	1.5ml Eppendorf	VWR International GmbH, Wien, Austria

3.1.2 Cell counting

Counting chamber	Bürker-Türk	LO-Laboroptik GmbH, Friedrichsdorf, Germany
Inverted Microscope	Axiovert S100TV	Carl Zeiss Jena GmbH, Jena, Germany
Pipette	PIPETMAN® P20	Gilson Inc., Middleton, USA
Pipette tips	10-200µl	Greiner Bio-One GmbH, Frickenhausen, Germany

3.1.3 Labelling

Antibody Labelling kit	Dylight™488	Pierce Biotechnology, Rockford, USA
Centrifuge	MIKRO 22R	Andreas Hettich GmbH&Co.KG, Tuttlingen, Germany
Pipette	PIPETMAN® P200	Gilson Inc., Middleton, USA
Pipette tips	10-200µl	Greiner Bio-One GmbH, Frickenhausen, Germany
Rotor	1159	Andreas Hettich GmbH&Co.KG, Tuttlingen, Germany

3.1.4 FCS

Ar-laser		LASOS Lasertechnik GmbH, Jena, Germany
Spectrofluorimeter	ConfoCor® 2	Carl Zeiss Jena GmbH, Jena, Germany
Objective		Carl Zeiss Jena GmbH, Jena, Germany
Chambered coverglass	LabTek™	Nalge Nunc International KK, Tokyo, Japan
Avalanche photodiodes		Perkin Elmer Inc., Massachusetts, USA
Hardware autocorrelator		ALV GmbH, Langen, Germany
PCR tubes		Brand GmbH&Co.KG, Wertheim, Germany
Pipette	PIPETMAN® P10	Gilson Inc., Middleton, USA
Pipette	PIPETMAN® P20	Gilson Inc., Middleton, USA
Pipette	PIPETMAN® P100	Gilson Inc., Middleton, USA
Pipette tips (micro)	0.5-10µl	Greiner Bio-One GmbH, Frickenhausen, Germany
Pipette tips	10-200µl	Greiner Bio-One GmbH, Frickenhausen, Germany
Pipette tips	200-1000µl	Greiner Bio-One GmbH, Frickenhausen, Germany

3.2 Chemicals and solutions

ddH2O		Millipore, Massachusetts, USA
Ethanol		Sigma-Aldrich Inc., St. Louis, USA
Rhodamine 6G		Sigma-Aldrich Inc., St. Louis, USA
Sodium bicarbonate		Sigma-Aldrich Inc., St. Louis, USA
Trypsin	(1x), 0.25% in PBS	PAA Laboratories GmbH, Pasching, Austria
DMEM		Sigma-Aldrich Inc., St. Louis, USA
PBS	(100x)	Sigma-Aldrich Inc., St. Louis, USA
Penicillin/Strepomycin	(100x)	EuroClone S.p.A., Siziano, Italy

3.3 Suspensions

AtT-20 cell line		ATCC, Rockville, USA
anti-ACTH IgG antibody	monoclonal (C-term.)	Fitzgerald Industries International, Concord, USA
anti-ACTH IgG antibody	monoclonal (N-term.)	Phoenix Pharmaceuticals Inc., Belmont, USA
CRH		Sigma-Aldrich Inc., St. Louis, USA
FBS		PAA Laboratories GmbH, Pasching, Austria

3.4 Software

FCS software	ConfoCor® Instrument Control	Carl Zeiss Jena GmbH, Jena, Germany
FCS fitting program I	FCS ACCESS Fit	Carl Zeiss Jena GmbH, Jena, Germany
FCS fitting program II		Prof. Köhler's group (running on LINUX)
Microsoft® Word	Office 2007	Microsoft Corporations, Redmond, USA
Microsoft® Excel	Office 2007	Microsoft Corporations, Redmond, USA
OriginPro®	Version 8	OriginLab Corporation, Northampton, USA
Symyx Draw	Version 3.2	Symyx Technologies Inc., Sunnyvale, USA

4 Methods

4.1 Fluorescent labelling of antibodies

For further measurements the quality of antibodies is of immense importance. To avoid long labelling reactions and maybe the degradation of antibodies as a consequence of temperature shift, the selection of the reactants plays a decisive role. As mentioned below the durability of a nucleophilic substitution is dependent on the binding speed in all steps and, thus, on the reactivity of both reactants: the nuceophile and the leaving group.

The conjugation of a monoclonal mouse anti-ACTH (N-terminal) IgG antibody to a DyLight 488 dye was performed by a DyLight Microscale Antibody Labelling Kit (Thermo Fisher Scientific, Waltham, Massachusetts, USA in cooperation with Pierce Biotechnology, Rockford, USA). This kit contained all sufficient reagents to obtain fluorescently labelled proteins in a few simple reaction steps. It was designed for labelling and subsequently purifying 100µg (1mg/ml) of anti-ACTH IgG antibodies.

The NHS ester, the most commonly used reactive group for labelling proteins, reacts ideally with all five primary amines – located on the lysine side chains of the antibody – forming a stable, covalent amide bond by releasing the NHS group. To avoid nonreactivity of fluorescent dyes it is very important to store NHS esters at -20°C till the labelling reaction occurs.

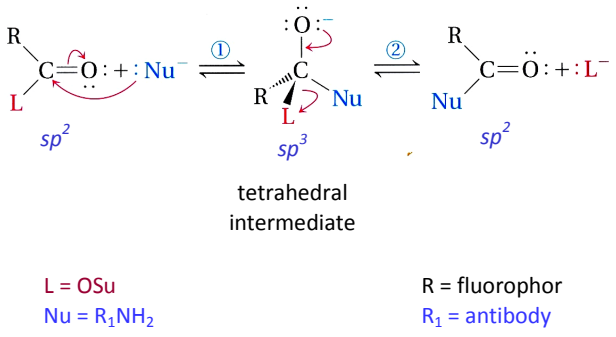

Fig. 4.1: Nucleophilic substitution on the carboxyl group (modified from [63])

A small trip to organic chemistry clarifies and demonstrates the mechanism of the labelling reaction in detail. The nucleophilic substitution on the carboxyl group occurs via an addition-elimination mechanism. The binding speed and the probability that the

reaction occurs is influenced by two facts: On the one hand the NHS-ester is a good leaving group because it favours a nucleophilic attack by delocalizing the negative charge from the carbon atom very well and thus leading to a partially positive charged carboxyl carbon atom. On the other hand primary amines are stronger nucleophiles than secondary or tertiary amines as their electron cloud is easier deformable, easier polarisable since the negative charge is clustered to the free electron pair at the nitrogen atom and not partially distributed over the residues, which are both hydrogen atoms.

①Addition step

The reaction starts with a nucleophilic attack on the carboxyl carbon atom of the trigonal, sp^2-hybridized NHS-ester forming a tetrahedral intermediate, where the carbon atom is sp^3-hybridized and bound to four residues.

②Elimination step

The negative charge in the intermediate state is now delocalized at the oxygen atom and results in a very instable C–L bond. Immediately afterwards the nucleofug – the leaving group – with the binding electron pair is eliminated, and the oxygen atom provides its free duplet to form a stable, trigonal, sp^2-hybridized carboxyl carbon atom again.

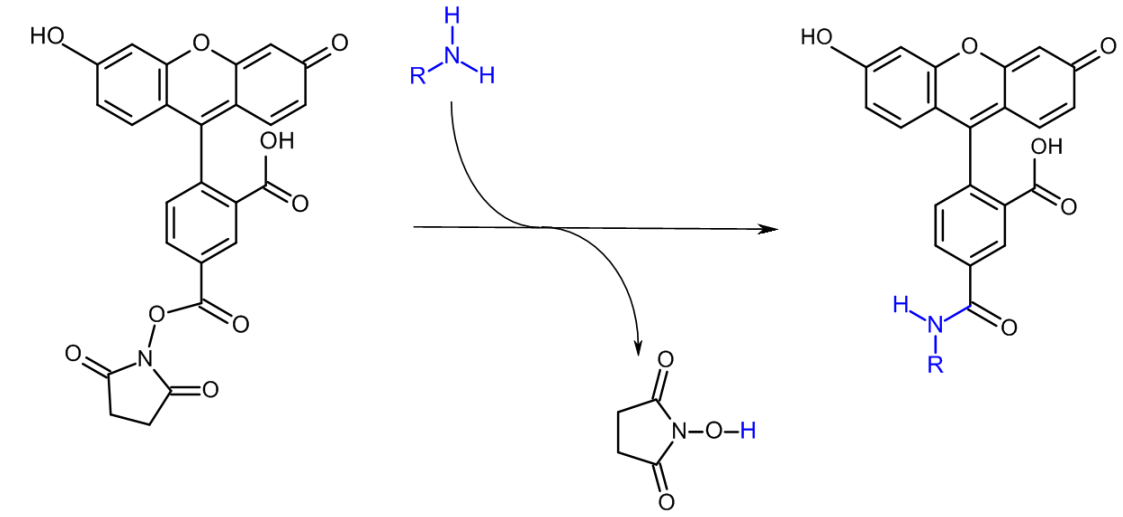

5-Carboxyfluorescein *N*-succinimidyl ester

Fluorescein Carboxylamid

Fig. 4.2: Labelling reaction of Fluorescein NHS ester to a primary amine of an IgG antibody

Recapitulatory the reactive nucleofug N-succinimide is substituted by an amine, which is a strong nucleophile in turn. The end product of this nucleophilic substitution is a labelled antibody. Fig. 4.2 shows the simplified form of the labelling reaction considering the chemical structure of all reactants if all proton transfer steps are excluded. The different colours of atoms and bonds should demonstrate the dynamic of electrons transfers in this substitution reaction.

4.1.1 Protein Labelling

100 µl of the prepared antibody solution (1 mg/ml) was added to the vial of the NHS ester, inverted 10 times and then centrifuged (Hettich-Centrifuge MIKRO 22R, Hettich-Rotor 1159) to enable an optimal labelling reaction in a short time. The collected reaction mixture was incubated for 60 minutes at room temperature protected from light.

4.1.2 Protein Purification

Subsequently, the protein purification was performed by column chromatography. The column was calibrated with 100 µl of a premixed uniform silica gel suspension which was filled into a spin column that contained a filter prior to the exit port to avoid effluence of the silica particles (Sephadex G-25M). Centrifugation for 45 seconds at 1000x*g* (3200 rpm) and 4°C removed the PBS solution and bedded the silica particles. The collected reaction mixture from the labelling step – a suspension of labelled antibodies and free unbound dyes – was loaded on the spin column.

Due to the fact that molecules migrate through the stationary phase with different retention times, labelled antibodies were separated from non-reacted dyes by modified silica particles of the stationary phase, which acted like a molecular filter: Non-conjugated fluorophores remained in the pores of the silica particles and, thereby, could be removed by gel filtration, because they retended in the stationary phase (visible as a coloured phase) whereas labelled and unlabelled antibodies were not retended and passed through the column because of a too small pore size of the stationary phase. The migration of the reaction mixture through the stationary phase was accelerated by centrifugation for 45 seconds at 1000x*g* (3200 rpm) and 4°C. The purified conjugates were collected in an Eppendorf tube and stored in single-use aliquots at -20°C to avoid repeated freeze/thaw cycles.

4.1.3 Protein ratio estimation

For all further measurements it was of indispensable importance to verify the existence of these purified labelled antibodies on the one hand and to determine the degree and the exact concentration of them on the other hand by the use of photometry.

Lambert Beer's law is a fundamental equation in optical spectroscopy and expresses that the amount of light emerging from a sample is diminished by three physical phenomena:

- the amount of light absorbed in any volume (concentration),
- the distance the light travels through the sample (optical path length) and
- the wavelength-dependent probability that a photon will be absorbed by the sample (extinction coefficient).

This relationship is expressed as

$$\mathbf{A} = \mathbf{lg}\left(\frac{\mathbf{I_0}}{\mathbf{I}}\right) = \boldsymbol{\varepsilon}\,\mathbf{c}\,\mathbf{d}$$

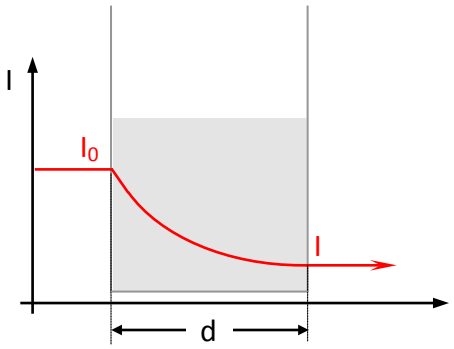

A	measured absorbance		
I	intensity of the absorbed light		
I_0	intensity of the initial light beam	c	concentration of absorbed sample [M]
ε	extinction coefficient [$M^{-1}cm^{-1}$]	d	optical path length [cm]

Based on the fact that upon protein conjugation the absorption maximum (A_{max}) of the bound fluorophore shifts to the right of the spectra an absorption spectra (see Fig. 4.3 and Tab. A.1) was recorded with a spectral photometer and the protein concentrations of labelled and unlabelled antibodies were calculated afterwards according to Lambert-Beer law. For this purpose 5 µl of the collected purified conjugates were added to 147.5 µl PBS (dilution of 1:30.5) in a quartz cuvette of 1 ml volume. PBS was used as the blank in this measurement.

As mentioned above the absorption maximum (A_{max}) of the dye shifts to the right of the spectrum from 488 nm to 493 nm upon protein conjugation and was considered as a specific correction factor (CF) in the equation below.

The UV absorption maximum at 280 nm wavelength, which was caused by the two aromatic amino acids Tryptophan and Tyrosine of the antibodies, indicated the presence of antibodies in the sample.

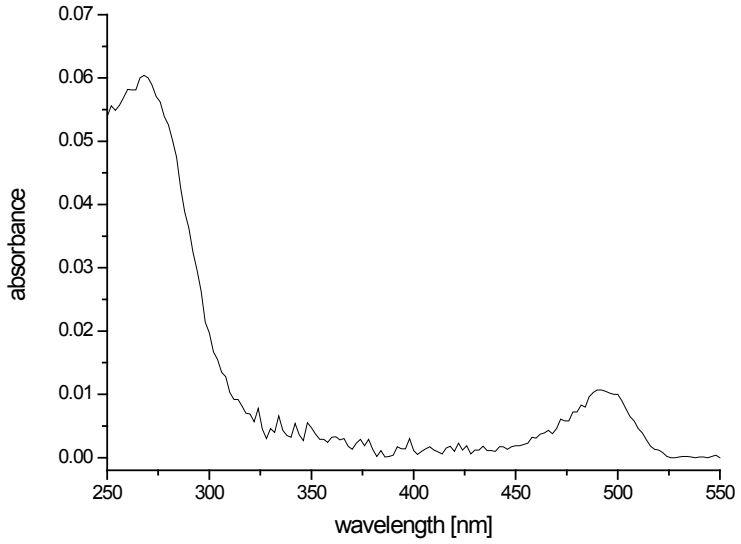

Fig. 4.3: Absorption spectra of DyLight488

Molarity of the antibody

In 1975 the Norwegian physician Per Brandtzaeg recommended the following formula to calculate protein concentrations in solution [43].

$$c_{ab,\,total} = \frac{A_{280} - (A_{max} \cdot CF)}{\varepsilon_{IgG} \cdot d} \cdot DF \approx \mathbf{7.411 \cdot 10^{-6}\ M}$$

$$c_{ab,labelled} = \frac{A_{max}}{\varepsilon_{fluor} \cdot d} \cdot DF \approx \mathbf{4.662 \cdot 10^{-6}\ M}$$

$A_{280} = 0.0526$ CF = 0.147

$A_{max} = A_{492} = 0.0107$ DF = 30.5

$\varepsilon_{IgG} \sim 210000\ M^{-1}cm^{-1}$ d = 1 cm

$\varepsilon_{flour} \sim 70000\ M^{-1}cm^{-1}$

Degree of labelling

$$\frac{\text{mole flour}}{\text{mole protein}} = \frac{c_{ab,\,labelled}}{c_{ab,\,total}} = \frac{4.662 \cdot 10^{-6}\,M}{7.411 \cdot 10^{-6}\,M} \approx \mathbf{0.629}$$

About 63% of the anti-ACTH IgG antibodies were successfully labelled with the fluorophore whereas the rest remained unlabeled in solution. Additional purification steps might enhance the degree of labelled antibodies in a solution but would result in the lost of a great amount of labelled antibodies as well. Nevertheless only fluorescent antibodies can monitor random motions of an antibody-ACTH complex inside a defined volume element during FCS measurements.

Assuming that the binding event of a labelled antibody to the N-terminal region of the ACTH molecule occurred in the same degree as its successful labelling reaction, a correction factor was included in all calculations regarding ACTH concentrations.

Correction factor (CF) for ACTH concentration:

$$CF_{FCS} = \frac{1}{0.629} \approx \mathbf{1.58963}$$

4.2 Cell culture

Cell seeding and incubation of AtT-20 cells were performed as described for the static ACTH release experiments [40] and was partially modified for this experimental approach.

4.2.1 Cell line and cell culture medium

AtT-20 cells (ATCC No. CCL-89) were purchased from the American Type Culture Collection (ATCC, Manassas, USA) and passaged at a subcultivation ratio of 1:4 every 5 days. For these experiments only cells with a passage number up to five were used.

The base medium used for this cell line was Dulbecco's Modified Eagle's Medium (DMEM). For a complete growth medium cell culture reagents were used in conjunction with the base cell culture medium to provide essential nutrients like FBS for the AtT-20 cell growth and to support cell maintenance: this was achieved with the antibiotics penicillin and streptomycin on the bacteriological side and with sodium bicarbonate on the chemical side. The bottom line was to avoid apoptosis of the AtT-20 cells induced by

pathogens and to remove any acidic impurities from the media by decomposing to water and the volatile carbon dioxide.

$$\begin{aligned} NaHCO_3 + H^+ &\rightarrow Na^+ + H_2CO_3 \\ H_2CO_3 &\rightarrow H_2O + CO_2\uparrow \\ \hline NaHCO_3 + H^+ &\rightarrow Na^+ + H_2O + CO_2\uparrow \end{aligned}$$

Therefore the base medium was supplemented with a final concentration of 10% foetal bovine serum, 1.5 g/l sodium bicarbonate, 10 u penicillin and 10 µg streptomycin.

4.2.2 Seeding AtT-20 cells

For this static ACTH release experiment the cells were seeded onto polystyrene 24-well tissue culture plates (Nalge Nunc International, Japan) at a density of $1.0x10^4$ cells/ml in each 16 mm well and grown in 1ml DMEM complete medium for 2-6 days without any medium change. AtT-20 cells were maintained in an incubator (HERAcell®, Thermo Scientific, USA) at 37°C, 6% CO_2 and 95% relative humidity. Samples were seeded in duplicate to ensure reproducible results.

4.2.3 Stimulating AtT-20 cells

CRH is one of several stress factors which stimulates the ACTH response in pituitary gland cells (see CRH).

A dose of 10 nM was chosen because it was shown in FCS measurements to induce maximal ACTH response in AtT-20 cells between 5-20 nM CRH (data shown in *Results and Discussion*). For this purpose the cells were treated with 10 nM CRH in the stationary phase after incubation times of 92 hours and 114 hours.

4.2.4 Preparing samples for FCS measurement and cell counting

For measuring the cell population and the ACTH concentration, the cells had to be separated from the extracellular space. Whenever working with cell culture all experimental steps were carried out under sterile conditions in a laminar flow. Finally quantitative answers for the secreted ACTH concentration per cell as well as for the ACTH rate per cell were given (Fig. 4.4).

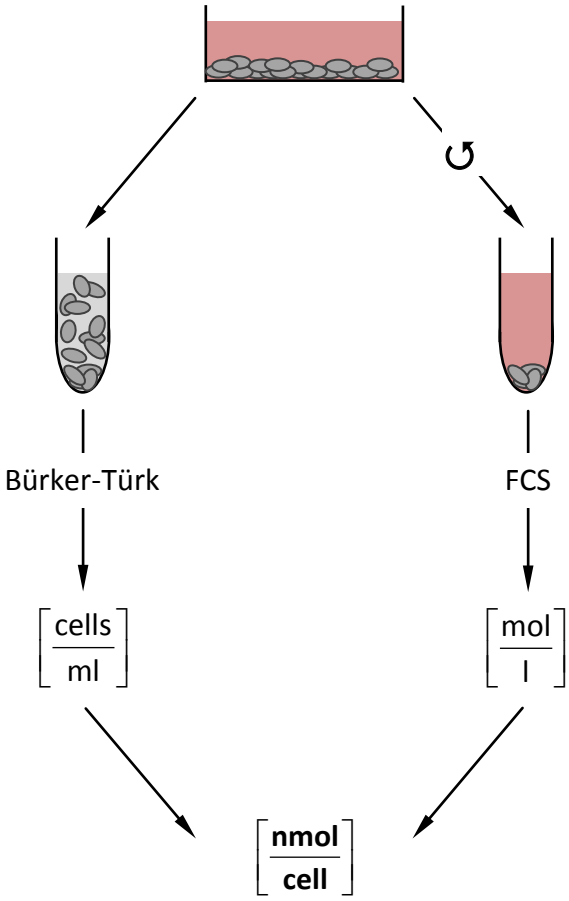

Fig. 4.4: Reduced overview of preparing AtT-20 cells (l.) and the supernatant (r.) for measurements

Supernatant (ACTH)

The supernatant, which mainly composed of the complete culture medium, secreted hormones, detached – mostly apoptotic – cells, degradation products and other trash, was removed careful from the cell layer and transferred into an Eppendorf tube. Subsequently the centrifugation at 3200 rpm and 37°C for 10 minutes ensured the separation of cell and trash material (pellet) from low-molecular weight compounds, which still remained in the supernatant.

As the FCS is a very sensitive spectroscopic technique, this step was of indispensible importance to avoid autofluorescence of the cell surface or unspecific antibody interactions with membrane proteins that may influence the results. Thereby the supernatant (about 1 ml) was transferred into a sterile tube and incubated at 37°C till FCS measurement occurred.

However the resulting cell pellet with an actually small amount of intact cells had to be taken into account in cell counting.

Cell pellet (AtT-20)

Once the medium was removed 200 µl of 0.25% (w/v) trypsin solution was added and the cells incubated at 37°C and 5% CO_2 for 5 minutes to achieve proteolysis of the adhesion matrix. Afterwards the cell layer was briefly rinsed with 800 µl DMEM to stop trypsinisation and transferred into that tube including the cell pellet of the pre-performed supernatant isolation. The cell layer cell suspension was gently mixed and loaded on a Bürker-Türk counting chamber immediately afterwards to calculate the number of AtT-20 cells.

4.3 Cell counting

The Bürker-Türk chamber, which was used in all measurements for calculating the population of AtT-20 cells, is one of various counting chambers available on the market differing only in their design of the counting net and the chamber depth.

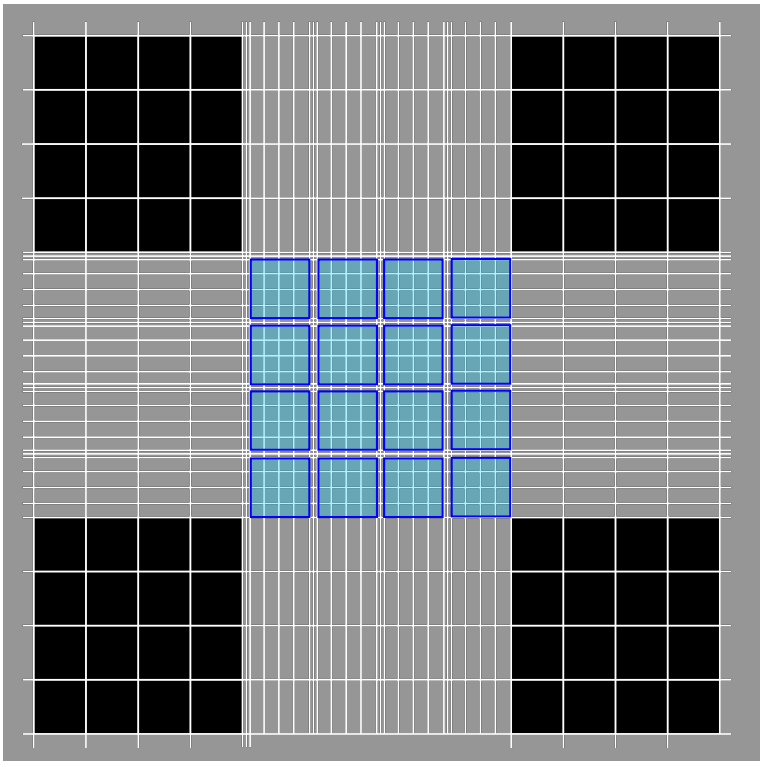

Fig. 4.5: Counting net and countable areas (in blue) of a Bürker-Türk counting chamber

The countable area (in Fig. 4.5 in blue) of a Bürker-Türk chamber consists of a large square in the middle which is divided into four times four group squares of 0.04 mm^2 each. Taking the chamber depth of 0.1 mm into account, the concentration of AtT-20 cells in a solution can be calculated as the number of cells in each group square corresponds to

a fixed volume of 0.004 mm^3. Through the low cell numbers in each group square, the countable area was expanded to all 16 group squares to diminish the probability of counting errors.

Immediately after completing each count the cover glass and the counting chamber were washed with a mild ethanol solution and dried afterwards.

General calculation formula

$$\frac{\text{cell number} \cdot DF}{\text{counted area}[mm^2] \cdot \text{chamber depth}[mm]} \cdot 1000 \equiv \frac{\text{cells}}{\text{ml}}$$

Parameters	
Chamber	Bürker-Türk
Counted area	16 group squares = 16 x 0.04 mm^2 = 0.64 mm^2
Chamber depth	0.1 mm

Regarding to these parameters the following simplified formula formed the basis for all calculations of AtT-20 cell numbers in this thesis (see *Results and Discussion*).

Simplified calculation formula

$$\frac{\textbf{cell number} \cdot \textbf{DF}}{\textbf{0.064 mm}^3} \cdot \textbf{1000} \equiv \frac{\textbf{cells}}{\textbf{ml}}$$

4.4 FCS-Setup

4.4.1 FCS-Measurement

However, from the instrumental as well as the chemical point of view a suitable measurement requires the right setup, which had to be found in a few tens of FCS measurements by changing the ratio of the antibodies, sample and buffer solution among each other. A variety of mechanisms can influence FCS measurements: dynamic photobleaching of molecules to a dark state, photo-induced isomerisation, protonation of

chromophores, photon anti-bunching and other processes are of particular concern and cause unwanted background signals.

Even lowest signal/noise-background during FCS measurements that allows detection of all low-abundance ACTH molecules with great selectivity and sensitivity was the goal of this setup. Finally the right adjustment enabled quick, constant and reproducible measurements as the shape sigmoid run of the autocorrelation function and the constant fluorescence intensity of each photon illustrated in chapter 4.4.2.

For this reason labelled as well as unlabelled antibodies were added in excess to the sample compared to the number of ACTH molecules expected in solution to ensure a quick and high potential binding of both antibodies to all ACTH molecules and to calculate exact ACTH concentrations by means of FCS in the end.

In fact FCS cannot be performed in too concentrated solutions with many fluorophores in the observed volume. Less fluorophores result in more fluctuations and more fluorophores result in smaller fluctuations and a more constant average signal [64].

'Detection mixture' for FCS measurements

Therefore, PBS (1x), purified antibody conjugates (100 µg/ml) binding to the N-terminal region of the ACTH molecule, unlabelled IgG antibodies (100 µg/ml) specific for the C-terminal region of adrenocorticotropin and a sample aliquot including ACTH molecules of unknown concentration were united in a volume ratio of 8 : 1 : 1 : 10, slightly stirred and incubated for 20 min at 37°C.

In a meanwhile a drop of the organic fluorescent dye Rhodamine 6G (diluted 1:200) was used to automatically position the chambered coverglass (Nalge Nunc International, Japan) in focus of the confocal optics of the spectrofluorimeter by a scanning procedure as well as to automatically adjust the pinhole to its right position (for the pinhole x = 4.739 mm, y = 4.812 mm and z = 6.294 mm; for the focus 5.600mm). A pinhole, which is introduced in the image plane of confocal optics, is responsible for limiting the detection volume in axial direction and thus blocking all light not arising from the focal region. The pinhole size was set to 45 µm, resulting in a confocal volume element of 0.17 µm in the lateral and 2.4 µm in the axial dimension.

For focussing light in a total space element of about 0.5 femtolitres small sample volumes (15-30 µl) are sufficient for FCS measurements.

After 20 min incubation time, a drop of sample was pipetted on the chambered coverglass and the fluctuations in fluorescence intensity were monitored in series of 30 measurements with identical setup (measurement time: 10 s; correlator scaling: 10 s) for each sample. A correct positioning was re-evaluated after 20 measurement series.

4.4.2 Calculating autocorrelation function G(τ)

The number of fluorescent molecules entering and leaving the detection volume (10^{-15} l) fluctuates incessantly. Binding events result in slower fluctuation components and modulate the fluorescence signal, which is additionally influenced by triplet crossing causing blinking on a characteristic microsecond-timescale. Fig. 4.6 shows that the fluorescent dye ideally displayed emission which persisted for a long time. This photostability of the fluorescent signal made it possible to monitor fluctuations via a long timescale.

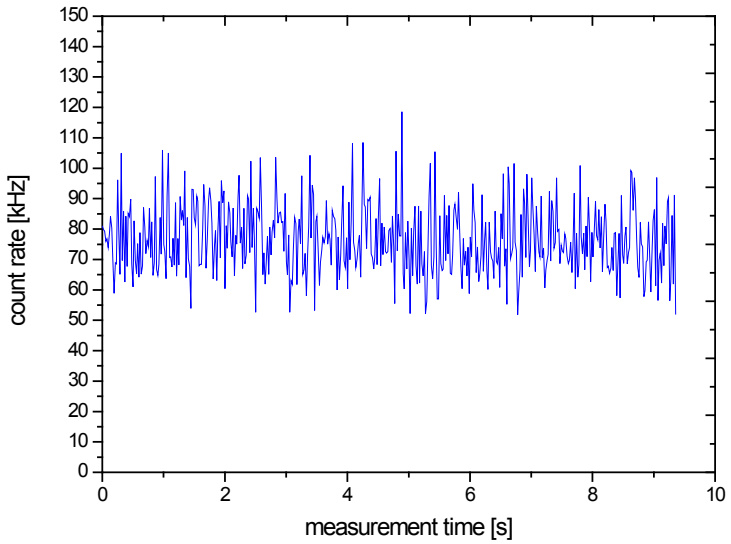

Fig. 4.6: Fluorescence Fluctuations monitored in a FCS measurement

As a higher number of measurements for each sample diminishes its deviation of the mean value and, thus, increase the accuracy of results enormously, a spate of 30 to 40 fluctuation measurements was carried out for each sample with identical FCS setup.

Subsequently, fluctuations were analyzed statistically by the autocorrelation function to yield accurate results. In addition, a model which incorporates descriptions of the sources of fluctuations was used for fitting this function to determine the physical parameters of interest.

The amplitude and speed of the fluctuations were used to calculate the correlation function. The intersection point of the autocorrelation curve with the ordinate is inversely proportional to the average number of fluorescent particles being observed. The red points on the curve in Fig. 4.6 indicate the different diffusion times derived from the function. A diffusion time of about 230 µs is related to the free antibody fraction whereas antibody(labelled)–ACTH–antibody(unlabelled) complexes need longer diffusion times through the focus of about 900-1200 µs.

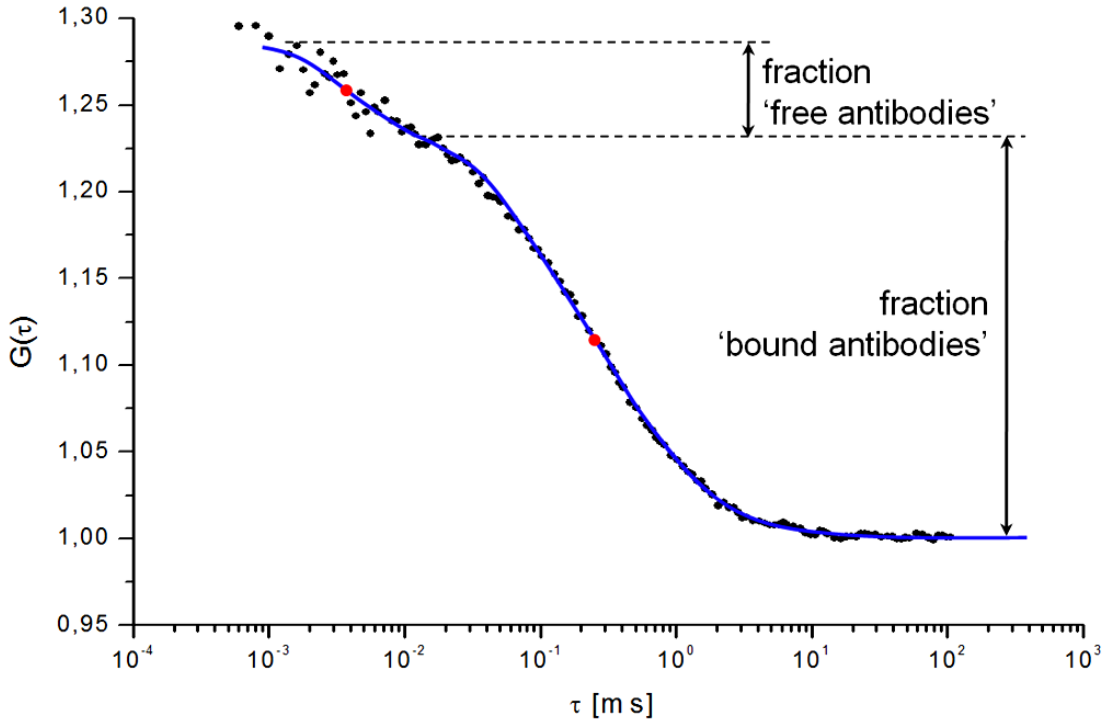

Fig. 4.7: Schematic representation of an autocorrelation function for a sample with 2 diffusion properties

The normalized autocorrelation function G(τ) describes fluctuations of a signal F(t) from the mean intensity at any time compared to fluctuations at any later time F(t+τ), and is given by

$$G(\tau) = \frac{\langle \delta F(t) \cdot \delta F(t+\tau) \rangle}{\langle F(t) \rangle^2}$$

where the angular brackets in the function represent the ensemble average and τ is known as the delay or correlation time over which the fluctuations are compared.

G(τ) depends on the measurement geometry and on the diffusion properties of the fluorescent species. The Stokes-Einstein relation mathematically describes the translational diffusion coefficient of a particle in a viscous medium [62],

$$D = \frac{k\,T}{f}$$

D	Diffusion coefficient
k	Boltzmann constant
T	Temperature
f	Friction coefficient for the particle in the fluid

where *f* depends on the geometry (Stokes radius) as well as the surrounding solution (viscosity of the solvent), and is given by [62]

$$f = 6\,\pi\,\eta\,r$$

f	friction coefficient for the particle in the fluid
η	viscosity of the solvent
r	hydrodynamic radius (Stokes radius)

For a single diffusing species (a one component model) in a Gaussian confocal volume the autocorrelation function G(τ) is written as [48][49],

$$G(\tau) = 1 + \frac{1}{N\left(1 + \frac{\tau}{\tau_D}\right)\sqrt{1 + \frac{\tau}{\left(\frac{z}{r}\right)^2 \tau_D}}}$$

where N is the particle number and τ_D the molecular diffusion time of the fluorescent molecule moving through the confocal volume in an axial (z) to radial (r) dimension [48][49]. The molecular diffusion time for a one photon excitation is given by the following relationship to the diffusion coefficient D [$cm^2\ s^{-1}$]

$$\tau_D = \frac{r^2}{4\,D}$$

The obtained autocorrelation functions were evaluated using a two component model by fixing the diffusion time of component 1 which was achieved from one component fitting of labelled antibodies (see the equation for a one component model above).

The analytical formula for the two component model, which was successfully applied in previous works of our scientific group [48][49], was used in a modified form (including triplet state in component 1) for this approach and is given by

$$\mathbf{G(\tau) = 1 + \frac{1}{N^2}\left[(1-Y)\,g_{D1}(\tau) + Y\,g_{D2}(\tau)\right]}$$

with

$N^2 = N_1\,N_2$

$$g(\tau) = \left(1 + \frac{\tau}{\tau_D}\right)^{-1}\left(1 + \frac{\tau}{\left(\frac{z}{r}\right)^2 \tau_D^2}\right)^{-0.5}$$

This yields values of diffusion times (τ_{D1}, τ_{D2}) and of the related mole fractions Y and (1–Y) for the two components. Based on this autocorrelation function the 2-component curve fit permits the direct reading of four parameters in the detection volume (Fig. 4.7):

- the diffusion time (τ_{D1}) of component 1
- the number of particles (p_1)of component 1
- the diffusion time (τ_{D2}) of component 2
- the number of particles (p_2)of component 2

Only in this way it was possible to computationally eliminate the desired ACTH-bound form (component 2) from unbound fluorescent antibodies (component 1) in the sample.

Assuming that exactly as many antibody(labelled)–ACTH–antibody(unlabelled) complexes were formed as ACTH molecules remained in solution, the concentration of ACTH was directly calculated from the number of particles of component 2.

5 Results and Discussion

5.1 Cell growth studies on AtT-20 pituitaries

As the main focus of our study was the investigation of stress response of pituitary glands within the HPA axis, experiments were centred on the AtT-20 cell type.

Prior to all *in vitro* studies a stable population of AtT-20 cells had to be established in a complete medium without any cell stimuli (e.g. CRH or cortisol) and the stress-independent basal ACTH level had to be measured in a second step.

Recent data supported well-known investigations from the past [40] and indicated that beside unwanted environmental factors (listed in Tab.1.2) the behaviour of the growing curve is strongly influenced by the initial cell concentrations. The higher the cell population from the outset, the sharper and quicker the increase in the growing curves during exponential phase (Tab.5.1).

Live image studies – performed with Zeiss AxioCam MRm by focussing on the cell layers in each 16mm-well – showed different characteristics in morphology and the same tendency in cell growing as mentioned above. Tab.5.2 corroborates this hypothesis of cell behaviour and illustrates that the cell population increases from the left to the right side (in each row of Tab.5.2) due to higher seeded cell numbers.

Initial cell concentrations of $5x10^4$ – $1x10^5$ cells per ml indicate a far quicker growing process (pointed out in columns in Tab.5.2). However, a population of $5x10^5$ AtT-20 cells per ml is too high and the growing process too quick for investigating anything. Already after about 30 hours cells run through the stationary phase, because no distinctive increase of the cell population is observed in the next 22 hours. A population decrease of 7% cells (Tab.5.1) indicates that the balance of living to dead cells is shifted to negative cell growth and the majority of cells begin to shrink after already 44 hours and go into apoptosis after 70 hours, which is observable as a cell detachment from the layer (see right column in Tab.5.2).

initial cell number	incubation time	cell counts per 16 squares								total polulation	+/- total population	in-/ decrease	in-/ decrease
[cells/ml]	[h]									[cells/ml]	[cells/ml]	[cells/ml]	[%]
5.0×10^{3}	22	1	0	1	0	0	1	1	1	9765.63	7324.22	4766	195.31
1.0×10^{4}	22	2	1	1	0	1	2	1	1	17578.13	6835.94	7578	175.78
5.0×10^{4}	22	7	3	4	4	5	3	7	6	76171.88	21484.38	26172	152.34
1.0×10^{5}	22	9	11	10	9	9	12	10	12	160156.25	16601.56	60156	160.16
5.0×10^{5}	22	10	12	12	9	11	9	10	10	648437.50	15136.72	148438	129.69
5.0×10^{3}	44	1	2	1	1	1	0	1	1	15625.00	3906.25	5859	160.00
1.0×10^{4}	44	3	2	2	1	2	2	2	1	29296.88	6835.94	11719	166.67
5.0×10^{4}	44	9	11	12	14	10	12	14	10	179687.50	23437.50	103516	235.90
1.0×10^{5}	44	20	25	26	21	19	19	24	21	341796.88	36621.09	181641	213.41
5.0×10^{5}	44	15	13	17	12	10	16	14	13	859375.00	27343.75	210938	132.53
5.0×10^{3}	76	2	3	1	2	2	3	1	2	31250.00	7812.50	15625	200.00
1.0×10^{4}	76	8	6	9	9	10	8	9	7	128906.25	15625.00	99609	440.00
5.0×10^{4}	76	19	16	16	20	15	17	21	19	279296.88	29296.88	99609	155.43
1.0×10^{5}	76	6	8	7	7	9	6	8	6	445312.50	14160.16	103516	130.29
5.0×10^{5}	76	14	16	11	13	13	10	14	12	804687.50	21972.66	-54688	93.64

DF (dilution factor) = 4 (1:4 cell suspension)

Tab.5.1: Cell growth studies on AtT-20 pituitaries by cell counting

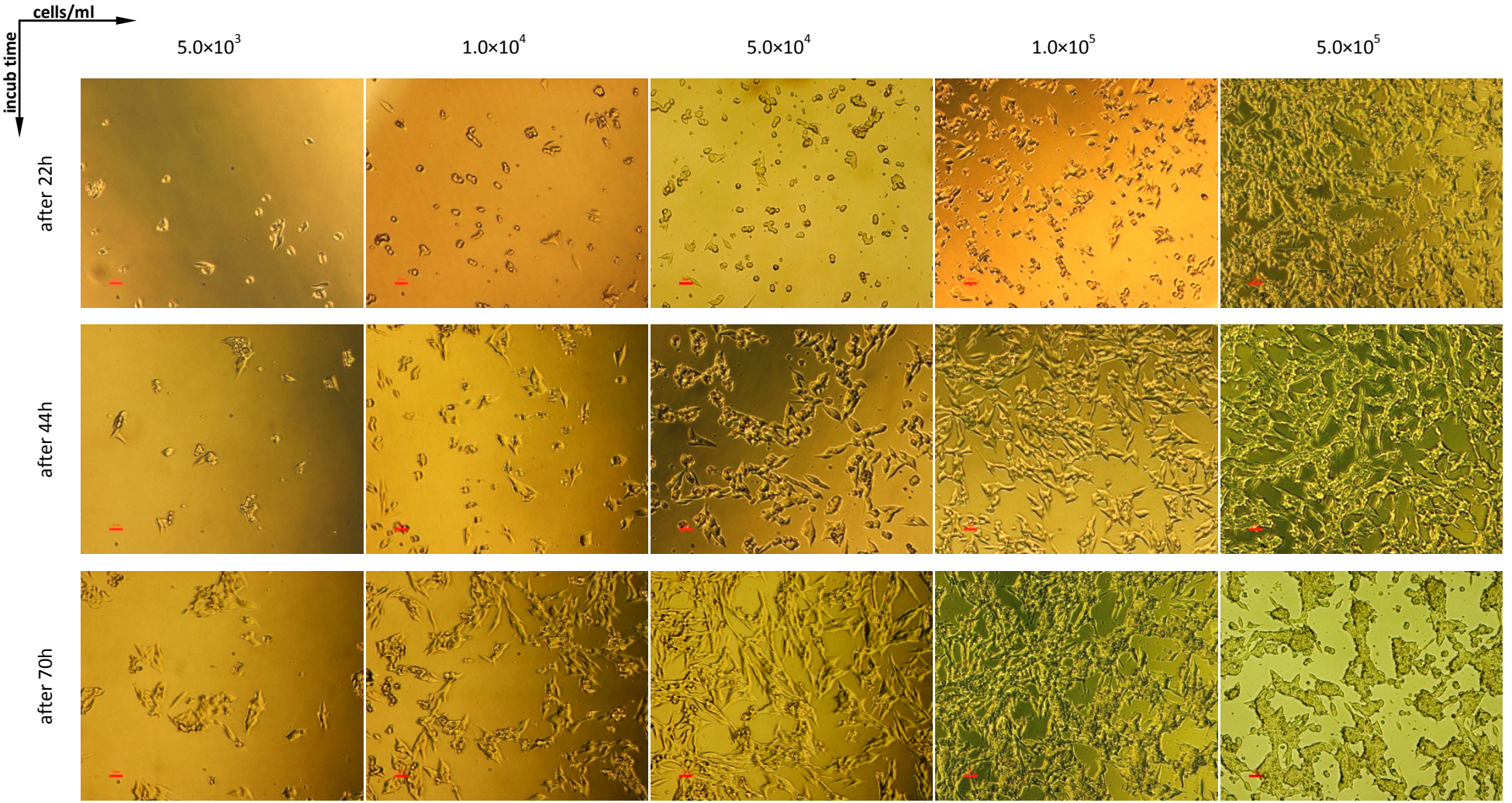

Tab.5.2: Morphological and cell growth studies on AtT-20 pituitaries by live-time imaging

Recapitulatory, the behaviour of AtT-20 cell growth is dependent to various populations of AtT-20 cells at the beginning. Furthermore an initial cell number higher than 10^4 cells per ml would result in temporally shorter phases of each AtT-20 cell growing circle and, thus, in temporally too short time windows for measuring real-time ACTH response to stress factors.

5.2 AtT-20 counts (seeded initial cell concentration: 10^4 cells/ml)

With respect to the quantification of our model the data further suggested, that in case of no medium change the stationary phase was most suitable for stimulating AtT-20 cells. An optimal use of this relatively short phase was achieved by adapting the initial cell concentration of 10^4 cells per ml for all *in vitro* experiments.

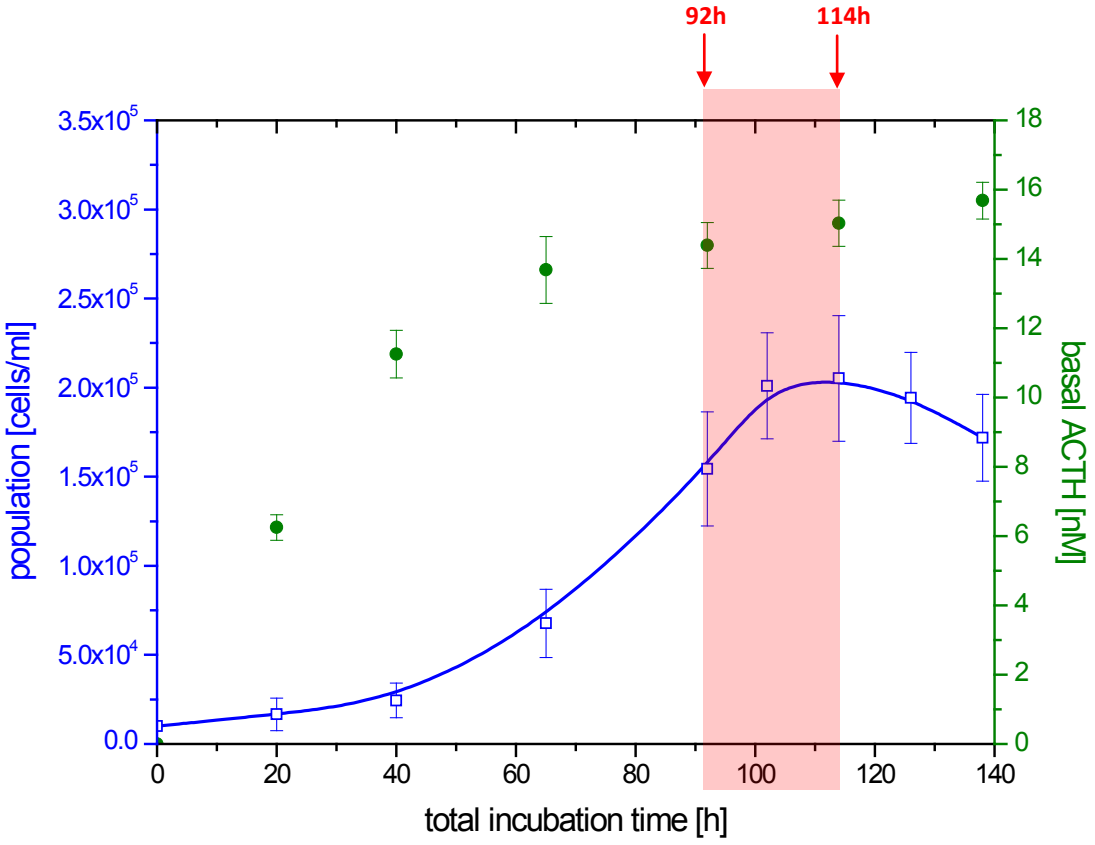

Fig. 5.1: AtT-20 cell growing curve compared with its total basal ACTH level over 138 h incubation time

The resulting time window for performing model studies (red area in Fig. 5.1) was increased to about 24 hours – starting after 92 hours and ending after 114 hours total incubation time – compared to only 14 hours for an outset of $5x10^4$ cells per ml in the stationary phase, and thus permitted the measurement of ACTH levels over a long period

of time. Furthermore the constant low ACTH output rate per cell and the constant number of cells in the stationary phase allowed the detection of even slight changes in ACTH levels.

5.3 'Idle currents' in the stand-by mode of AtT-20 cells

The basal ACTH rate, which indicates a permanent and constant secretion of this peptide hormone in AtT-20 cells, is triggered by inevitable signals (Tab.1.2) in the extracellular space caused by handling [31] and, thus, of immense importance for interpreting the ACTH response to stress in the right way. Metaphorically spoken a basal level to a certain time is the 'idle current' of ACTH secreted by the AtT-20 cell.

Therefore fluctuations of the basal ACTH level are observable depending on whether an up- (e.g. CRH) or down-regulating factor (e.g. cortisol) binds to the receptors on the cell surface.

time	population	+/-	ACTH	+/-	ACTH/cell	ACTH/cell/h
[h]	[cells/ml]	[cells/ml]	[nM]	[nM]	[nM.ml/cell]	[nM.ml.h/cell]
0	10000	0	0	0	0	0
20	16602	9156	6.249	0.372	9.4651E-04	4.7325E-05
40	24415	9766	11.253	0.691	6.4049E-04	3.2025E-05
65	67709	19098	13.684	0.967	5.6140E-05	2.2456E-06
92	154390	32039	14.391	0.660	8.1608E-06	3.0225E-07
114	205163	35327	15.027	0.666	1.2523E-05	5.6925E-07
138	171875	24306	15.685	0.529	-1.9770E-05	-8.2375E-07

Tab.5.3: Basal ACTH concentration and basal output rate in 'stand by'-mode

The basal ACTH secretion is characterised by a strong increase in the first 65 hours of incubation (Tab.5.3, illustrated in Fig. 5.2). Nevertheless a plateau level of ACTH is reached after an 80-hour incubation period. It could be interpreted as a shut down mechanism of the secretion machinery in AtT-20 cells due to a large pH change to an acidic milieu in the medium mainly caused by the degradation products of AtT-20 cells and nutrition depletion in the medium.

Fig. 5.3 points out the basal ACTH rate per cell in one hour, which represents the most significant value as the cell population is taken into account as well. Thereby the same tendency as discussed for the total basal ACTH concentrations in the extracellular space

can be observed: A high ACTH secretion level per cell in the first 60 hours, followed by a reduced ACTH output to a minimum in the stationary phase (between 95 hours and 120 hours incubation time) as a result of nutrient lost and the shutdown of cell growth.

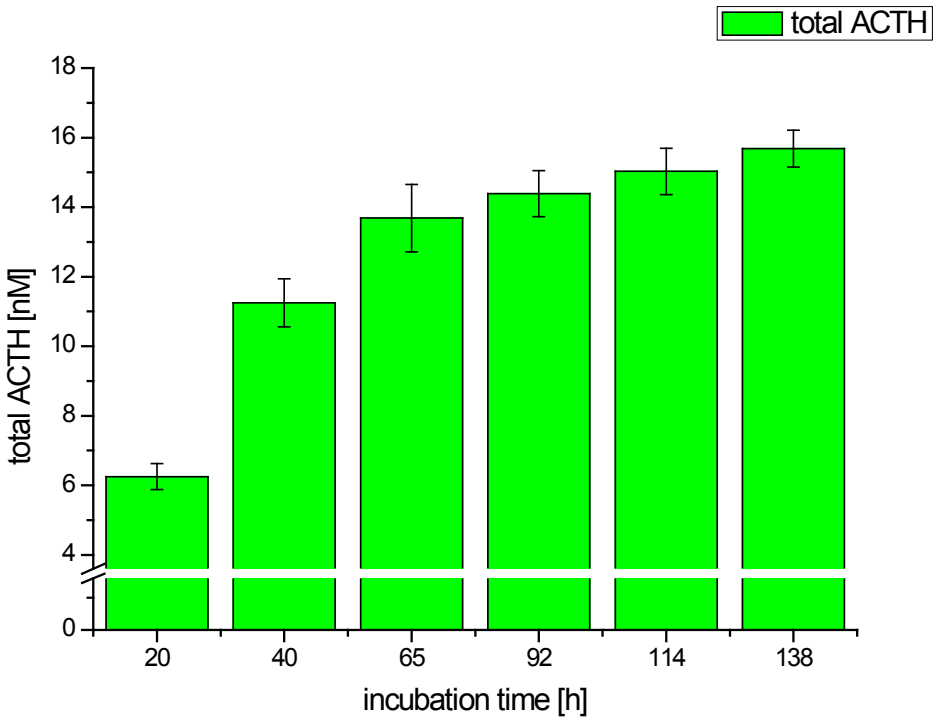

Fig. 5.2: Total basal ACTH level of AtT-20 cells over 138 h incubation time

As soon as the nutrient's level diminishes radically (after about 120 hours incubation time), the cell has to constrain its metabolism to a minimum to survive. Since the pathway of ACTH synthesis only plays a subsidiary role for AtT-20 cells in case of life or death the secretion of ACTH is shut down first to ensure cell survival.

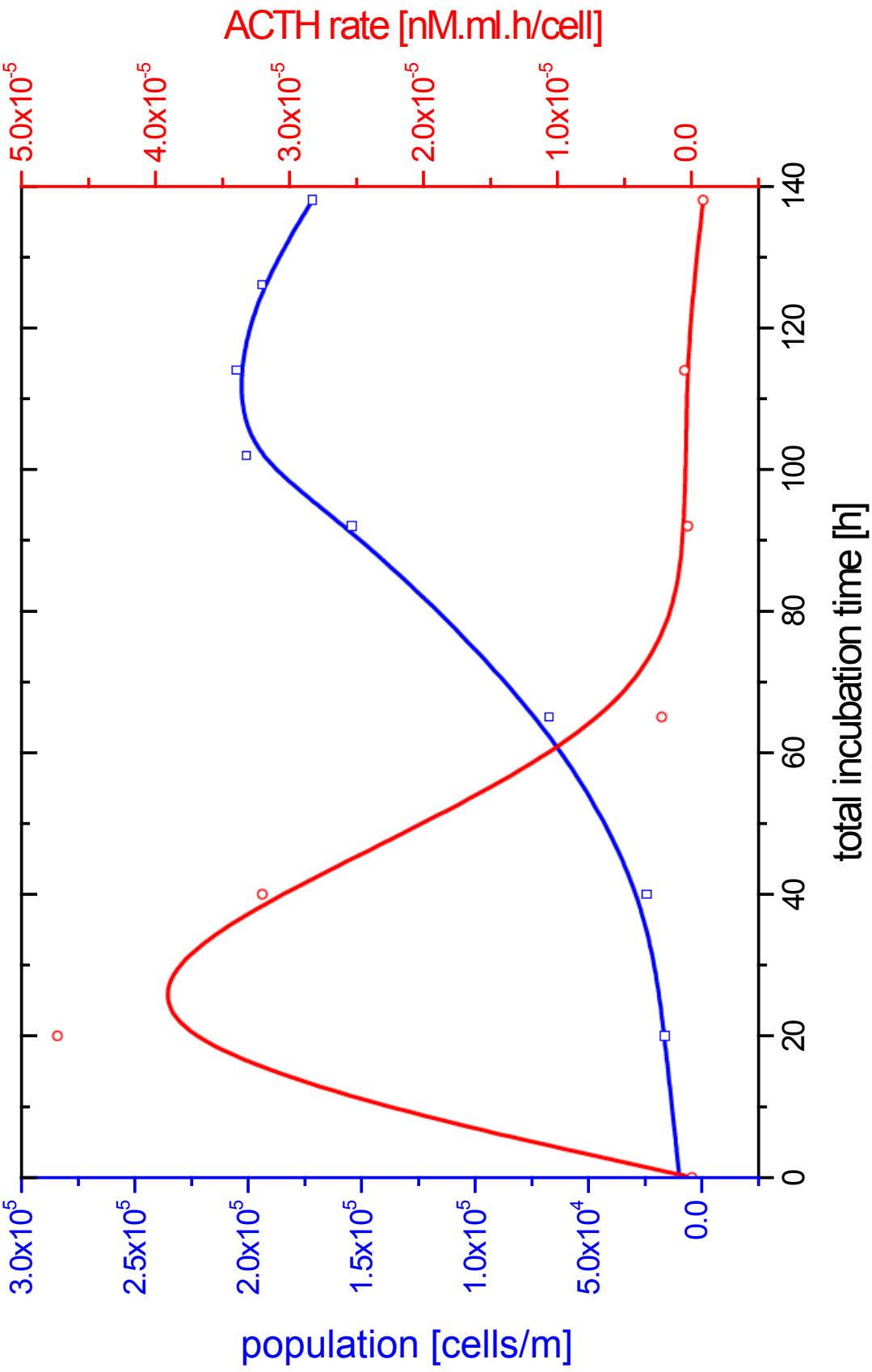

Fig. 5.3: Basal ACTH output rate of an AtT-20 cell over 138 h incubation time

5.4 Molarity of a signal controls its ACTH response

The first goal of our study was to find the right extracellular CRH concentration for measuring highly different ACTH secretion levels compared to those in the basal state.

As the firing frequency of action potentials in neurons reflects the magnitude of intensity of any stimulus the same is true in case of hormone signalling in the HPA axis network.

Due to higher stress intensities, neurons located in the periventricular hypothalamus increase the frequency of CRH release into the blood of the portal circulation. Within 15 seconds CRH travels in short distance to the anterior pituitary where it stimulates ACTH release [61]. Our data (Tab.5.4 and Tab.5.5) of an *in vitro* HPA axis model suggests that the molarity of CRH controls its ACTH response in AtT-20 pituitaries and affects its cell growing as well. An incubation of CRH in a concentration range of 5-10 nM over 22 hours showed a strong increase in the total ACTH level (Fig. 5.5B), as well as in the cell population (Fig. 5.6A), which indicates that CRH in low molarities mediates a higher rate of ACTH secretion (Fig. 5.4), whereas CRH concentrations higher than 54 nM won't have any significant effects on ACTH secretion rate compared to basal levels.

Several anterior pituitary hormones exert short-loop negative feedback on the hypothalamus resulting in lower or even inhibition of CRH output rate [69] *in vivo*. Surprisingly this short-loop negative feedback mechanism has no influence for our *in vitro* model as no hypothalamic cells exist, which would generate a response.

However, an adaptive function of this feedback mechanism is that it maintains the plasma concentration of the final hormone in a sequence relatively constant whenever a disease-induced primary change occurs in the secretion or metabolism of that hormone [69]. Transformed to our study there could be evidence of a protective mechanism in AtT-20 cells, which is triggered by a CRH overload in the extracellular space, beside the described short-loop negative feedback, which down-regulates ACTH secretion as well as cell growth if a threshold of stress intensity is reached leading to a far increased ACTH output rate and affecting the balance of homeostasis.

These results suggested that the highest ACTH response exerts from extracellular CRH concentrations of 5-20 nM. Therefore a stress signal of 10 nM CRH was used for all further measurements on AtT-20 pituitaries.

time		total population	+/-	population + 10nM CRH	total ACTH	+/-
[h]		[cells/ml]	[cells/ml]	[cells/ml]	[nM]	[nM]
92		154390	32039		14.391	0.660
114		205163	35327	50773	15.027	0.666
114	+5nMCRH(22h)	335938	27344	181548	16.771	0.916
114	+10nMCRH(22h)	324219	19532	169829	16.898	1.065
114	+36nMCRH(22h)	302084	28936	147694	16.151	0.904
114	+54nMCRH(22h)	237500	22500	83110	15.364	1.389

Tab.5.4: Cell- and ACTH response through different CRH concentrations (part I)

time		ACTH after 22h CRH	ACTH/cell	ACTH rate	+/- basal ACTH rate
[h]		[nM]	[nM.ml/cell]	[nM.ml.h/cell]	[nM.ml.h/cell]
92		0			
114		0.636	1.2523E-05	5.6925E-07	
114	+5nMCRH(22h)	2.380	1.3108E-05	5.9580E-07	2.6558E-08
114	+10nMCRH(22h)	2.507	1.4761E-05	6.7095E-07	1.0171E-07
114	+36nMCRH(22h)	1.760	1.1915E-05	5.4157E-07	-2.7672E-08
114	+54nMCRH(22h)	0.973	1.1706E-05	5.3207E-07	-3.7173E-08

Tab.5.5: Cell- and ACTH response through different CRH concentrations (part II)

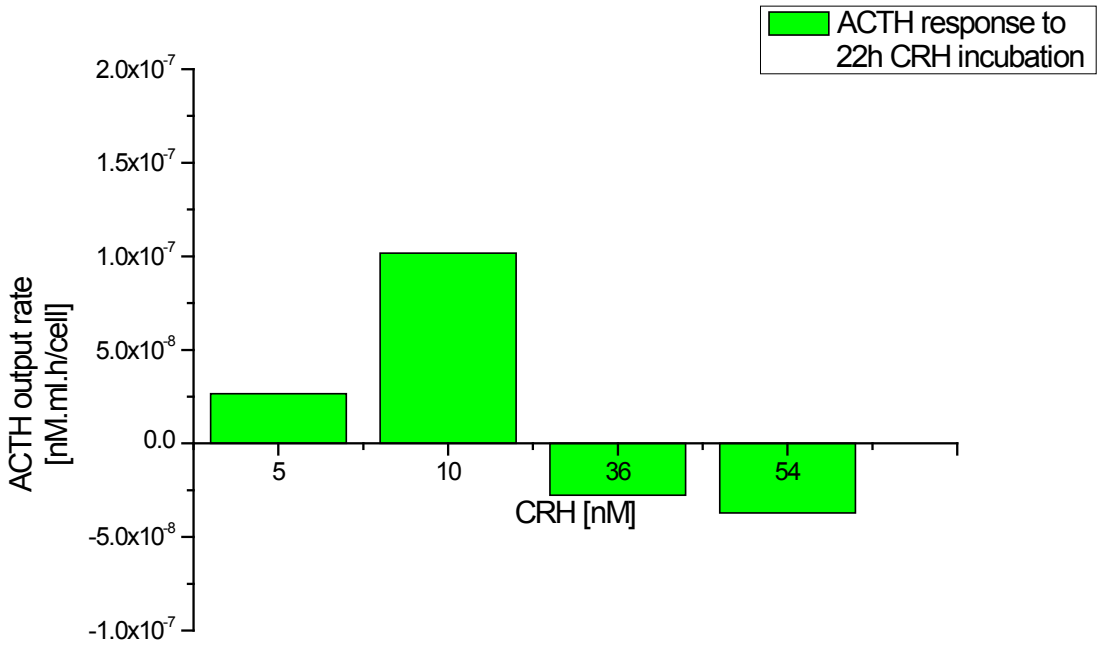

Fig. 5.4: Extracellular ACTH secretion rate through different CRH concentrations

A

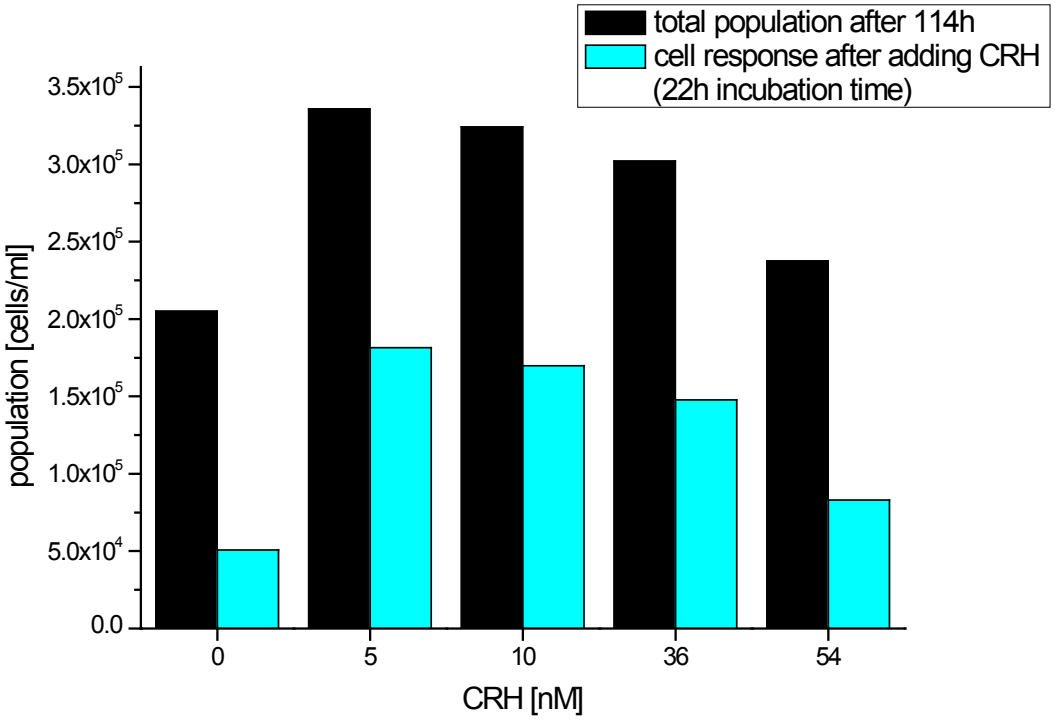

B

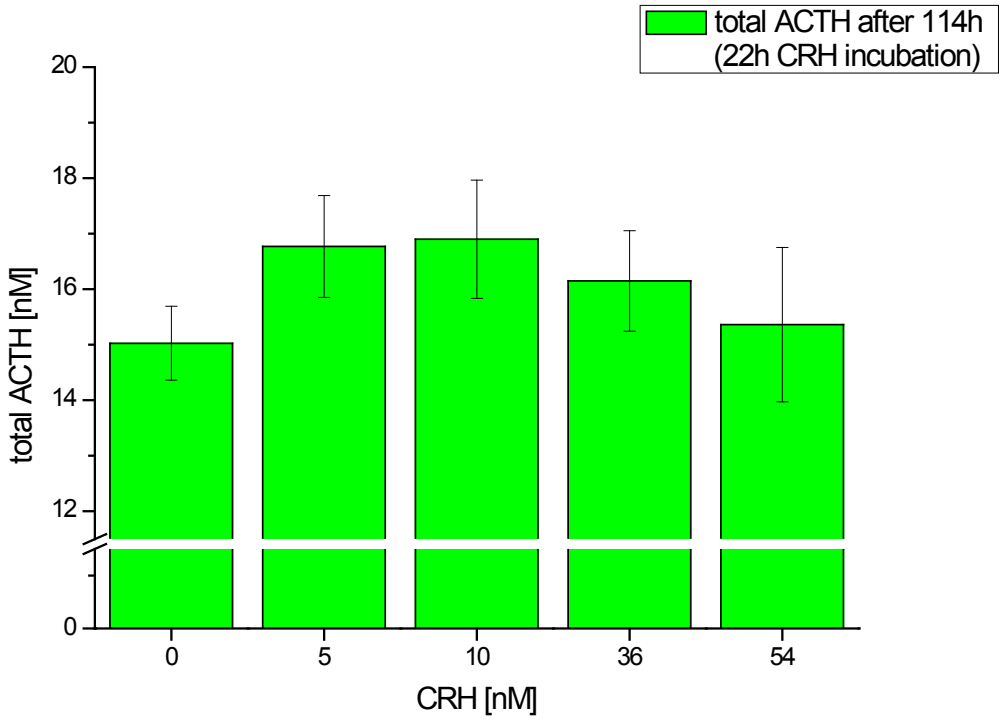

Fig. 5.5: Comparison of cell- (A) and ACTH concentrations (B) through different CRH concentrations

5.5 Real-time ACTH response to CRH at two time windows

Real-time measurements were performed within two time borders: One at the crossover of the exponential to the stationary phase (after 92 hours of incubation time) and the other at the end of the stationary phase (after 114 hours). Fig. 5.6 (data from Tab.5.6, Tab.5.7) illustrates the rapid and highest ACTH response per cell to a stress signal within a minute! The secretion of ACTH molecules into the extracellular space is flattened in the next two hours nearly to the basal rate. These observations are consistent with previous reports showing the glucocorticoid-induced inhibition of ACTH secretion [4][56] and thus indicating similar pathways for stimulating and inhibiting factors of ACTH secretion.

However, there is evidence of the activation of a non-genomic pathway by specific CRH receptors complexes [23], appearing immediately in a few seconds and minutes after CRH binding to its membrane receptor. ACTH is transported in clathrin-coated vesicles [30][36] via post-Golgi vesicle trafficking on microtubules to the proximity of the release site. Then vesicles are loaded onto an actin/myosin system for distal transport through the actin cortex to just below the plasma membrane, where vesicle tethering or docking to the membrane occurs [24]. These docked vesicles form the releasable pool, which is ready for takeoff. Stimulated by a stress signal (e.g. CRH), the docked vesicles fuse with the plasma membrane and ACTH molecules are released into the extracellular space.

Time delays in the secretion of ACTH-vesicles, which are tethered to the membrane, as a result of a longer transport route to the membrane are comprehensible and are mainly included in the measured ACTH levels after 15 minutes CRH incubation time.

Furthermore we found out that the ACTH response to the same CRH signal leads to a delay after 114 hours total incubation time compared to the one after 92 hours, which could be directly linked to the worsen cell growing conditions due to the loss of nutrients in the medium and the shutdown of the cytoplasmic machinery of cells in the battle against apoptosis.

Additionally, the latter, long-term effect of CRH is known to involve an increase in ACTH via the translation of the POMC mRNA [23]. This pathway is necessary for ‘filling up’ the pool of released ACTH vesicles beneath the plasma membrane as well. It is not clear up to now at which time the systemic switch from the non-genomic to the genomic pathway occurs *in vitro*, but this will be the goal for further studies in the future.

time		total population	+/-	total ACTH	+/-
[h]		[cells/ml]	[cells/ml]	[nM]	[nM]
92		154390	32039	14.391	0.660
	+10nMCRH(1min)	154390	32039	14.787	1.024
	+10nMCRH(15min)	154390	32039	15.124	0.677
	+10nMCRH(30min)	154390	32039	15.429	1.060
	+10nMCRH(1h)	154390	32039	15.532	0.608
	+10nMCRH(2h)	154390	32039	16.151	1.056
116	+10nMCRH(22h)	324219	19532	16.898	1.065
114		205163	35327	15.027	0.666
	+10nMCRH(1min)	205163	35327	15.167	0.467
	+10nMCRH(15min)	205163	35327	15.621	1.462
	+10nMCRH(30min)	205163	35327	15.683	0.561
	+10nMCRH(1h)	205163	35327	15.869	0.882
	+10nMCRH(2h)	205163	35327	17.152	1.110
136	+10nMCRH(22h)	425000	44375	18.090	0.763

Tab.5.6: ACTH response to CRH at different incubation times (after 92 h and 114 h, part I)

time		ACTH after CRH incubation	ACTH/cell	ACTH rate
[h]		[nM]	[nM.ml/cell]	[nM.ml.h/cell]
92		0		
	+10nMCRH(1min)	0.396	2.5638E-06	1.5383E-04
	+10nMCRH(15min)	0.733	2.1828E-06	8.7312E-06
	+10nMCRH(30min)	1.038	1.9769E-06	3.9537E-06
	+10nMCRH(1h)	1.141	6.6925E-07	6.6925E-07
	+10nMCRH(2h)	1.760	4.0052E-06	2.0026E-06
116	+10nMCRH(22h)	2.507	4.3993E-06	1.8330E-07
114		0		
	+10nMCRH(1min)	0.140	6.8184E-07	4.0910E-05
	+10nMCRH(15min)	0.595	2.2160E-06	8.8639E-06
	+10nMCRH(30min)	0.657	3.0218E-07	6.0435E-07
	+10nMCRH(1h)	0.843	9.0653E-07	9.0653E-07
	+10nMCRH(2h)	2.125	6.2527E-06	3.1264E-06
136	+10nMCRH(22h)	3.063	4.2663E-06	1.7776E-07

Tab.5.7: ACTH response to CRH at different incubation times (after 92 h and 114 h, part II)

A

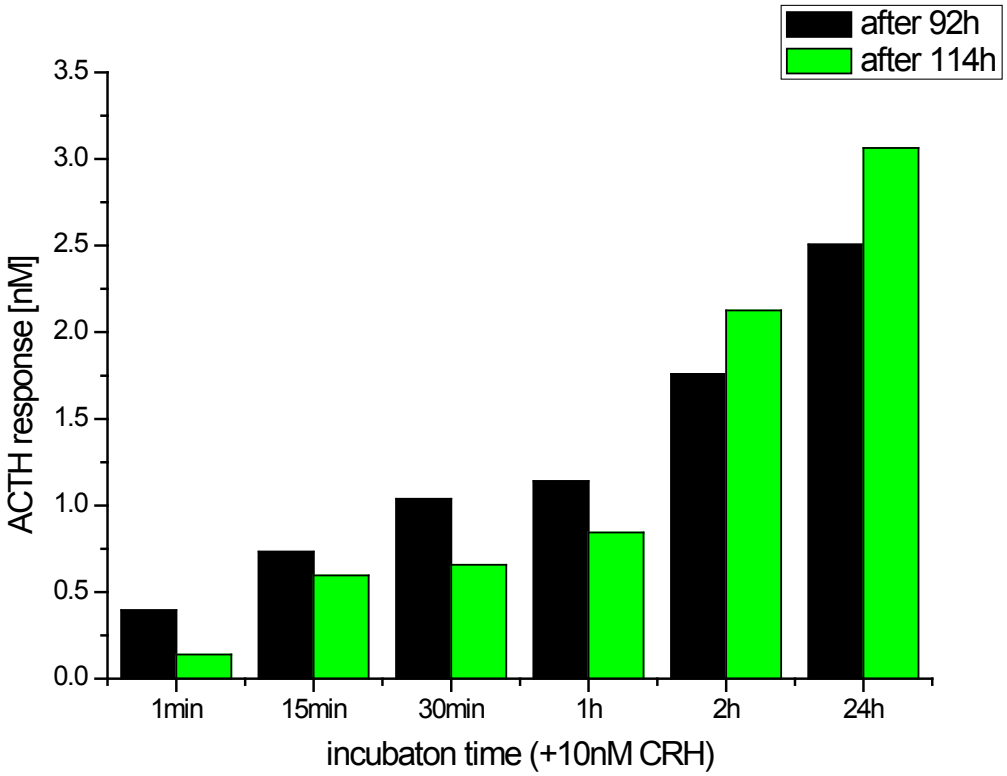

B

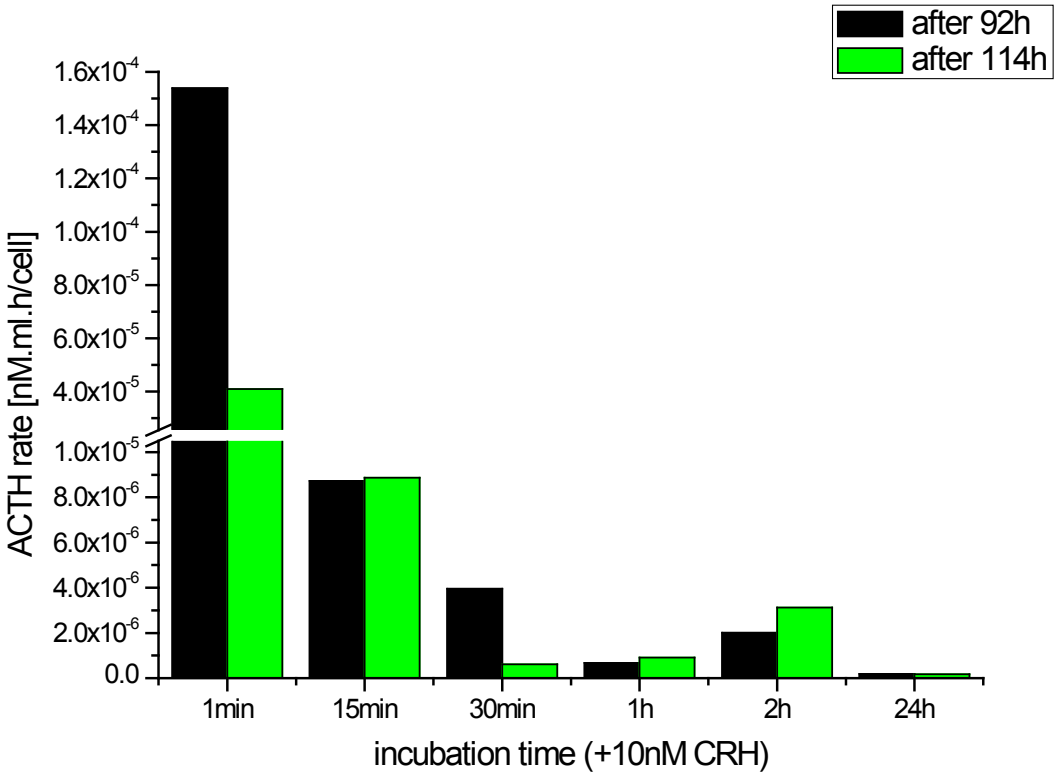

Fig. 5.6: Comparison of total ACTH response (A) and ACTH output rate (B) at two time windows

6 Appendix

6.1 Absorption spectra of the labelled antibody

λ	A	λ	A	λ	A	λ	A	λ	A
[nm]		[nm]		[nm]		[nm]		[nM]	
250	0.0539	**310**	0.0103	**370**	0.0013	**430**	0.0012	**490**	0.0107
252	0.0556	**312**	0.0092	**372**	0.0023	**432**	0.0012	**492**	0.0107
254	0.0549	**314**	0.0092	**374**	0.0029	**434**	0.0018	**494**	0.0105
256	0.0557	**316**	0.0082	**376**	0.0019	**436**	0.0011	**496**	0.0102
258	0.0569	**318**	0.0070	**378**	0.0029	**438**	0.0011	**498**	0.0100
260	0.0582	**320**	0.0069	**380**	0.0013	**440**	0.0010	**500**	0.0100
262	0.0581	**322**	0.0057	**382**	0.0002	**442**	0.0017	**502**	0.0090
264	0.0581	**324**	0.0078	**384**	0.0011	**444**	0.0017	**504**	0.0077
266	0.0600	**326**	0.0045	**386**	0.0001	**446**	0.0013	**506**	0.0065
268	0.0604	**328**	0.0030	**388**	0.0002	**448**	0.0017	**508**	0.0058
270	0.0600	**330**	0.0046	**390**	0.0004	**450**	0.0019	**510**	0.0046
272	0.0589	**332**	0.0040	**392**	0.0017	**452**	0.0019	**512**	0.0039
274	0.0571	**334**	0.0066	**394**	0.0014	**454**	0.0021	**514**	0.0028
276	0.0562	**336**	0.0043	**396**	0.0014	**456**	0.0023	**516**	0.0018
278	0.0539	**338**	0.0035	**398**	0.0030	**458**	0.0032	**518**	0.0013
280	0.0526	**340**	0.0032	**400**	0.0011	**460**	0.0031	**520**	0.0012
282	0.0502	**342**	0.0054	**402**	0.0005	**462**	0.0037	**522**	0.0008
284	0.0475	**344**	0.0036	**404**	0.0010	**464**	0.0039	**524**	0.0002
286	0.0426	**346**	0.0027	**406**	0.0014	**466**	0.0043	**526**	0
288	0.0388	**348**	0.0055	**408**	0.0017	**468**	0.0038	**528**	0
290	0.0363	**350**	0.0047	**410**	0.0012	**470**	0.0046	**530**	0.0001
292	0.0325	**352**	0.0037	**412**	0.0009	**472**	0.0061	**532**	0.0002
294	0.0296	**354**	0.0029	**414**	0.0006	**474**	0.0058	**534**	0.0002
296	0.0263	**356**	0.0029	**416**	0.0015	**476**	0.0058	**536**	0.0001
298	0.0214	**358**	0.0024	**418**	0.0018	**478**	0.0072	**538**	0
300	0.0197	**360**	0.0032	**420**	0.0010	**480**	0.0072	**540**	0.0001
302	0.0167	**362**	0.0033	**422**	0.0023	**482**	0.0083	**542**	0.0001
304	0.0155	**364**	0.0028	**424**	0.0012	**484**	0.0080	**544**	0
306	0.0135	**366**	0.0030	**426**	0.0019	**486**	0.0096	**546**	0.0002
308	0.0128	**368**	0.0018	**428**	0.0006	**488**	0.0103	**548**	0.0004

Tab.6.1: Absorption spectra of DyLight488

6.2 AtT-20 counts

Basically, all cell numbers were counted with a Bürker-Türk counting chamber (for further information see Fig. 4.5) and the total cell population was deduced from that counts following the formula in chapter 4.3. Each sample was incubated under the same conditions (37°C, 5% CO_2, 95% humidity) and prepared for cell counting in the same way (see chapter 4.2.4) to ensure reproducible and comparable results.

Incub. time	Cell counts per 16 squares										total polulation	+/-
[h]											[cells/ml]	[cells/ml]
22	2	2	0	1	2	2	1	0	1	1	16602	9156
	2	0	1	1	1	0						
40	1	1	2	1	1	1	1	1	1	3	24414	9766
	2	2	3	0	1	1	1	2	2	1		
	2	2	2	2	2	1	2	1	2	3		
	1	2										
67	4	3	7	5	4	2	6	3	4	6	67708	19098
	5	6	6	1	4	6	6	4	4	5		
	3	3	3	4								
92	7	9	7	7	8	7	10	13	12	9	154390	32039
	8	8	9	6	7	10	9	10	12	7		
	15	7	9	12	12	9	12	10	14	11		
	11	9	12	8	12	12	12	10	11	15		
	13	9	13	9	7	9	7	11	10	12		
	15	6	8	9	9	6	7	13	7	12		
	10	13	7	11	7	8	7	7	8	10		
	8	12	9	10	11	10	12	13	9	13		
	6	10	14	15								
102	8	12	9	16	13	14	9	15	14	11	200994	29701
	14	15	13	13	10	14	13	16	16	15		
	11	12										
114	13	14	14	9	13	16	14	16	11	13	205163	35327
	14	15	10	10	9	13	8	8	16	15		
	9	12	8	16	14	9	12	14	13	12		
	16	16	15	18	17	13	16	15	17	14		
	17	15	12	13	11	9						
126	14	14	9	11	15	12	12				194196	25511
138	12	11	14	9	12	8	11	13	9		171875	24305

Tab.6.2: Basal population of AtT-20 cells

Incub. time		Cell counts per 16 squares							total polulation	+/-
[h]									[cells/ml]	[cells/ml]
114	+ 5nM CRH (24h)	25	24	19	23	19	20	21	335938	27344
		20	24	21	20	22				
114	+ 10nM CRH (24h)	23	20	19	21				324219	19532
114	+ 36nM CRH (24h)	17	22	22		21	20	18	302084	28936
		15	19		20					
114	+ 54nM CRH (24h)	17	14	13	17	15			237500	22500
138	+ 10nM CRH (24h)	23	32	27	34	24	27	25	425000	44375
		28	29	23						
138	+ 10nM CRH (48h)	26	22	27	32	28	22	31	429688	50782
		32								

Tab.6.3: Effect of extracellular stress signals to the population of AtT-20 cells

6.3 2-component fits

For calculating the exact ACTH concentration the diffusion time of the first component was fixed to computationally eliminate the particle numbers of the unbound fluorescent antibodies (chapter 4.4.2). Subsequently the correction factor (CF_{FCS}) had to be taken into account for all ACTH concentrations obtained from computationally fits of FCS data.

Tab.6.4 summarizes the calculated ACTH concentrations obtained from the 2-component fits, which are listed on the following pages, and the actual concentration in consideration of the correction factor (CF_{FCS} ~ 1.58963).

time		c (ACTH) 2-comp fit	+/- 2-comp fit	c (ACTH) corrected	+/- corrected
[h]		[nM]	[nM]	[nM]	[nM]
20	Basal	3.931	0.234	**6.249**	0.372
40	Basal	7.079	0.435	**11.253**	0.691
65	Basal	8.608	0.608	**13.684**	0.967
92	Basal	9.053	0.415	**14.391**	0.660
114	Basal	9.453	0.419	**15.027**	0.666
138	basal	9.867	0.333	**15.685**	0.529
92	+ 10nM CRH (1min)	9.302	0.644	**14.787**	1.024
92	+ 10nM CRH (15min)	9.514	0.426	**15.124**	0.677
92	+ 10nM CRH (30min)	9.706	0.667	**15.429**	1.060
92	+ 10nM CRH (1h)	9.771	0.382	**15.532**	0.608
92	+ 10nM CRH (2h)	10.160	0.665	**16.151**	1.056
114	+ 10nM CRH (22h)	10.630	0.670	**16.898**	1.065
114	+ 10nM CRH (1min)	9.541	0.294	**15.167**	0.467
114	+ 10nM CRH (15min)	9.827	0.920	**15.621**	1.462
114	+ 10nM CRH (30min)	9.866	0.353	**15.683**	0.561
114	+ 10nM CRH (1h)	9.983	0.555	**15.869**	0.882
114	+ 10nM CRH (2h)	10.790	0.698	**17.152**	1.110
136	+ 10nM CRH (22h)	11.380	0.480	**18.090**	0.763
114	+5nMCRH(24h)	10.55	0.576	**16.771**	0.916
114	+10nMCRH(24h)	10.63	0.670	**16.898**	1.065
114	+36nMCRH(24h)	10.16	0.569	**16.151**	0.904
114	+54nMCRH(24h)	9.665	0.874	**15.364**	1.389

Tab.6.4: Summarized ACTH concentrations (including correction factor)

134

2fit	c_2	t_2	p_2	c_1	t_1	p_1	tauT	Triplet	chi^2
#	[M]	[s]		[M]	[s]		[s]		
5	4.003E-09	1.745E-03	0.532	2.464E-08	2.300E-04	3.275	7.400E-06	0.28	2.820E-03
6	3.760E-09	2.089E-03	0.499	2.504E-08	2.300E-04	3.328	7.400E-06	0.30	1.940E-03
7	3.778E-09	2.287E-03	0.502	2.412E-08	2.300E-04	3.206	8.100E-06	0.27	1.250E-03
8	3.914E-09	1.547E-03	0.520	2.521E-08	2.300E-04	3.350	8.400E-06	0.29	2.030E-03
10	3.833E-09	2.162E-03	0.509	2.421E-08	2.300E-04	3.218	7.000E-06	0.29	2.240E-03
11	3.729E-09	1.477E-03	0.496	2.438E-08	2.300E-04	3.240	7.900E-06	0.28	1.440E-03
12	3.971E-09	1.727E-03	0.528	2.435E-08	2.300E-04	3.236	8.800E-06	0.28	2.100E-03
14	3.366E-09	2.098E-03	0.447	2.439E-08	2.300E-04	3.242	7.000E-06	0.28	2.440E-03
16	3.560E-09	1.786E-03	0.473	2.435E-08	2.300E-04	3.235	6.500E-06	0.28	2.250E-03
17	4.434E-09	1.562E-03	0.589	2.462E-08	2.300E-04	3.272	9.700E-06	0.28	1.970E-03
18	3.388E-09	1.836E-03	0.450	2.588E-08	2.300E-04	3.439	7.700E-06	0.29	1.370E-03
21	3.391E-09	2.077E-03	0.451	2.484E-08	2.300E-04	3.300	7.900E-06	0.27	2.350E-03
23	3.637E-09	2.300E-03	0.483	2.486E-08	2.300E-04	3.304	6.500E-06	0.30	2.110E-03
27	4.309E-09	1.960E-03	0.573	2.368E-08	2.300E-04	3.147	7.400E-06	0.28	1.790E-03
29	3.739E-09	1.833E-03	0.497	2.630E-08	2.300E-04	3.495	9.000E-06	0.30	2.030E-03
33	4.154E-09	1.672E-03	0.552	2.352E-08	2.300E-04	3.125	8.100E-06	0.29	1.620E-03
34	4.488E-09	1.511E-03	0.596	2.479E-08	2.300E-04	3.295	9.000E-06	0.28	2.060E-03
36	4.396E-09	1.628E-03	0.584	2.433E-08	2.300E-04	3.234	8.100E-06	0.28	1.770E-03
38	3.799E-09	1.760E-03	0.505	2.537E-08	2.300E-04	3.372	7.100E-06	0.29	2.370E-03
40	4.030E-09	2.027E-03	0.536	2.415E-08	2.300E-04	3.209	7.500E-06	0.29	1.670E-03
41	3.667E-09	2.211E-03	0.487	2.561E-08	2.300E-04	3.404	7.900E-06	0.28	2.050E-03
46	3.998E-09	1.978E-03	0.531	2.481E-08	2.300E-04	3.297	7.400E-06	0.29	2.170E-03
47	4.249E-09	1.751E-03	0.565	2.307E-08	2.300E-04	3.065	7.400E-06	0.26	2.810E-03
48	4.339E-09	2.302E-03	0.577	2.417E-08	2.300E-04	3.212	9.400E-06	0.28	1.570E-03
49	4.364E-09	2.116E-03	0.580	2.413E-08	2.300E-04	3.207	7.300E-06	0.29	2.280E-03
50	4.005E-09	1.776E-03	0.532	2.353E-08	2.300E-04	3.127	7.300E-06	0.27	2.460E-03
51	3.686E-09	2.019E-03	0.490	2.518E-08	2.300E-04	3.346	7.200E-06	0.30	1.590E-03
52	4.155E-09	2.052E-03	0.552	2.391E-08	2.300E-04	3.177	7.900E-06	0.28	1.490E-03
53	3.743E-09	1.655E-03	0.498	2.438E-08	2.300E-04	3.239	7.800E-06	0.28	1.900E-03
54	3.848E-09	1.346E-03	0.511	2.545E-08	2.300E-04	3.382	8.900E-06	0.27	2.090E-03
55	4.146E-09	1.824E-03	0.551	2.450E-08	2.300E-04	3.256	7.800E-06	0.28	1.560E-03
56	4.002E-09	1.525E-03	0.532	2.417E-08	2.300E-04	3.212	8.900E-06	0.27	2.180E-03
57	4.038E-09	2.268E-03	0.537	2.489E-08	2.300E-04	3.307	7.700E-06	0.29	2.090E-03
58	3.795E-09	1.725E-03	0.505	2.445E-08	2.300E-04	3.249	8.100E-06	0.27	2.090E-03
59	3.792E-09	1.424E-03	0.504	2.457E-08	2.300E-04	3.266	9.000E-06	0.26	2.140E-03
$\bar{x}$	**3.931E-09**	1.840E-03	0.522						
$\bar{x} \pm$	**2.341E-10**	2.351E-04	0.031						

Tab.6.5: 2-component fit for calculating basal ACTH after 20 h

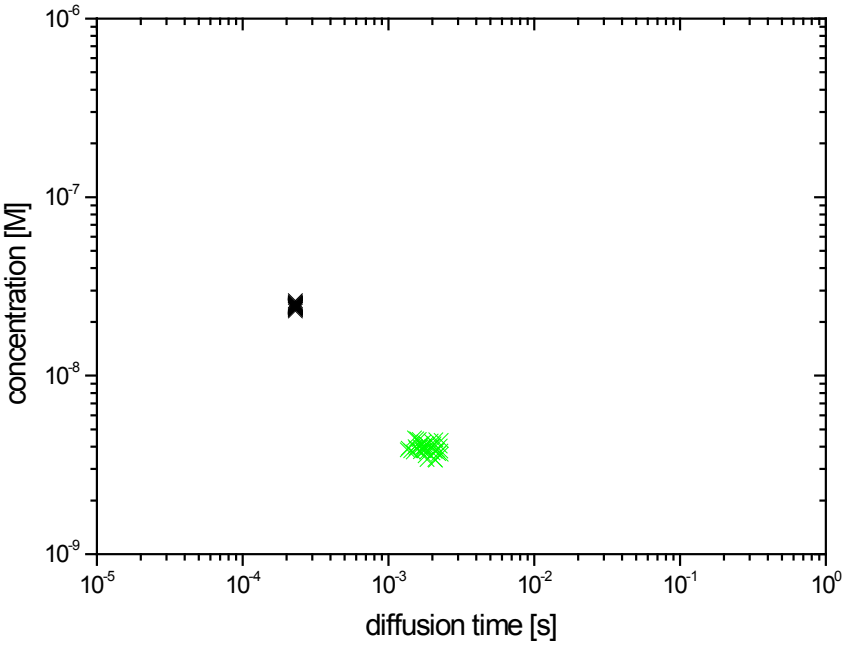

Fig. 6.1: Concdiff-plot of 2-component fit after 20 h total incubation time

2fit	c_2	t_2	p_2	c_1	t_1	p_1	tauT	Triplet	chi²
#	[M]	[s]		[M]	[s]		[s]		
3	6.769E-09	1.294E-03	0.899	2.122E-08	1.970E-04	2.820	6.200E-06	0.20	1.580E-03
11	7.488E-09	1.319E-03	0.995	2.115E-08	1.970E-04	2.811	6.300E-06	0.20	1.200E-03
12	7.791E-09	9.796E-04	1.035	2.001E-08	1.970E-04	2.659	6.100E-06	0.21	1.690E-03
14	7.505E-09	1.327E-03	0.997	2.020E-08	1.970E-04	2.684	6.400E-06	0.20	1.060E-03
16	7.748E-09	1.111E-03	1.030	1.943E-08	1.970E-04	2.582	5.500E-06	0.21	1.820E-03
25	6.735E-09	1.184E-03	0.895	2.134E-08	1.970E-04	2.836	6.700E-06	0.19	8.710E-04
27	7.511E-09	1.043E-03	0.998	2.012E-08	1.970E-04	2.673	6.300E-06	0.20	1.110E-03
31	6.946E-09	1.325E-03	0.923	2.114E-08	1.970E-04	2.809	5.300E-06	0.22	1.340E-03
32	7.768E-09	1.051E-03	1.032	2.070E-08	1.970E-04	2.751	6.900E-06	0.21	1.250E-03
33	7.088E-09	1.345E-03	0.942	2.090E-08	1.970E-04	2.777	5.100E-06	0.23	1.370E-03
34	7.979E-09	1.028E-03	1.060	2.031E-08	1.970E-04	2.699	6.400E-06	0.22	1.260E-03
36	7.038E-09	1.219E-03	0.935	2.092E-08	1.970E-04	2.779	5.200E-06	0.22	1.100E-03
41	7.390E-09	1.006E-03	0.982	2.000E-08	1.970E-04	2.658	4.700E-06	0.23	1.190E-03
45	6.816E-09	9.811E-04	0.906	2.072E-08	1.970E-04	2.754	4.800E-06	0.21	1.350E-03
47	7.628E-09	1.276E-03	1.014	2.080E-08	1.970E-04	2.764	5.800E-06	0.21	1.360E-03
55	6.299E-09	1.194E-03	0.837	2.083E-08	1.970E-04	2.768	4.400E-06	0.21	1.520E-03
59	7.722E-09	1.110E-03	1.026	1.990E-08	1.970E-04	2.644	6.800E-06	0.20	1.430E-03
60	7.562E-09	1.028E-03	1.005	2.021E-08	1.970E-04	2.686	6.500E-06	0.20	1.540E-03
61	7.999E-09	1.042E-03	1.063	1.917E-08	1.970E-04	2.547	6.400E-06	0.19	1.250E-03
63	7.758E-09	8.781E-04	1.031	1.997E-08	1.970E-04	2.654	4.800E-06	0.22	1.560E-03

119

65	8.066E-09	9.614E-04	1.072	1.910E-08	1.970E-04	2.539	5.000E-06	0.21	1.320E-03
67	7.930E-09	9.197E-04	1.054	1.962E-08	1.970E-04	2.607	5.500E-06	0.20	1.360E-03
76	7.724E-09	1.083E-03	1.026	2.040E-08	1.970E-04	2.711	5.800E-06	0.23	1.100E-03
80	7.206E-09	1.483E-03	0.958	2.168E-08	1.970E-04	2.881	6.400E-06	0.22	1.010E-03
81	7.610E-09	1.256E-03	1.011	2.124E-08	1.970E-04	2.823	6.100E-06	0.23	1.100E-03
82	6.541E-09	1.708E-03	0.869	2.183E-08	1.970E-04	2.901	5.100E-06	0.23	2.050E-03
83	6.444E-09	1.562E-03	0.856	2.162E-08	1.970E-04	2.873	5.800E-06	0.22	9.690E-04
84	7.248E-09	1.034E-03	0.963	2.076E-08	1.970E-04	2.759	5.100E-06	0.22	1.420E-03
87	7.910E-09	1.114E-03	1.051	1.957E-08	1.970E-04	2.600	6.500E-06	0.21	1.310E-03
89	6.511E-09	1.668E-03	0.865	2.116E-08	1.970E-04	2.812	4.700E-06	0.22	1.570E-03
90	7.009E-09	1.143E-03	0.931	2.195E-08	1.970E-04	2.917	6.700E-06	0.22	1.410E-03
93	7.814E-09	1.018E-03	1.038	1.962E-08	1.970E-04	2.607	5.400E-06	0.22	2.390E-03
95	6.062E-09	1.474E-03	0.806	2.183E-08	1.970E-04	2.901	5.000E-06	0.21	1.380E-03
96	7.070E-09	1.308E-03	0.939	2.122E-08	1.970E-04	2.820	5.600E-06	0.21	1.050E-03
99	6.153E-09	1.225E-03	0.818	2.288E-08	1.970E-04	3.040	4.500E-06	0.23	9.810E-04
100	6.588E-09	1.110E-03	0.875	2.225E-08	1.970E-04	2.957	5.900E-06	0.23	1.250E-03
101	6.554E-09	1.144E-03	0.871	2.181E-08	1.970E-04	2.898	6.100E-06	0.21	1.340E-03
102	6.647E-09	1.096E-03	0.883	2.320E-08	1.970E-04	3.083	5.100E-06	0.24	1.170E-03
104	6.801E-09	1.295E-03	0.904	2.060E-08	1.970E-04	2.738	5.900E-06	0.20	1.430E-03
105	6.326E-09	1.173E-03	0.841	2.236E-08	1.970E-04	2.971	5.900E-06	0.21	1.000E-03
106	6.353E-09	1.509E-03	0.844	2.292E-08	1.970E-04	3.046	5.800E-06	0.21	1.300E-03
109	7.237E-09	1.244E-03	0.962	2.141E-08	1.970E-04	2.845	5.800E-06	0.23	1.570E-03
110	7.340E-09	1.069E-03	0.975	2.154E-08	1.970E-04	2.863	6.300E-06	0.21	1.050E-03
111	7.320E-09	1.243E-03	0.973	2.063E-08	1.970E-04	2.741	5.600E-06	0.23	1.480E-03
112	7.593E-09	1.318E-03	1.009	2.154E-08	1.970E-04	2.862	6.500E-06	0.22	1.270E-03
119	6.749E-09	1.529E-03	0.897	2.212E-08	1.970E-04	2.940	6.000E-06	0.22	1.240E-03
120	7.513E-09	1.203E-03	0.998	2.108E-08	1.970E-04	2.802	6.800E-06	0.21	1.050E-03
124	7.523E-09	1.148E-03	0.999	2.169E-08	1.970E-04	2.882	6.400E-06	0.23	1.380E-03
125	6.601E-09	1.303E-03	0.877	2.101E-08	1.970E-04	2.792	4.700E-06	0.22	1.690E-03
126	6.162E-09	1.684E-03	0.819	2.304E-08	1.970E-04	3.061	6.900E-06	0.21	1.150E-03
128	7.336E-09	1.133E-03	0.975	2.172E-08	1.970E-04	2.886	6.900E-06	0.21	1.120E-03
132	6.453E-09	1.217E-03	0.857	2.193E-08	1.970E-04	2.915	5.900E-06	0.22	1.150E-03
133	7.205E-09	1.197E-03	0.958	2.136E-08	1.970E-04	2.839	6.600E-06	0.21	1.310E-03
136	6.271E-09	1.436E-03	0.833	2.217E-08	1.970E-04	2.946	5.600E-06	0.22	1.540E-03
137	7.151E-09	1.359E-03	0.950	2.084E-08	1.970E-04	2.770	5.100E-06	0.22	1.630E-03
138	6.265E-09	1.512E-03	0.832	2.227E-08	1.970E-04	2.959	6.000E-06	0.22	1.090E-03
142	6.673E-09	1.390E-03	0.887	2.191E-08	1.970E-04	2.911	5.900E-06	0.20	1.570E-03
145	6.945E-09	1.158E-03	0.923	2.124E-08	1.970E-04	2.823	4.800E-06	0.23	2.020E-03
146	6.111E-09	1.274E-03	0.812	2.250E-08	1.970E-04	2.990	5.100E-06	0.22	1.630E-03
149	6.224E-09	1.515E-03	0.827	2.310E-08	1.970E-04	3.070	6.600E-06	0.21	9.090E-04
153	6.466E-09	1.239E-03	0.859	2.206E-08	1.970E-04	2.932	5.400E-06	0.22	1.100E-03

	154	6.798E-09	1.322E-03	0.903	2.194E-08	1.970E-04	2.916	5.200E-06	0.23	1.740E-03
122	2	6.858E-09	1.020E-03	0.911	1.950E-08	2.060E-04	2.591	5.000E-06	0.18	2.260E-03
	5	6.970E-09	9.817E-04	0.926	1.994E-08	2.060E-04	2.650	6.300E-06	0.18	1.420E-03
	6	6.686E-09	1.161E-03	0.889	2.058E-08	2.060E-04	2.735	3.700E-06	0.23	3.170E-03
	11	7.354E-09	1.162E-03	0.977	1.845E-08	2.060E-04	2.451	5.900E-06	0.19	1.660E-03
	12	6.962E-09	1.180E-03	0.925	1.980E-08	2.060E-04	2.632	5.900E-06	0.18	1.770E-03
	14	7.302E-09	1.088E-03	0.970	1.825E-08	2.060E-04	2.426	5.600E-06	0.18	1.950E-03
	17	7.126E-09	1.130E-03	0.947	1.985E-08	2.060E-04	2.638	7.200E-06	0.19	2.110E-03
	21	7.454E-09	1.193E-03	0.991	1.978E-08	2.060E-04	2.628	5.900E-06	0.19	2.070E-03
	22	7.436E-09	1.194E-03	0.988	1.951E-08	2.060E-04	2.593	4.700E-06	0.20	1.710E-03
	33	7.065E-09	1.154E-03	0.939	2.048E-08	2.060E-04	2.722	7.000E-06	0.18	1.650E-03
	35	7.138E-09	1.035E-03	0.949	2.036E-08	2.060E-04	2.706	5.000E-06	0.21	2.590E-03
	36	6.913E-09	1.249E-03	0.919	1.970E-08	2.060E-04	2.618	5.700E-06	0.20	1.800E-03
	46	6.941E-09	1.154E-03	0.922	1.987E-08	2.060E-04	2.640	5.500E-06	0.20	2.050E-03
	48	6.794E-09	1.319E-03	0.903	1.897E-08	2.060E-04	2.521	5.400E-06	0.19	1.800E-03
	50	6.997E-09	1.174E-03	0.930	1.950E-08	2.060E-04	2.591	5.800E-06	0.18	1.720E-03
	51	7.576E-09	1.272E-03	1.007	1.929E-08	2.060E-04	2.563	7.200E-06	0.18	1.820E-03
	54	7.043E-09	1.185E-03	0.936	2.047E-08	2.060E-04	2.720	5.100E-06	0.20	1.550E-03
	59	7.097E-09	1.385E-03	0.943	2.008E-08	2.060E-04	2.669	7.100E-06	0.19	1.170E-03
	60	7.613E-09	1.261E-03	1.012	1.947E-08	2.060E-04	2.587	6.600E-06	0.19	1.100E-03
	$\bar{x}$	**7.079E-09**	1.220E-03	0.941						
	$\bar{x}$ ±	**4.349E-10**	1.365E-04	0.058						

Tab.6.6: 2-component fit for calculating basal ACTH after 40 h

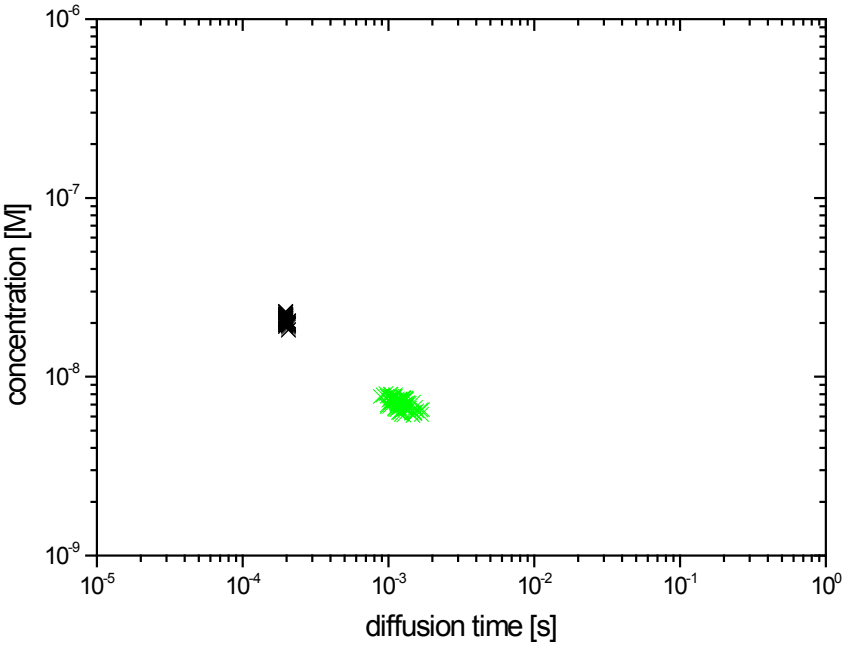

Fig. 6.2: Concdiff-plot of 2-component fit after 40 h total incubation time

	2fit	c_2	t_2	p_2	c_1	t_1	p_1	tauT	Triplet	chi²
144	#	[M]	[s]		[M]	[s]		[s]		
	2	9.281E-09	1.432E-03	1.233	1.876E-08	2.290E-04	2.493	5.300E-06	0.17	1.490E-03
	3	9.313E-09	9.602E-04	1.238	1.998E-08	2.290E-04	2.655	5.600E-06	0.17	1.810E-03
	5	9.515E-09	9.703E-04	1.265	1.798E-08	2.290E-04	2.389	5.500E-06	0.17	2.080E-03
	7	8.268E-09	1.358E-03	1.099	1.926E-08	2.290E-04	2.560	4.200E-06	0.17	1.190E-03
	9	9.278E-09	1.144E-03	1.233	1.752E-08	2.290E-04	2.328	4.300E-06	0.19	1.260E-03
	14	8.600E-09	1.084E-03	1.143	1.924E-08	2.290E-04	2.557	6.700E-06	0.15	1.060E-03
	15	9.092E-09	1.093E-03	1.208	1.749E-08	2.290E-04	2.324	3.400E-06	0.18	1.570E-03
	18	7.582E-09	1.274E-03	1.008	1.923E-08	2.290E-04	2.556	3.600E-06	0.19	1.590E-03
	19	7.995E-09	1.062E-03	1.062	1.922E-08	2.290E-04	2.554	3.900E-06	0.17	1.260E-03
	20	9.823E-09	9.843E-04	1.305	1.700E-08	2.290E-04	2.260	4.900E-06	0.18	1.460E-03
	25	7.781E-09	1.246E-03	1.034	1.910E-08	2.290E-04	2.538	5.000E-06	0.17	1.160E-03
	26	7.541E-09	1.284E-03	1.002	1.862E-08	2.290E-04	2.474	4.700E-06	0.15	1.590E-03
	30	8.658E-09	1.047E-03	1.151	1.873E-08	2.290E-04	2.489	5.000E-06	0.15	2.330E-03
	31	9.244E-09	1.184E-03	1.228	1.756E-08	2.290E-04	2.334	6.200E-06	0.17	1.170E-03
	38	9.084E-09	9.617E-04	1.207	1.694E-08	2.290E-04	2.251	5.300E-06	0.15	2.080E-03
	40	8.201E-09	1.206E-03	1.090	1.807E-08	2.290E-04	2.401	5.900E-06	0.16	1.860E-03
	42	9.015E-09	1.268E-03	1.198	1.856E-08	2.290E-04	2.467	5.300E-06	0.17	1.530E-03
	43	9.792E-09	8.690E-04	1.301	1.797E-08	2.290E-04	2.388	6.400E-06	0.16	1.290E-03
	45	7.906E-09	9.831E-04	1.051	1.871E-08	2.290E-04	2.487	4.000E-06	0.16	1.030E-03
	47	9.150E-09	1.015E-03	1.216	1.844E-08	2.290E-04	2.450	5.300E-06	0.17	1.460E-03
	49	8.906E-09	9.489E-04	1.184	1.755E-08	2.290E-04	2.333	5.000E-06	0.17	1.620E-03
	51	8.041E-09	1.150E-03	1.069	1.882E-08	2.290E-04	2.501	5.200E-06	0.16	1.720E-03
	56	8.385E-09	1.176E-03	1.114	1.757E-08	2.290E-04	2.335	5.000E-06	0.16	1.650E-03
	58	8.284E-09	1.194E-03	1.101	1.874E-08	2.290E-04	2.491	4.400E-06	0.17	2.160E-03
146	1	8.524E-09	1.107E-03	1.133	1.930E-08	2.290E-04	2.565	3.500E-06	0.20	1.430E-03
	3	9.259E-09	1.180E-03	1.230	1.892E-08	2.290E-04	2.515	4.800E-06	0.18	2.260E-03
	5	7.885E-09	1.423E-03	1.048	1.978E-08	2.290E-04	2.629	3.900E-06	0.19	1.380E-03
	6	8.125E-09	1.249E-03	1.080	1.961E-08	2.290E-04	2.606	4.300E-06	0.17	1.800E-03
	11	7.016E-09	1.310E-03	0.932	2.052E-08	2.290E-04	2.727	4.300E-06	0.16	1.800E-03
	13	8.829E-09	1.116E-03	1.173	1.896E-08	2.290E-04	2.519	5.100E-06	0.17	1.850E-03
	18	8.528E-09	1.047E-03	1.133	2.010E-08	2.290E-04	2.671	5.600E-06	0.16	2.340E-03
	20	8.899E-09	1.172E-03	1.183	1.907E-08	2.290E-04	2.534	6.200E-06	0.19	2.360E-03
	22	8.381E-09	1.206E-03	1.114	1.965E-08	2.290E-04	2.611	4.300E-06	0.18	1.920E-03
	23	9.478E-09	9.721E-04	1.260	1.898E-08	2.290E-04	2.523	6.000E-06	0.18	1.570E-03
	25	9.223E-09	9.822E-04	1.226	1.856E-08	2.290E-04	2.467	3.900E-06	0.18	1.590E-03
	28	9.854E-09	9.405E-04	1.309	1.828E-08	2.290E-04	2.429	5.600E-06	0.16	1.640E-03
	29	8.156E-09	1.257E-03	1.084	2.069E-08	2.290E-04	2.750	5.900E-06	0.16	1.890E-03
	30	8.176E-09	1.312E-03	1.086	1.984E-08	2.290E-04	2.637	5.800E-06	0.17	1.640E-03
	31	8.916E-09	1.301E-03	1.185	1.942E-08	2.290E-04	2.581	5.900E-06	0.17	1.950E-03

32	8.227E-09	1.253E-03	1.093	2.061E-08	2.290E-04	2.739	7.800E-06	0.16	2.300E-03
34	9.101E-09	1.106E-03	1.209	1.947E-08	2.290E-04	2.588	6.300E-06	0.19	1.320E-03
35	7.662E-09	1.396E-03	1.018	1.976E-08	2.290E-04	2.626	4.300E-06	0.19	1.860E-03
36	9.662E-09	9.532E-04	1.284	1.984E-08	2.290E-04	2.637	6.400E-06	0.18	1.410E-03
37	7.538E-09	1.276E-03	1.002	2.060E-08	2.290E-04	2.738	5.300E-06	0.16	1.780E-03
38	9.421E-09	1.012E-03	1.252	1.836E-08	2.290E-04	2.441	5.100E-06	0.16	1.430E-03
41	7.871E-09	1.365E-03	1.046	2.046E-08	2.290E-04	2.718	5.000E-06	0.17	1.490E-03
43	8.066E-09	1.004E-03	1.072	2.081E-08	2.290E-04	2.766	4.100E-06	0.18	1.060E-03
45	9.369E-09	8.927E-04	1.245	1.895E-08	2.290E-04	2.518	5.300E-06	0.17	2.060E-03
47	7.639E-09	1.511E-03	1.015	1.950E-08	2.290E-04	2.592	5.500E-06	0.16	3.130E-03
48	8.326E-09	1.178E-03	1.106	1.889E-08	2.290E-04	2.510	4.100E-06	0.16	1.880E-03
49	7.872E-09	1.274E-03	1.046	2.004E-08	2.290E-04	2.664	6.300E-06	0.17	1.360E-03
51	9.629E-09	1.193E-03	1.280	1.875E-08	2.290E-04	2.491	6.600E-06	0.17	1.380E-03
52	8.443E-09	1.182E-03	1.122	2.063E-08	2.290E-04	2.742	6.600E-06	0.17	1.200E-03
55	8.963E-09	1.148E-03	1.191	1.826E-08	2.290E-04	2.427	4.700E-06	0.16	2.120E-03
56	9.065E-09	9.469E-04	1.205	1.849E-08	2.290E-04	2.457	7.300E-06	0.15	1.430E-03
57	8.386E-09	1.141E-03	1.114	1.932E-08	2.290E-04	2.567	4.700E-06	0.18	1.970E-03
59	7.192E-09	1.576E-03	0.956	2.080E-08	2.290E-04	2.764	4.700E-06	0.15	1.340E-03
60	8.834E-09	1.302E-03	1.174	1.938E-08	2.290E-04	2.575	6.400E-06	0.16	1.450E-03
$\bar{x}$	**8.608E-09**	1.158E-03	1.144						
$\bar{x} \pm$	**6.081E-10**	1.307E-04	0.081						

Tab.6.7: 2-component fit for calculating basal ACTH after 65 h

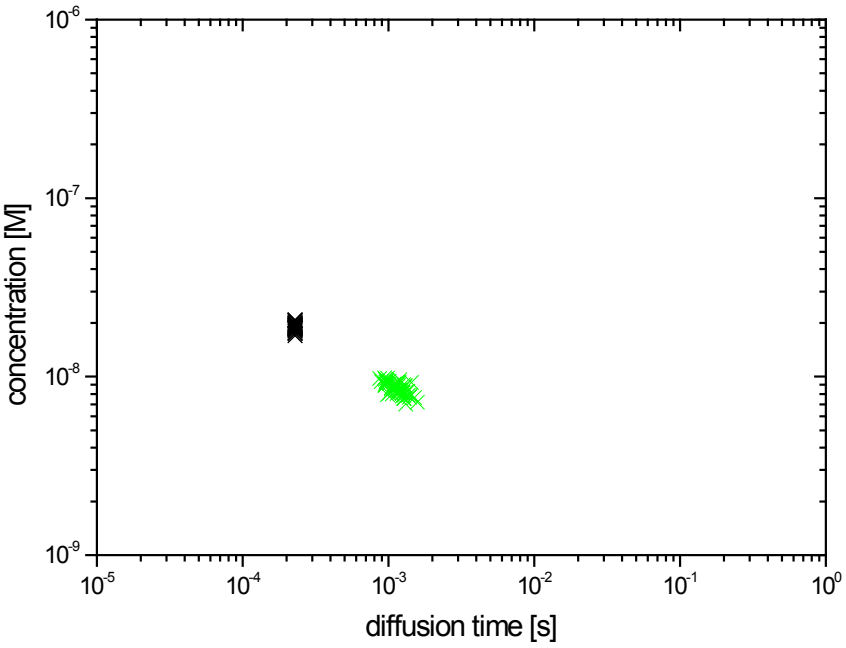

Fig. 6.3: Concdiff-plot of 2-component fit after 65 h total incubation time

	2fit	c_2	t_2	p_2	c_1	t_1	p_1	tauT	Triplet	chi^2
149	#	[M]	[s]		[M]	[s]		[s]		
	1	9.104E-09	8.932E-04	1.210	1.800E-08	2.130E-04	2.391	5.100E-06	0.16	2.330E-03
	4	8.339E-09	1.047E-03	1.108	1.690E-08	2.130E-04	2.246	3.700E-06	0.21	2.350E-03
	5	8.714E-09	1.098E-03	1.158	1.693E-08	2.130E-04	2.250	7.500E-06	0.17	1.800E-03
	8	8.070E-09	1.167E-03	1.072	1.746E-08	2.130E-04	2.321	6.000E-06	0.18	2.880E-03
	9	1.014E-08	1.043E-03	1.347	1.544E-08	2.130E-04	2.052	9.100E-06	0.17	1.710E-03
	10	9.313E-09	9.445E-04	1.238	1.572E-08	2.130E-04	2.089	4.900E-06	0.19	1.770E-03
	11	9.220E-09	8.186E-04	1.225	1.569E-08	2.130E-04	2.085	4.400E-06	0.19	2.920E-03
	12	9.888E-09	8.579E-04	1.314	1.559E-08	2.130E-04	2.072	4.600E-06	0.20	3.340E-03
	17	9.492E-09	8.664E-04	1.261	1.575E-08	2.130E-04	2.093	4.600E-06	0.18	1.550E-03
	19	9.509E-09	8.351E-04	1.264	1.624E-08	2.130E-04	2.159	5.700E-06	0.18	2.050E-03
	21	8.723E-09	9.681E-04	1.159	1.647E-08	2.130E-04	2.188	5.800E-06	0.17	3.010E-03
	24	9.792E-09	9.877E-04	1.301	1.553E-08	2.130E-04	2.064	8.500E-06	0.15	1.270E-03
	25	8.069E-09	9.966E-04	1.072	1.726E-08	2.130E-04	2.293	3.300E-06	0.19	2.050E-03
	26	9.417E-09	9.117E-04	1.251	1.575E-08	2.130E-04	2.093	7.100E-06	0.17	1.750E-03
	28	9.287E-09	9.313E-04	1.234	1.570E-08	2.130E-04	2.086	5.800E-06	0.18	1.620E-03
	36	9.062E-09	8.000E-04	1.204	1.721E-08	2.130E-04	2.287	7.200E-06	0.15	2.690E-03
	37	8.485E-09	1.028E-03	1.128	1.591E-08	2.130E-04	2.114	4.400E-06	0.18	3.630E-03
186	1	9.265E-09	1.295E-03	1.231	2.415E-08	2.310E-04	3.209	6.500E-06	0.16	1.190E-03
	2	8.908E-09	1.410E-03	1.184	2.253E-08	2.310E-04	2.994	5.100E-06	0.19	1.320E-03
	3	8.551E-09	1.303E-03	1.136	2.316E-08	2.310E-04	3.077	4.400E-06	0.21	1.870E-03
	6	9.322E-09	1.221E-03	1.239	2.194E-08	2.310E-04	2.916	7.500E-06	0.16	1.590E-03
	7	8.683E-09	1.093E-03	1.154	2.280E-08	2.310E-04	3.029	6.300E-06	0.18	1.810E-03
	8	9.009E-09	1.335E-03	1.197	2.188E-08	2.310E-04	2.908	8.400E-06	0.17	1.970E-03
	10	9.892E-09	9.819E-04	1.315	2.219E-08	2.310E-04	2.948	7.700E-06	0.18	2.700E-03
	14	8.981E-09	1.110E-03	1.193	2.231E-08	2.310E-04	2.965	5.100E-06	0.19	1.420E-03
	17	9.445E-09	1.118E-03	1.255	2.141E-08	2.310E-04	2.845	8.900E-06	0.17	1.240E-03
	18	8.266E-09	1.476E-03	1.099	2.378E-08	2.310E-04	3.160	4.900E-06	0.19	3.390E-03
	23	8.243E-09	1.353E-03	1.095	2.213E-08	2.310E-04	2.940	6.100E-06	0.16	2.840E-03
	26	9.086E-09	1.320E-03	1.207	2.179E-08	2.310E-04	2.896	5.300E-06	0.19	2.070E-03
	28	9.095E-09	1.088E-03	1.209	2.182E-08	2.310E-04	2.899	5.600E-06	0.18	2.260E-03
	30	8.985E-09	1.024E-03	1.194	2.136E-08	2.310E-04	2.838	6.600E-06	0.17	1.570E-03
	31	9.102E-09	1.236E-03	1.210	2.095E-08	2.310E-04	2.784	6.700E-06	0.16	1.990E-03
	33	9.454E-09	1.223E-03	1.256	2.139E-08	2.310E-04	2.843	6.700E-06	0.17	1.740E-03
	36	9.443E-09	8.606E-04	1.255	2.191E-08	2.310E-04	2.912	6.300E-06	0.18	1.750E-03
	37	8.515E-09	1.322E-03	1.132	2.271E-08	2.310E-04	3.018	6.700E-06	0.18	1.650E-03
	$\bar{x}$	**9.053E-09**	1.085E-03	1.203						
	$\bar{x} \pm$	**4.149E-10**	1.559E-04	0.055						

Tab.6.8: 2-component fit for calculating basal ACTH after 92 h

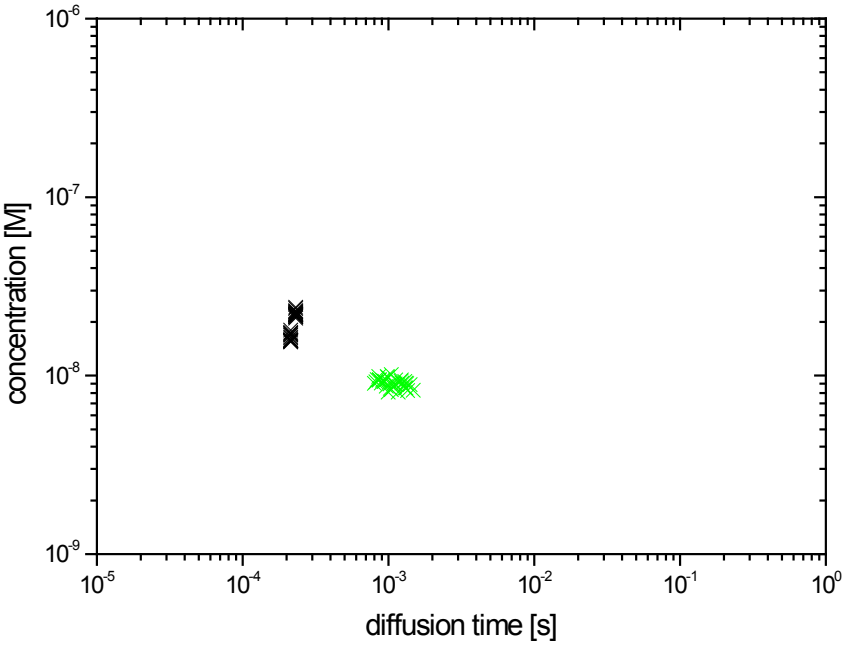

Fig. 6.4: Concdiff-plot of 2-component fit after 92 h total incubation time

	2fit	c_2	t_2	p_2	c_1	t_1	p_1	tauT	Triplet	chi²
162	#	[M]	[s]		[M]	[s]		[s]		
	4	9.786E-09	1.106E-03	1.300	2.074E-08	2.140E-04	2.756	7.600E-06	0.16	2.040E-03
	5	9.455E-09	1.164E-03	1.256	1.972E-08	2.140E-04	2.621	6.400E-06	0.16	1.800E-03
	7	9.774E-09	1.184E-03	1.299	1.923E-08	2.140E-04	2.556	6.900E-06	0.17	1.450E-03
	14	9.100E-09	1.271E-03	1.209	2.366E-08	2.140E-04	3.144	3.400E-06	0.2	1.530E-03
	16	9.725E-09	1.037E-03	1.292	2.290E-08	2.140E-04	3.043	2.100E-06	0.24	2.000E-03
	17	9.106E-09	1.022E-03	1.210	2.006E-08	2.140E-04	2.665	4.100E-06	0.18	2.630E-03
	20	9.571E-09	1.355E-03	1.272	1.943E-08	2.140E-04	2.582	6.300E-06	0.16	1.730E-03
	21	9.342E-09	1.583E-03	1.241	2.345E-08	2.140E-04	3.116	3.100E-06	0.2	1.480E-03
	23	9.457E-09	1.295E-03	1.257	2.388E-08	2.140E-04	3.174	4.700E-06	0.15	1.660E-03
	24	9.354E-09	1.167E-03	1.243	2.457E-08	2.140E-04	3.266	5.100E-06	0.17	1.180E-03
	27	9.105E-09	1.088E-03	1.210	1.935E-08	2.140E-04	2.572	4.200E-06	0.19	2.340E-03
	32	9.361E-09	1.424E-03	1.244	2.476E-08	2.140E-04	3.290	6.200E-06	0.14	2.570E-03
	33	9.555E-09	1.200E-03	1.270	2.373E-08	2.140E-04	3.154	4.200E-06	0.18	2.400E-03
	37	9.402E-09	1.104E-03	1.249	2.534E-08	2.140E-04	3.367	4.500E-06	0.18	1.380E-03
203	4	1.017E-08	9.799E-04	1.351	1.723E-08	2.140E-04	2.289	4.900E-06	0.16	2.000E-03
	5	9.075E-09	1.125E-03	1.206	1.855E-08	2.140E-04	2.465	5.200E-06	0.19	3.600E-03
	8	9.573E-09	1.109E-03	1.272	1.733E-08	2.140E-04	2.303	6.400E-06	0.14	2.730E-03
	10	9.882E-09	1.116E-03	1.313	1.710E-08	2.140E-04	2.272	4.700E-06	0.18	2.800E-03
	14	9.182E-09	1.178E-03	1.220	1.775E-08	2.140E-04	2.359	7.900E-06	0.14	2.040E-03
	18	8.772E-09	1.013E-03	1.166	1.853E-08	2.140E-04	2.462	4.500E-06	0.17	2.180E-03

20	1.011E-08	9.335E-04	1.343	1.649E-08	2.140E-04	2.191	5.800E-06	0.16	2.010E-03
21	9.254E-09	1.086E-03	1.230	1.765E-08	2.140E-04	2.346	3.700E-06	0.19	3.060E-03
23	9.034E-09	1.118E-03	1.201	1.831E-08	2.140E-04	2.434	6.100E-06	0.16	2.120E-03
28	9.067E-09	1.136E-03	1.205	1.772E-08	2.140E-04	2.355	5.300E-06	0.17	2.130E-03
30	9.554E-09	1.109E-03	1.270	1.660E-08	2.140E-04	2.206	3.000E-06	0.19	2.840E-03
36	1.015E-08	1.037E-03	1.349	1.582E-08	2.140E-04	2.103	4.400E-06	0.19	2.270E-03
38	9.064E-09	1.062E-03	1.204	1.828E-08	2.140E-04	2.429	5.400E-06	0.17	2.530E-03
$\bar{x}$	**9.453E-09**	1.148E-03	1.255						
$\bar{x} \pm$	**4.185E-10**	9.916E-05	0.039						

Tab.6.9: 2-component fit for calculating basal ACTH after 114 h

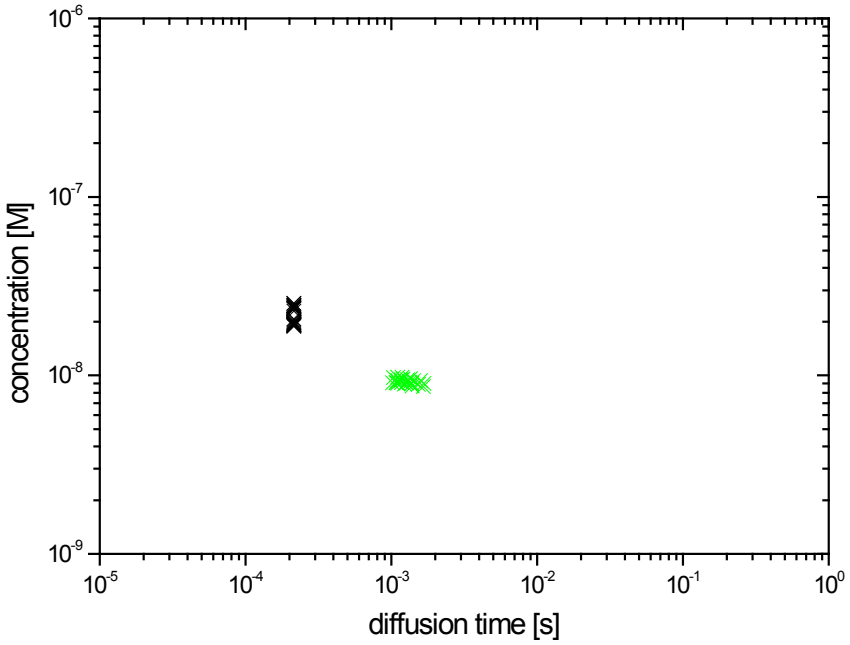

Fig. 6.5: Concdiff-plot of 2-component fit after 114 h total incubation time

173	2fit	c_2	t_2	p_2	c_1	t_1	p_1	tauT	Triplet	chi²
	#	[M]	[s]		[M]	[s]		[s]		
	9	9.927E-09	1.021E-03	1.319	2.052E-08	2.370E-04	2.727	4.000E-06	0.17	2.140E-03
	10	9.955E-09	1.213E-03	1.323	2.312E-08	2.370E-04	3.072	6.400E-06	0.19	2.140E-03
	13	9.627E-09	1.535E-03	1.279	2.063E-08	2.370E-04	2.741	5.900E-06	0.16	1.780E-03
	14	9.439E-09	1.417E-03	1.254	2.355E-08	2.370E-04	3.129	1.000E-05	0.16	2.450E-03
	18	1.006E-08	1.128E-03	1.337	2.154E-08	2.370E-04	2.862	6.200E-06	0.14	1.720E-03
	18	1.006E-08	1.128E-03	1.337	2.154E-08	2.370E-04	2.862	6.200E-06	0.14	1.720E-03
	21	9.688E-09	1.249E-03	1.287	2.308E-08	2.370E-04	3.067	1.000E-05	0.15	1.860E-03
	22	9.338E-09	1.428E-03	1.241	2.359E-08	2.370E-04	3.135	6.200E-06	0.16	1.740E-03

	23	1.001E-08	1.201E-03	1.330	2.116E-08	2.370E-04	2.812	4.200E-06	0.18	1.890E-03
	23	1.001E-08	1.201E-03	1.330	2.116E-08	2.370E-04	2.812	4.200E-06	0.18	1.890E-03
	24	9.696E-09	9.992E-04	1.289	2.121E-08	2.370E-04	2.819	2.900E-06	0.21	1.940E-03
	29	9.819E-09	1.473E-03	1.305	2.246E-08	2.370E-04	2.985	6.800E-06	0.16	1.840E-03
	30	1.042E-08	1.372E-03	1.385	2.071E-08	2.370E-04	2.752	6.100E-06	0.17	2.110E-03
	31	9.433E-09	1.567E-03	1.254	2.309E-08	2.370E-04	3.069	5.700E-06	0.17	1.670E-03
	33	9.242E-09	1.270E-03	1.228	2.111E-08	2.370E-04	2.806	3.300E-06	0.18	2.060E-03
174	4	1.040E-08	1.433E-03	1.383	2.237E-08	2.370E-04	2.972	5.800E-06	0.18	1.650E-03
	11	9.636E-09	1.319E-03	1.281	2.407E-08	2.370E-04	3.199	4.400E-06	0.20	1.410E-03
	15	1.040E-08	1.277E-03	1.383	2.318E-08	2.370E-04	3.080	5.000E-06	0.15	2.420E-03
	16	1.037E-08	1.158E-03	1.379	2.245E-08	2.370E-04	2.983	5.200E-06	0.19	1.990E-03
	18	1.065E-08	1.188E-03	1.415	2.213E-08	2.370E-04	2.940	5.200E-06	0.17	1.730E-03
	22	9.639E-09	1.113E-03	1.281	2.388E-08	2.370E-04	3.173	5.800E-06	0.15	1.810E-03
	24	9.433E-09	1.169E-03	1.254	2.257E-08	2.370E-04	3.000	3.000E-06	0.21	2.190E-03
	25	1.047E-08	1.179E-03	1.391	2.238E-08	2.370E-04	2.974	5.700E-06	0.16	2.530E-03
	27	9.541E-09	1.398E-03	1.268	2.397E-08	2.370E-04	3.185	2.700E-06	0.22	2.170E-03
	29	9.397E-09	1.234E-03	1.249	2.379E-08	2.370E-04	3.162	6.200E-06	0.16	1.610E-03
	31	9.713E-09	1.153E-03	1.291	2.337E-08	2.370E-04	3.105	4.600E-06	0.16	1.520E-03
	34	9.541E-09	1.359E-03	1.268	2.343E-08	2.370E-04	3.114	5.200E-06	0.17	1.570E-03
	38	1.015E-08	1.348E-03	1.349	2.336E-08	2.370E-04	3.104	9.000E-06	0.14	2.530E-03
	40	1.009E-08	1.438E-03	1.341	2.266E-08	2.370E-04	3.012	4.700E-06	0.15	2.740E-03
	$\bar{x}$	**9.867E-09**	1.275E-03	1.311						
	$\bar{x} \pm$	**3.330E-10**	1.236E-04	0.044						

Tab.6.10: 2-component fit for calculating basal ACTH after 138 h

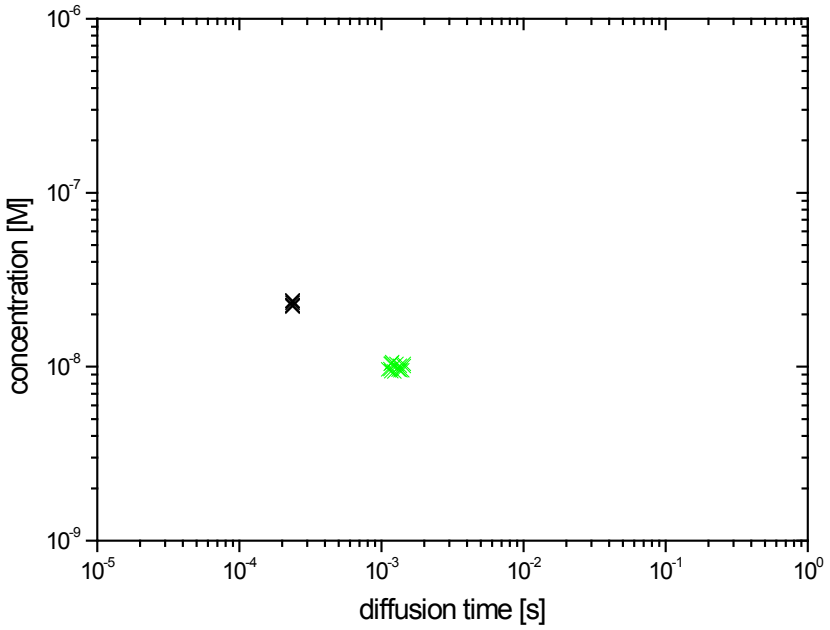

Fig. 6.6: Concdiff-plot of 2-component fit after 138 h total incubation time

	2fit	c_2	t_2	p_2	c_1	t_1	p_1	tauT	Triplet	chi²
151	#	[M]	[s]		[M]	[s]		[s]		
	5	8.438E-09	1.403E-03	1.121	2.274E-08	2.130E-04	3.022	4.400E-06	0.19	1.870E-03
	10	8.902E-09	1.290E-03	1.183	2.171E-08	2.130E-04	2.885	6.100E-06	0.18	1.520E-03
	12	1.012E-08	1.061E-03	1.344	2.114E-08	2.130E-04	2.809	5.100E-06	0.19	1.680E-03
	17	1.006E-08	8.733E-04	1.337	1.986E-08	2.130E-04	2.640	6.200E-06	0.16	1.160E-03
	18	8.526E-09	1.232E-03	1.133	2.213E-08	2.130E-04	2.941	4.800E-06	0.18	1.310E-03
	19	1.014E-08	1.159E-03	1.348	1.969E-08	2.130E-04	2.616	5.900E-06	0.17	1.320E-03
	23	9.699E-09	1.150E-03	1.289	2.027E-08	2.130E-04	2.693	5.100E-06	0.18	1.290E-03
	24	9.095E-09	1.158E-03	1.209	2.174E-08	2.130E-04	2.889	4.000E-06	0.18	1.930E-03
	25	8.691E-09	1.328E-03	1.155	2.035E-08	2.130E-04	2.704	4.100E-06	0.17	1.710E-03
	26	8.909E-09	1.009E-03	1.184	2.148E-08	2.130E-04	2.855	4.100E-06	0.17	1.330E-03
	28	9.781E-09	1.089E-03	1.300	2.111E-08	2.130E-04	2.806	7.700E-06	0.17	2.040E-03
	29	9.053E-09	1.206E-03	1.203	2.157E-08	2.130E-04	2.867	4.600E-06	0.19	1.180E-03
	30	8.529E-09	1.053E-03	1.133	2.110E-08	2.130E-04	2.804	4.300E-06	0.18	1.270E-03
	32	9.675E-09	9.789E-04	1.286	2.074E-08	2.130E-04	2.756	6.200E-06	0.17	1.300E-03
	33	8.913E-09	1.089E-03	1.184	2.110E-08	2.130E-04	2.805	5.600E-06	0.18	1.120E-03
	35	9.457E-09	1.117E-03	1.257	2.112E-08	2.130E-04	2.807	5.600E-06	0.17	9.930E-04
	36	9.779E-09	9.800E-04	1.300	1.953E-08	2.130E-04	2.595	4.700E-06	0.17	1.060E-03
	39	9.534E-09	9.739E-04	1.267	1.989E-08	2.130E-04	2.644	5.800E-06	0.17	1.690E-03
181	1	1.065E-08	9.977E-04	1.416	2.291E-08	2.310E-04	3.044	4.300E-06	0.22	1.340E-03
	3	8.954E-09	1.127E-03	1.190	2.118E-08	2.310E-04	2.815	3.700E-06	0.21	2.310E-03
	7	8.567E-09	1.293E-03	1.139	2.209E-08	2.310E-04	2.935	5.100E-06	0.18	1.980E-03
	8	9.224E-09	1.310E-03	1.226	2.070E-08	2.310E-04	2.751	7.300E-06	0.16	1.740E-03
	9	8.922E-09	9.939E-04	1.186	2.252E-08	2.310E-04	2.993	1.000E-05	0.16	1.770E-03
	11	8.387E-09	1.230E-03	1.115	2.195E-08	2.310E-04	2.917	7.000E-06	0.16	1.920E-03
	12	8.318E-09	1.697E-03	1.105	2.224E-08	2.310E-04	2.955	7.500E-06	0.17	1.570E-03
	13	1.032E-08	1.049E-03	1.372	2.061E-08	2.310E-04	2.739	1.000E-05	0.16	1.710E-03
	18	8.973E-09	1.074E-03	1.192	2.164E-08	2.310E-04	2.876	1.000E-05	0.15	2.800E-03
	21	9.486E-09	9.244E-04	1.261	2.134E-08	2.310E-04	2.836	6.600E-06	0.18	2.070E-03
	26	1.006E-08	8.878E-04	1.337	2.033E-08	2.310E-04	2.701	5.300E-06	0.20	2.300E-03
	28	8.888E-09	1.399E-03	1.181	2.078E-08	2.310E-04	2.761	6.800E-06	0.18	2.060E-03
	30	1.041E-08	9.603E-04	1.383	2.000E-08	2.310E-04	2.657	8.200E-06	0.17	2.240E-03
	30	1.041E-08	9.603E-04	1.383	2.000E-08	2.310E-04	2.657	8.200E-06	0.17	2.240E-03
	32	1.008E-08	1.140E-03	1.339	2.067E-08	2.310E-04	2.747	7.600E-06	0.19	1.780E-03
	34	1.019E-08	1.025E-03	1.355	2.024E-08	2.310E-04	2.690	7.800E-06	0.17	1.550E-03
	35	8.398E-09	1.274E-03	1.116	2.150E-08	2.310E-04	2.858	5.700E-06	0.17	2.110E-03
	36	9.996E-09	1.081E-03	1.328	2.059E-08	2.310E-04	2.736	5.500E-06	0.18	2.340E-03
	38	8.163E-09	1.469E-03	1.085	2.182E-08	2.310E-04	2.900	4.800E-06	0.19	2.070E-03
	39	9.234E-09	9.852E-04	1.227	2.125E-08	2.310E-04	2.824	5.800E-06	0.16	2.900E-03
	41	8.224E-09	1.153E-03	1.093	2.273E-08	2.310E-04	3.021	5.700E-06	0.19	2.350E-03

43	8.909E-09	1.168E-03	1.184	2.164E-08	2.310E-04	2.876	8.000E-06	0.17	2.400E-03
44	1.042E-08	8.956E-04	1.385	2.135E-08	2.310E-04	2.838	8.500E-06	0.19	1.800E-03
50	8.194E-09	1.100E-03	1.089	2.209E-08	2.310E-04	2.936	4.700E-06	0.18	1.250E-03
$\bar{x}$	**9.302E-09**	**1.127E-03**	1.236						
$\bar{x} \pm$	**6.444E-10**	**1.318E-04**	0.086						

Tab.6.11: 2-component fit for calculating ACTH response to 10nM CRH (1 min) after 92 h

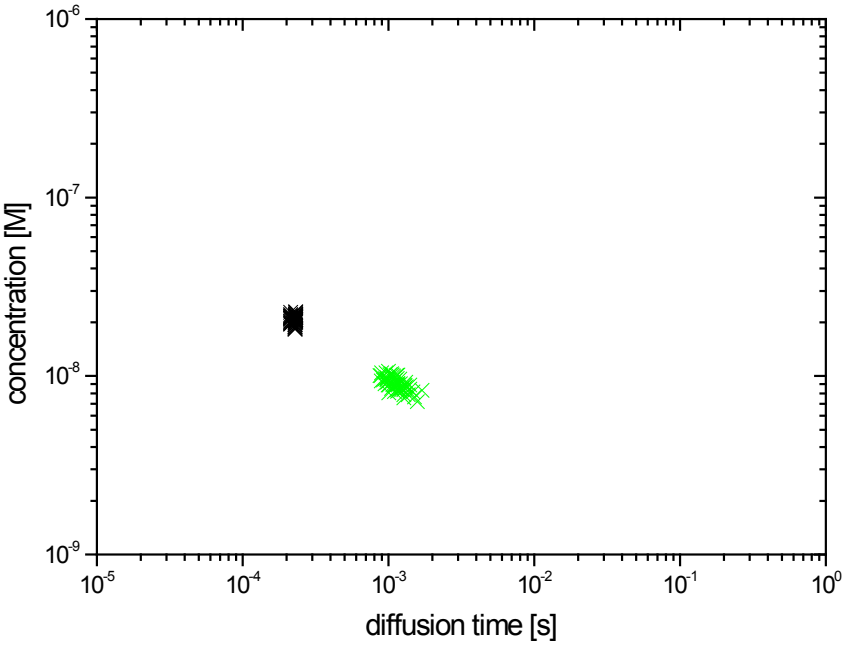

Fig. 6.7: Concdiff-plot of 2-component fit to 10nM CRH (1 min) after 92 h

2fit	c_2	t_2	p_2	c_1	t_1	p_1	tauT	Triplet	chi²
#	[M]	[s]		[M]	[s]		[s]		
1	8.977E-09	9.973E-04	1.193	2.045E-08	2.130E-04	2.718	4.300E-06	0.16	2.440E-03
2	1.025E-08	1.136E-03	1.362	2.015E-08	2.130E-04	2.678	1.000E-05	0.15	1.830E-03
3	9.532E-09	1.070E-03	1.267	2.020E-08	2.130E-04	2.684	7.000E-06	0.18	1.510E-03
4	9.099E-09	1.159E-03	1.209	1.894E-08	2.130E-04	2.517	5.900E-06	0.17	1.910E-03
5	9.798E-09	1.029E-03	1.302	1.871E-08	2.130E-04	2.486	7.100E-06	0.16	2.840E-03
8	1.028E-08	8.581E-04	1.366	1.785E-08	2.130E-04	2.372	5.000E-06	0.19	2.370E-03
10	9.113E-09	1.087E-03	1.211	1.976E-08	2.130E-04	2.626	4.500E-06	0.18	2.670E-03
17	9.793E-09	9.606E-04	1.301	1.830E-08	2.130E-04	2.432	6.700E-06	0.18	1.590E-03
18	8.898E-09	1.323E-03	1.183	1.916E-08	2.130E-04	2.547	6.100E-06	0.16	1.670E-03
19	9.618E-09	1.076E-03	1.278	1.837E-08	2.130E-04	2.441	6.700E-06	0.16	1.660E-03
22	8.943E-09	1.089E-03	1.188	1.830E-08	2.130E-04	2.431	4.600E-06	0.19	3.040E-03
23	9.270E-09	1.052E-03	1.232	1.932E-08	2.130E-04	2.568	3.600E-06	0.23	2.350E-03

148

	24	9.381E-09	1.122E-03	1.247	1.881E-08	2.130E-04	2.500	7.000E-06	0.16	2.430E-03
	25	9.829E-09	9.859E-04	1.306	1.780E-08	2.130E-04	2.366	7.300E-06	0.16	2.150E-03
	26	1.005E-08	8.852E-04	1.335	1.775E-08	2.130E-04	2.359	3.600E-06	0.22	2.430E-03
	27	9.453E-09	1.059E-03	1.256	1.807E-08	2.130E-04	2.402	6.300E-06	0.17	1.690E-03
	31	9.284E-09	1.142E-03	1.234	1.903E-08	2.130E-04	2.529	4.700E-06	0.18	1.780E-03
	34	9.704E-09	8.702E-04	1.290	1.913E-08	2.130E-04	2.542	6.400E-06	0.17	2.540E-03
	36	9.057E-09	1.114E-03	1.204	1.860E-08	2.130E-04	2.472	6.900E-06	0.16	1.360E-03
	40	9.199E-09	1.054E-03	1.222	1.819E-08	2.130E-04	2.417	4.600E-06	0.20	1.720E-03
183	2	9.796E-09	1.251E-03	1.302	2.081E-08	2.310E-04	2.765	7.500E-06	0.16	2.090E-03
	9	1.000E-08	9.021E-04	1.329	1.919E-08	2.310E-04	2.550	6.100E-06	0.15	1.900E-03
	10	1.045E-08	1.021E-03	1.388	1.981E-08	2.310E-04	2.633	7.600E-06	0.18	2.350E-03
	12	9.455E-09	1.318E-03	1.256	2.034E-08	2.310E-04	2.702	5.700E-06	0.18	1.640E-03
	14	8.729E-09	1.347E-03	1.160	2.045E-08	2.310E-04	2.717	5.300E-06	0.18	2.430E-03
	15	9.542E-09	1.183E-03	1.268	2.075E-08	2.310E-04	2.758	8.600E-06	0.15	2.460E-03
	16	9.796E-09	1.251E-03	1.302	2.081E-08	2.310E-04	2.765	7.500E-06	0.16	2.090E-03
	17	9.849E-09	1.130E-03	1.309	2.081E-08	2.310E-04	2.766	9.900E-06	0.15	2.020E-03
	18	9.133E-09	1.144E-03	1.214	2.172E-08	2.310E-04	2.887	5.300E-06	0.18	2.950E-03
	19	9.714E-09	8.529E-04	1.291	2.149E-08	2.310E-04	2.856	6.100E-06	0.17	2.170E-03
	20	1.036E-08	9.696E-04	1.377	1.905E-08	2.310E-04	2.532	6.400E-06	0.17	1.680E-03
	21	9.708E-09	9.834E-04	1.290	2.054E-08	2.310E-04	2.729	3.300E-06	0.21	1.660E-03
	23	1.022E-08	1.104E-03	1.358	2.030E-08	2.310E-04	2.698	9.500E-06	0.16	1.930E-03
	25	8.417E-09	1.196E-03	1.119	2.207E-08	2.310E-04	2.933	5.300E-06	0.19	1.540E-03
	26	8.623E-09	9.882E-04	1.146	2.093E-08	2.310E-04	2.781	4.000E-06	0.20	2.140E-03
	27	1.002E-08	1.148E-03	1.332	2.163E-08	2.310E-04	2.875	1.000E-05	0.16	1.760E-03
	32	9.669E-09	1.017E-03	1.285	2.131E-08	2.310E-04	2.832	8.900E-06	0.16	1.470E-03
	34	9.175E-09	1.036E-03	1.219	2.078E-08	2.310E-04	2.761	5.500E-06	0.19	1.620E-03
	37	8.895E-09	1.027E-03	1.182	2.101E-08	2.310E-04	2.791	4.600E-06	0.18	2.330E-03
	39	9.896E-09	1.179E-03	1.315	2.036E-08	2.310E-04	2.706	6.700E-06	0.17	2.250E-03
	40	1.018E-08	1.050E-03	1.352	2.076E-08	2.310E-04	2.759	6.200E-06	0.18	2.090E-03
	43	9.348E-09	1.064E-03	1.242	2.155E-08	2.310E-04	2.863	6.500E-06	0.18	1.640E-03
	46	8.463E-09	1.187E-03	1.125	2.171E-08	2.310E-04	2.885	4.600E-06	0.20	2.060E-03
	48	9.651E-09	8.375E-04	1.283	2.137E-08	2.310E-04	2.840	4.900E-06	0.19	2.400E-03
	$\bar{x}$	**9.514E-09**	1.074E-03	1.264						
	$\bar{x} \pm$	**4.258E-10**	9.691E-05	0.057						

Tab.6.12: 2-component fit for calculating ACTH response to 10nM CRH (15 min) after 92 h

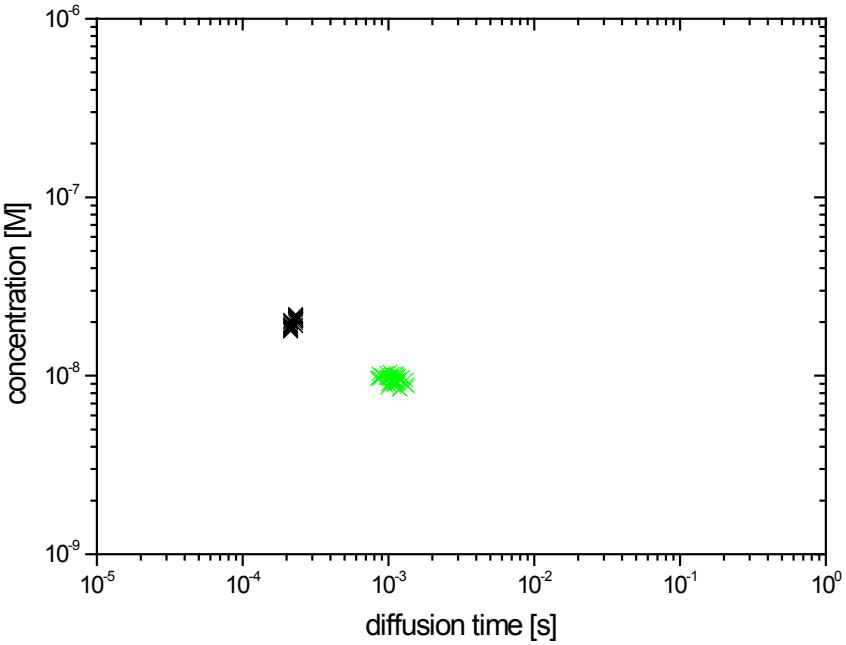

Fig. 6.8: Concdiff-plot of 2-component fit to 10nM CRH (15 min) after 92 h

2fit	c_2	t_2	p_2	c_1	t_1	p_1	tauT	Triplet	chi²
#	[M]	[s]		[M]	[s]		[s]		
1	9.826E-09	8.873E-04	1.306	2.039E-08	2.310E-04	2.709	4.700E-06	0.18	1.200E-03
2	1.102E-08	8.746E-04	1.464	2.011E-08	2.310E-04	2.672	6.100E-06	0.20	2.040E-03
3	1.067E-08	8.900E-04	1.418	1.927E-08	2.310E-04	2.561	7.200E-06	0.17	1.830E-03
6	8.585E-09	1.023E-03	1.141	1.984E-08	2.310E-04	2.636	6.600E-06	0.18	1.910E-03
7	9.249E-09	9.803E-04	1.229	1.998E-08	2.310E-04	2.655	8.700E-06	0.17	1.800E-03
10	9.908E-09	8.000E-04	1.317	2.040E-08	2.310E-04	2.711	6.400E-06	0.20	1.760E-03
11	9.496E-09	8.493E-04	1.262	1.960E-08	2.310E-04	2.605	5.300E-06	0.21	2.350E-03
14	9.809E-09	9.729E-04	1.304	1.717E-08	2.310E-04	2.282	6.500E-06	0.17	1.340E-03
15	9.898E-09	9.604E-04	1.315	1.892E-08	2.310E-04	2.515	9.900E-06	0.17	1.340E-03
16	9.557E-09	9.226E-04	1.270	1.880E-08	2.310E-04	2.498	6.600E-06	0.17	1.970E-03
20	9.074E-09	1.042E-03	1.206	1.913E-08	2.310E-04	2.543	7.500E-06	0.17	2.370E-03
26	1.015E-08	8.759E-04	1.348	1.911E-08	2.310E-04	2.540	4.900E-06	0.20	2.250E-03
27	1.121E-08	8.156E-04	1.490	1.681E-08	2.310E-04	2.234	7.900E-06	0.17	2.230E-03
29	8.924E-09	8.526E-04	1.186	1.884E-08	2.310E-04	2.504	5.200E-06	0.18	1.530E-03
30	1.007E-08	8.239E-04	1.339	1.858E-08	2.310E-04	2.469	5.400E-06	0.19	1.440E-03
31	8.928E-09	9.834E-04	1.186	1.983E-08	2.310E-04	2.635	6.400E-06	0.17	2.180E-03
33	1.104E-08	8.931E-04	1.467	1.768E-08	2.310E-04	2.350	6.500E-06	0.19	1.400E-03
39	8.588E-09	1.059E-03	1.141	2.014E-08	2.310E-04	2.676	6.800E-06	0.18	1.510E-03
43	1.017E-08	9.057E-04	1.352	1.861E-08	2.310E-04	2.473	8.400E-06	0.18	1.790E-03
48	8.890E-09	1.124E-03	1.181	1.908E-08	2.310E-04	2.536	5.000E-06	0.19	1.910E-03

50	8.768E-09	1.078E-03	1.165	1.908E-08	2.310E-04	2.536	5.900E-06	0.17	1.690E-03
x̄	**9.706E-09**	9.340E-04	1.290						
x̄ ±	**6.669E-10**	7.783E-05	0.088						

Tab.6.13: 2-component fit for calculating ACTH response to 10nM CRH (30 min) after 92 h

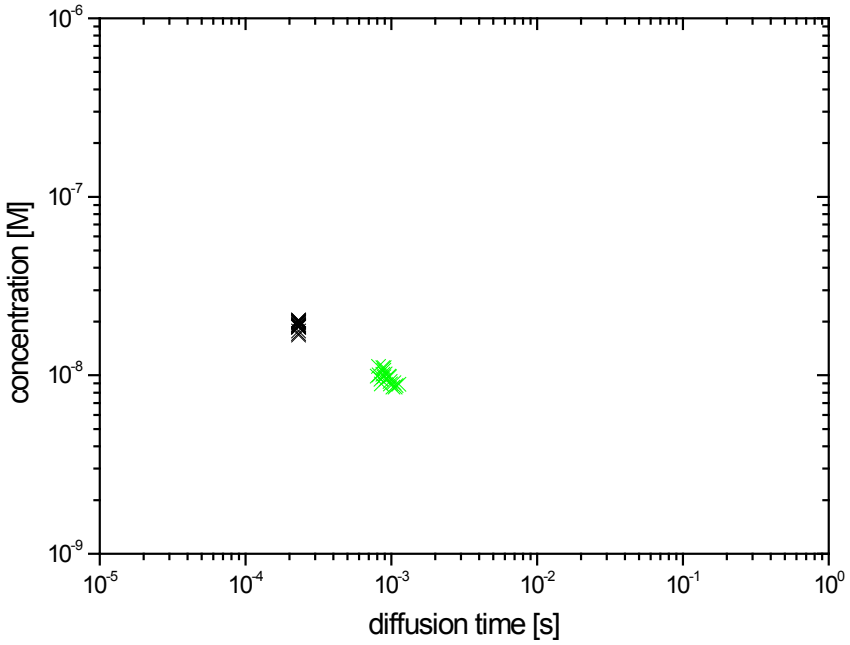

Fig. 6.9: Concdiff-plot of 2-component fit to 10nM CRH (30 min) after 92 h

150	2fit	c_2	t_2	p_2	c_1	t_1	p_1	tauT	Triplet	chi²
	#	[M]	[s]		[M]	[s]		[s]		
	3	1.027E-08	1.147E-03	1.365	2.102E-08	2.130E-04	2.793	4.200E-06	0.18	2.450E-03
	4	9.046E-09	1.269E-03	1.202	2.242E-08	2.130E-04	2.979	4.500E-06	0.18	2.490E-03
	5	9.812E-09	1.211E-03	1.304	1.930E-08	2.130E-04	2.565	7.400E-06	0.16	2.190E-03
	6	9.807E-09	1.051E-03	1.303	1.977E-08	2.130E-04	2.627	5.500E-06	0.15	2.360E-03
	8	9.020E-09	1.166E-03	1.199	1.974E-08	2.130E-04	2.623	5.800E-06	0.17	1.840E-03
	9	1.031E-08	1.045E-03	1.370	1.832E-08	2.130E-04	2.435	5.500E-06	0.17	1.830E-03
	10	9.246E-09	1.158E-03	1.229	2.078E-08	2.130E-04	2.761	8.400E-06	0.14	2.010E-03
	11	1.030E-08	1.067E-03	1.368	1.951E-08	2.130E-04	2.592	7.700E-06	0.13	1.990E-03
	12	9.818E-09	1.040E-03	1.305	1.973E-08	2.130E-04	2.622	4.800E-06	0.19	2.870E-03
	13	9.341E-09	1.109E-03	1.241	2.030E-08	2.130E-04	2.697	6.800E-06	0.16	2.990E-03
	14	1.048E-08	1.019E-03	1.393	1.897E-08	2.130E-04	2.521	6.400E-06	0.16	2.980E-03
	15	1.032E-08	1.043E-03	1.371	2.025E-08	2.130E-04	2.691	6.100E-06	0.20	1.650E-03
	17	9.339E-09	1.124E-03	1.241	2.114E-08	2.130E-04	2.809	5.500E-06	0.17	1.140E-03
	18	1.059E-08	1.026E-03	1.407	1.973E-08	2.130E-04	2.622	5.100E-06	0.17	1.110E-03

20	9.966E-09	1.015E-03	1.324	1.982E-08	2.130E-04	2.634	5.600E-06	0.18	2.150E-03
21	8.972E-09	1.158E-03	1.192	1.977E-08	2.130E-04	2.628	6.000E-06	0.17	2.780E-03
22	9.958E-09	1.074E-03	1.323	1.859E-08	2.130E-04	2.471	5.500E-06	0.16	2.740E-03
24	1.005E-08	8.858E-04	1.335	2.071E-08	2.130E-04	2.752	6.700E-06	0.18	2.710E-03
26	1.015E-08	1.021E-03	1.349	1.926E-08	2.130E-04	2.559	5.100E-06	0.18	2.470E-03
29	9.189E-09	8.799E-04	1.221	2.109E-08	2.130E-04	2.802	5.500E-06	0.19	3.010E-03
31	9.783E-09	1.118E-03	1.300	1.971E-08	2.130E-04	2.620	5.700E-06	0.16	2.620E-03
32	9.642E-09	1.176E-03	1.281	1.995E-08	2.130E-04	2.651	6.200E-06	0.16	1.970E-03
35	1.006E-08	8.278E-04	1.337	1.876E-08	2.130E-04	2.493	5.600E-06	0.16	3.690E-03
36	9.465E-09	1.083E-03	1.258	2.154E-08	2.130E-04	2.862	7.700E-06	0.19	1.670E-03
37	9.485E-09	9.462E-04	1.261	2.072E-08	2.130E-04	2.753	6.700E-06	0.18	3.660E-03
40	8.998E-09	1.214E-03	1.196	1.982E-08	2.130E-04	2.634	5.000E-06	0.16	1.120E-03
42	9.750E-09	9.773E-04	1.296	1.986E-08	2.130E-04	2.640	6.000E-06	0.15	2.740E-03
43	9.543E-09	9.778E-04	1.268	1.999E-08	2.130E-04	2.656	6.200E-06	0.15	2.280E-03
44	9.660E-09	1.194E-03	1.284	2.038E-08	2.130E-04	2.709	6.200E-06	0.15	2.380E-03
45	1.002E-08	9.604E-04	1.331	1.941E-08	2.130E-04	2.579	5.800E-06	0.19	3.630E-03
46	1.042E-08	8.568E-04	1.384	1.901E-08	2.130E-04	2.526	5.600E-06	0.16	1.760E-03
47	1.008E-08	9.760E-04	1.339	1.971E-08	2.130E-04	2.619	5.800E-06	0.16	2.230E-03
50	9.567E-09	9.428E-04	1.271	1.943E-08	2.130E-04	2.582	4.100E-06	0.17	2.790E-03
$\bar{x}$	**9.771E-09**	1.053E-03	1.298						
$\bar{x} \pm$	**3.823E-10**	8.900E-05	0.051						

Tab.6.14: 2-component fit for calculating ACTH response to 10nM CRH (1 h) after 92 h

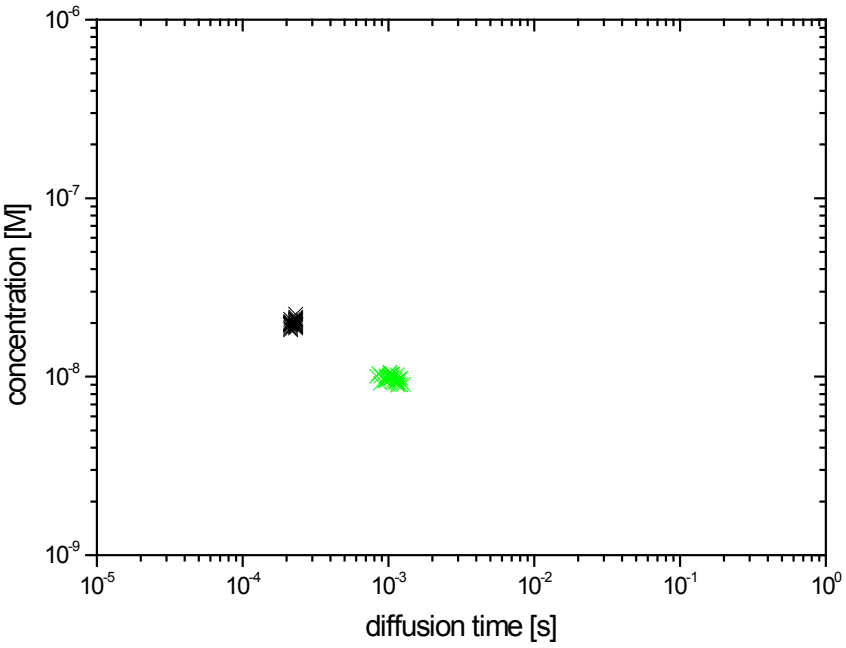

Fig. 6.10: Concdiff-plot of 2-component fit to 10nM CRH (1 h) after 92 h

184

2fit	c_2	t_2	p_2	c_1	t_1	p_1	tauT	Triplet	chi²
#	[M]	[s]		[M]	[s]		[s]		
1	1.151E-08	1.094E-03	1.530	2.252E-08	2.310E-04	2.992	8.500E-06	0.17	1.010E-03
2	1.014E-08	1.338E-03	1.348	2.253E-08	2.310E-04	2.995	6.300E-06	0.19	1.270E-03
4	1.010E-08	9.464E-04	1.342	2.267E-08	2.310E-04	3.013	7.900E-06	0.17	1.600E-03
5	1.011E-08	1.101E-03	1.343	2.265E-08	2.310E-04	3.010	8.600E-06	0.17	1.530E-03
8	9.242E-09	1.401E-03	1.228	2.256E-08	2.310E-04	2.998	5.700E-06	0.19	2.110E-03
12	1.024E-08	9.997E-04	1.361	2.026E-08	2.310E-04	2.692	6.500E-06	0.17	1.230E-03
15	9.491E-09	1.212E-03	1.261	2.281E-08	2.310E-04	3.032	6.800E-06	0.17	2.200E-03
16	9.240E-09	1.225E-03	1.228	2.009E-08	2.310E-04	2.670	5.000E-06	0.17	1.790E-03
21	1.141E-08	1.028E-03	1.516	2.036E-08	2.310E-04	2.706	7.700E-06	0.20	1.570E-03
22	9.908E-09	1.147E-03	1.317	2.150E-08	2.310E-04	2.857	8.200E-06	0.15	2.670E-03
24	1.116E-08	1.029E-03	1.483	2.028E-08	2.310E-04	2.695	8.100E-06	0.18	1.380E-03
25	1.096E-08	1.064E-03	1.456	2.140E-08	2.310E-04	2.844	8.400E-06	0.17	1.820E-03
26	9.140E-09	1.292E-03	1.215	2.217E-08	2.310E-04	2.946	5.400E-06	0.17	1.700E-03
28	9.255E-09	1.270E-03	1.230	2.210E-08	2.310E-04	2.937	9.300E-06	0.14	1.330E-03
31	1.155E-08	9.454E-04	1.536	1.924E-08	2.310E-04	2.557	7.400E-06	0.18	2.380E-03
37	9.403E-09	1.030E-03	1.250	2.204E-08	2.310E-04	2.929	6.900E-06	0.17	2.290E-03
38	9.733E-09	1.091E-03	1.293	2.194E-08	2.310E-04	2.916	6.100E-06	0.18	1.510E-03
39	1.026E-08	1.092E-03	1.364	1.901E-08	2.310E-04	2.527	5.200E-06	0.16	2.170E-03
$\bar{x}$	**1.016E-08**	1.128E-03	1.350						
$\bar{x} \pm$	**6.645E-10**	1.098E-04	0.088						

Tab.6.15: 2-component fit for calculating ACTH response to 10nM CRH (2 h) after 92 h

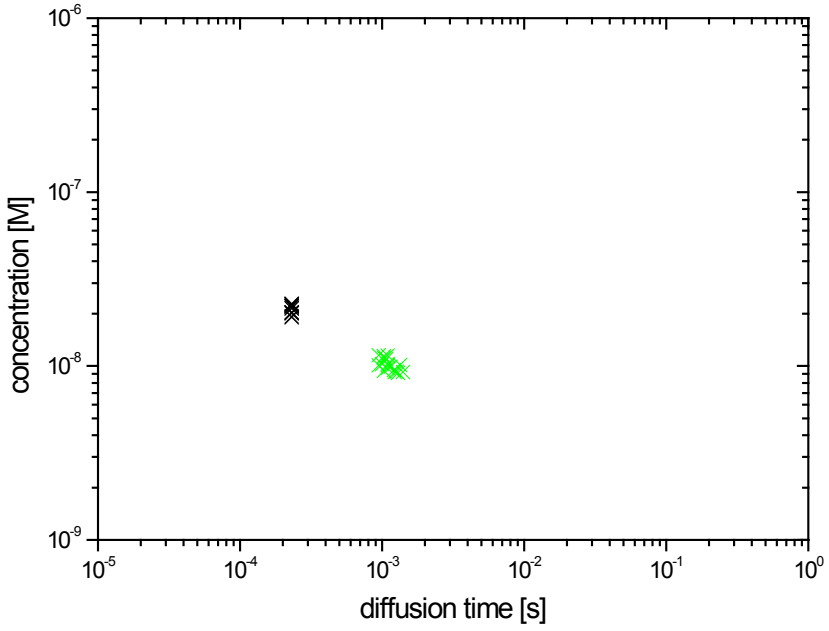

Fig. 6.11: Concdiff-plot of 2-component fit to 10nM CRH (2 h) after 92 h

2fit	c_2	t_2	p_2	c_1	t_1	p_1	tauT	Triplet	chi²
#	[M]	[s]		[M]	[s]		[s]		
2	9.390E-09	1.060E-03	1.250	1.930E-08	2.140E-04	2.570	4.500E-06	0.19	2.210E-03
10	9.710E-09	1.030E-03	1.290	1.910E-08	2.140E-04	2.530	9.100E-06	0.16	1.950E-03
13	9.130E-09	1.160E-03	1.210	2.000E-08	2.140E-04	2.660	6.300E-06	0.19	1.920E-03
14	9.670E-09	1.060E-03	1.280	1.950E-08	2.140E-04	2.600	6.600E-06	0.19	2.410E-03
15	9.060E-09	1.100E-03	1.200	1.980E-08	2.140E-04	2.630	8.200E-06	0.18	2.280E-03
17	1.010E-08	9.890E-04	1.340	1.980E-08	2.140E-04	2.630	5.800E-06	0.19	2.820E-03
18	9.980E-09	1.030E-03	1.330	1.880E-08	2.140E-04	2.500	5.500E-06	0.19	2.150E-03
23	9.320E-09	1.080E-03	1.240	1.970E-08	2.140E-04	2.620	5.200E-06	0.20	2.550E-03
25	9.730E-09	9.560E-04	1.290	1.880E-08	2.140E-04	2.500	6.200E-06	0.18	3.040E-03
27	9.120E-09	1.090E-03	1.210	2.020E-08	2.140E-04	2.680	5.600E-06	0.20	2.930E-03
38	9.460E-09	1.080E-03	1.260	2.020E-08	2.140E-04	2.680	6.400E-06	0.18	2.670E-03
40	9.820E-09	1.050E-03	1.310	2.000E-08	2.140E-04	2.660	8.000E-06	0.18	3.680E-03
$\bar{x}$	**9.541E-09**	1.057E-03	1.268						
$\bar{x} \pm$	**2.942E-10**	3.840E-05	0.039						

Tab.6.16: 2-component fit for calculating ACTH response to 10nM CRH (1 min) after 114 h

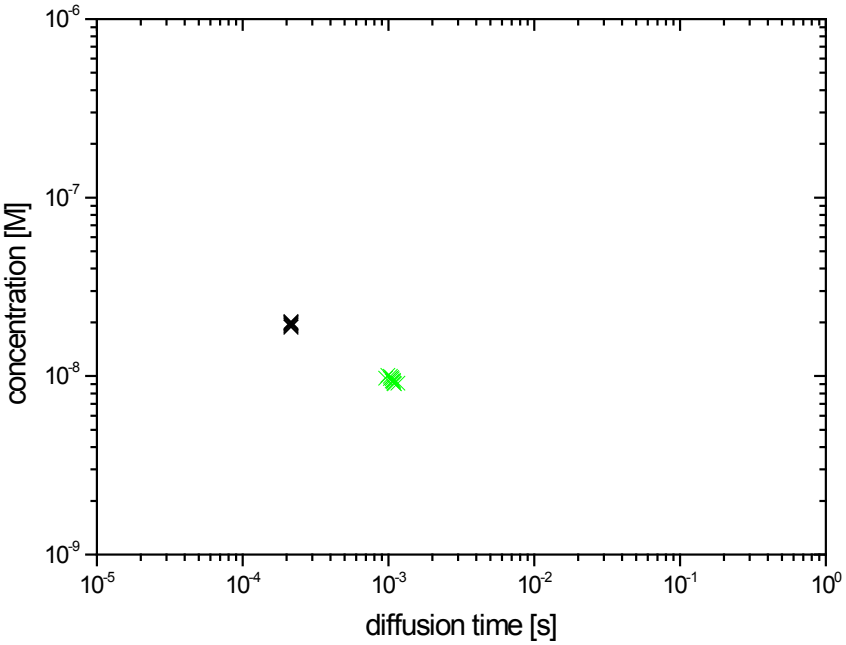

Fig. 6.12: Concdiff-plot of 2-component fit to 10nM CRH (1 min) after 114 h

193

2fit	c_2	t_2	p_2	c_1	t_1	p_1	tauT	Triplet	chi^2
#	[M]	[s]		[M]	[s]		[s]		
2	8.543E-09	1.520E-03	1.135	2.405E-08	2.140E-04	3.196	3.800E-06	0.18	1.840E-03
4	1.158E-08	9.644E-04	1.538	2.082E-08	2.140E-04	2.766	4.400E-06	0.20	2.400E-03
5	1.105E-08	1.086E-03	1.468	2.083E-08	2.140E-04	2.769	4.100E-06	0.21	1.350E-03
7	1.058E-08	9.657E-04	1.406	2.159E-08	2.140E-04	2.870	3.800E-06	0.23	2.150E-03
8	8.321E-09	1.394E-03	1.106	2.285E-08	2.140E-04	3.037	4.500E-06	0.18	1.830E-03
9	9.615E-09	1.245E-03	1.278	2.230E-08	2.140E-04	2.964	4.500E-06	0.20	2.810E-03
11	9.166E-09	1.227E-03	1.218	2.300E-08	2.140E-04	3.056	3.300E-06	0.21	3.200E-03
12	8.469E-09	1.658E-03	1.125	2.281E-08	2.140E-04	3.032	6.000E-06	0.16	2.320E-03
14	9.659E-09	1.264E-03	1.284	2.165E-08	2.140E-04	2.876	5.800E-06	0.18	1.420E-03
15	1.026E-08	1.103E-03	1.364	2.234E-08	2.140E-04	2.969	5.400E-06	0.19	1.280E-03
16	8.769E-09	1.309E-03	1.165	2.286E-08	2.140E-04	3.037	4.200E-06	0.19	1.890E-03
17	1.118E-08	1.071E-03	1.486	2.100E-08	2.140E-04	2.791	5.500E-06	0.20	2.100E-03
20	9.472E-09	1.275E-03	1.259	2.318E-08	2.140E-04	3.080	6.100E-06	0.18	1.270E-03
22	1.069E-08	1.074E-03	1.421	2.117E-08	2.140E-04	2.813	6.600E-06	0.19	1.420E-03
23	8.554E-09	1.340E-03	1.137	2.258E-08	2.140E-04	3.000	4.900E-06	0.18	1.830E-03
24	1.155E-08	1.078E-03	1.535	2.107E-08	2.140E-04	2.799	7.800E-06	0.18	1.060E-03
25	9.679E-09	1.213E-03	1.286	2.268E-08	2.140E-04	3.014	4.900E-06	0.21	1.420E-03
26	1.092E-08	9.245E-04	1.452	2.115E-08	2.140E-04	2.810	5.600E-06	0.19	1.470E-03
28	8.582E-09	1.365E-03	1.141	2.405E-08	2.140E-04	3.196	3.700E-06	0.18	1.830E-03
29	9.328E-09	1.270E-03	1.240	2.349E-08	2.140E-04	3.121	3.700E-06	0.23	1.210E-03
30	1.093E-08	1.129E-03	1.453	2.169E-08	2.140E-04	2.882	7.000E-06	0.18	1.510E-03
31	9.681E-09	1.000E-03	1.286	2.325E-08	2.140E-04	3.090	5.000E-06	0.18	1.640E-03
32	1.089E-08	8.712E-04	1.447	2.083E-08	2.140E-04	2.769	6.000E-06	0.17	1.760E-03
34	1.090E-08	1.026E-03	1.448	2.095E-08	2.140E-04	2.784	6.000E-06	0.17	2.570E-03
35	8.889E-09	1.505E-03	1.181	2.270E-08	2.140E-04	3.016	5.900E-06	0.15	1.980E-03
36	8.924E-09	1.170E-03	1.186	2.295E-08	2.140E-04	3.050	3.100E-06	0.25	1.720E-03
37	1.062E-08	8.000E-04	1.411	2.205E-08	2.140E-04	2.930	5.900E-06	0.20	1.710E-03
38	9.950E-09	1.241E-03	1.322	2.289E-08	2.140E-04	3.041	4.400E-06	0.22	1.840E-03
39	8.245E-09	1.343E-03	1.096	2.377E-08	2.140E-04	3.159	2.600E-06	0.21	1.500E-03
$\bar{x}$	**9.827E-09**	1.187E-03	1.306						
$\bar{x} \pm$	**9.202E-10**	1.627E-04	0.122						

Tab.6.17: 2-component fit for calculating ACTH response to 10nM CRH (15 min) after 114 h

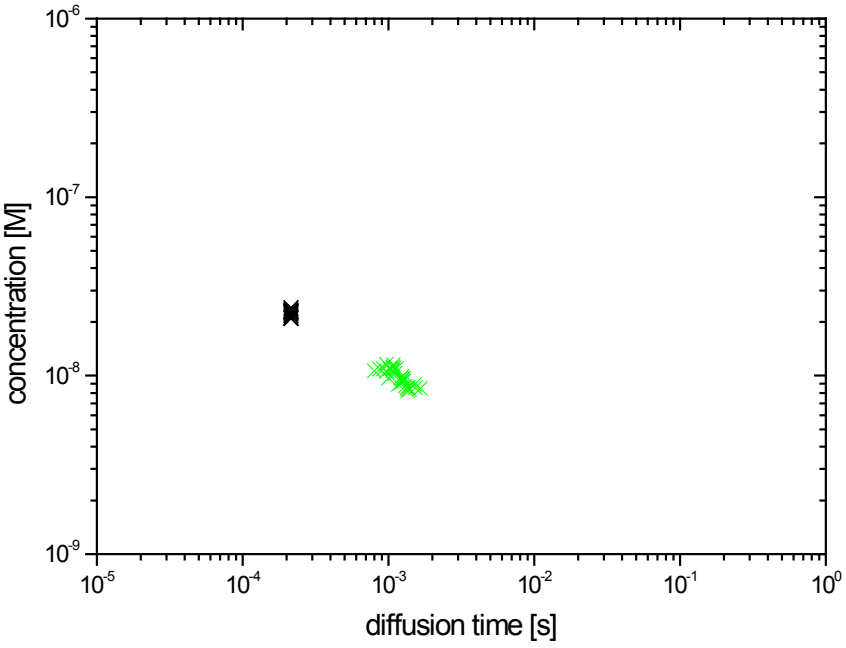

Fig. 6.13: Concdiff-plot of 2-component fit to 10nM CRH (15 min) after 114 h

164	2fit	c_2	t_2	p_2	c_1	t_1	p_1	tauT	Triplet	chi²
	#	[M]	[s]		[M]	[s]		[s]		
	1	9.905E-09	9.943E-04	1.316	2.262E-08	2.140E-04	3.005	3.100E-06	0.19	2.150E-03
	5	1.042E-08	1.278E-03	1.385	2.162E-08	2.140E-04	2.873	5.900E-06	0.17	1.530E-03
	11	9.420E-09	1.210E-03	1.252	2.278E-08	2.140E-04	3.027	3.700E-06	0.19	1.620E-03
	14	1.008E-08	9.713E-04	1.340	2.240E-08	2.140E-04	2.977	1.000E-05	0.15	1.250E-03
	25	9.831E-09	1.211E-03	1.306	2.138E-08	2.140E-04	2.842	4.300E-06	0.18	2.530E-03
	27	1.009E-08	1.077E-03	1.341	2.163E-08	2.140E-04	2.874	5.300E-06	0.16	2.550E-03
	31	9.290E-09	1.315E-03	1.235	2.115E-08	2.140E-04	2.811	4.100E-06	0.17	2.340E-03
	33	9.158E-09	1.213E-03	1.217	2.239E-08	2.140E-04	2.976	4.300E-06	0.15	1.570E-03
	35	9.953E-09	1.318E-03	1.323	2.015E-08	2.140E-04	2.678	4.600E-06	0.16	1.730E-03
	37	1.051E-08	1.029E-03	1.396	1.977E-08	2.140E-04	2.627	2.700E-06	0.21	1.890E-03
	$\bar{x}$	**9.866E-09**	1.162E-03	1.311						
	$\bar{x} \pm$	**3.528E-10**	1.150E-04	0.047						

Tab.6.18: 2-component fit for calculating ACTH response to 10nM CRH (30 min) after 114 h

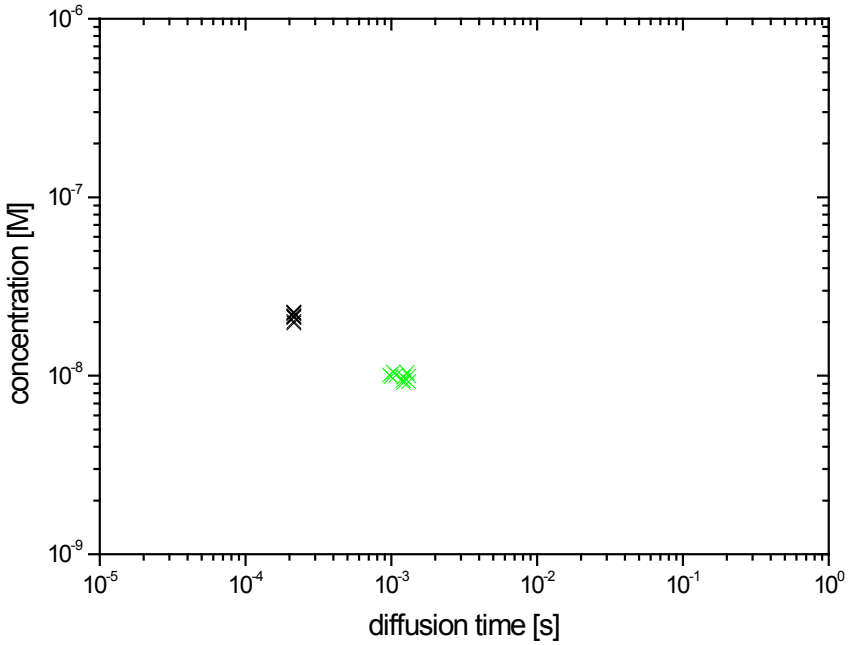

Fig. 6.14: Concdiff-plot of 2-component fit to 10nM CRH (30 min) after 114 h

163

2fit	c_2	t_2	p_2	c_1	t_1	p_1	tauT	Triplet	chi²
#	[M]	[s]		[M]	[s]		[s]		
1	1.035E-08	1.040E-03	1.376	2.329E-08	2.140E-04	3.095	5.500E-06	0.16	1.530E-03
2	9.027E-09	1.588E-03	1.200	2.525E-08	2.140E-04	3.355	9.900E-06	0.18	1.410E-03
4	1.006E-08	1.376E-03	1.337	2.208E-08	2.140E-04	2.934	3.700E-06	0.21	1.630E-03
5	8.753E-09	1.616E-03	1.163	2.403E-08	2.140E-04	3.194	4.100E-06	0.18	1.340E-03
7	1.086E-08	1.243E-03	1.443	2.282E-08	2.140E-04	3.032	6.000E-06	0.17	1.510E-03
8	9.680E-09	1.433E-03	1.286	2.442E-08	2.140E-04	3.245	7.200E-06	0.17	1.410E-03
9	9.114E-09	1.595E-03	1.211	2.236E-08	2.140E-04	2.972	4.400E-06	0.19	1.820E-03
10	1.095E-08	1.339E-03	1.456	2.388E-08	2.140E-04	3.173	8.100E-06	0.18	1.730E-03
12	1.039E-08	1.113E-03	1.381	2.281E-08	2.140E-04	3.031	6.600E-06	0.16	1.440E-03
13	1.094E-08	1.211E-03	1.454	2.159E-08	2.140E-04	2.870	4.500E-06	0.20	2.640E-03
14	1.035E-08	1.437E-03	1.375	2.238E-08	2.140E-04	2.975	6.000E-06	0.17	9.020E-04
16	1.017E-08	1.128E-03	1.352	2.161E-08	2.140E-04	2.872	5.500E-06	0.17	1.510E-03
17	9.015E-09	1.314E-03	1.198	2.259E-08	2.140E-04	3.003	4.100E-06	0.19	1.610E-03
18	1.040E-08	1.059E-03	1.383	2.208E-08	2.140E-04	2.934	4.800E-06	0.19	1.420E-03
19	1.088E-08	1.036E-03	1.446	2.202E-08	2.140E-04	2.927	6.800E-06	0.18	1.560E-03
20	9.720E-09	1.393E-03	1.292	2.138E-08	2.140E-04	2.842	4.200E-06	0.20	1.250E-03
22	9.690E-09	1.116E-03	1.288	2.233E-08	2.140E-04	2.967	6.600E-06	0.17	1.360E-03
24	1.124E-08	1.164E-03	1.494	2.013E-08	2.140E-04	2.675	6.400E-06	0.18	2.170E-03
27	1.035E-08	1.152E-03	1.375	2.208E-08	2.140E-04	2.934	5.600E-06	0.17	1.810E-03
28	9.766E-09	1.152E-03	1.298	2.191E-08	2.140E-04	2.911	6.400E-06	0.15	1.680E-03

	29	9.983E-09	1.176E-03	1.327	2.227E-08	2.140E-04	2.959	7.700E-06	0.15	1.230E-03
	30	9.301E-09	1.105E-03	1.236	2.270E-08	2.140E-04	3.016	6.700E-06	0.15	1.340E-03
	31	9.716E-09	1.088E-03	1.291	2.227E-08	2.140E-04	2.960	4.500E-06	0.15	2.750E-03
	33	1.018E-08	1.074E-03	1.353	2.293E-08	2.140E-04	3.047	5.500E-06	0.20	1.520E-03
	34	9.994E-09	1.015E-03	1.328	2.357E-08	2.140E-04	3.132	5.100E-06	0.19	1.390E-03
	35	9.620E-09	1.415E-03	1.278	2.405E-08	2.140E-04	3.196	5.700E-06	0.18	1.540E-03
	36	1.021E-08	1.398E-03	1.357	2.201E-08	2.140E-04	2.924	5.400E-06	0.18	1.010E-03
	37	1.062E-08	1.137E-03	1.412	2.266E-08	2.140E-04	3.012	4.900E-06	0.20	1.830E-03
	39	8.617E-09	1.299E-03	1.145	2.388E-08	2.140E-04	3.174	3.800E-06	0.19	1.630E-03
194	2	9.084E-09	1.070E-03	1.207	1.792E-08	2.140E-04	2.382	3.100E-06	0.19	2.250E-03
	4	1.091E-08	9.445E-04	1.449	1.605E-08	2.140E-04	2.133	6.100E-06	0.18	1.890E-03
	5	9.581E-09	8.786E-04	1.273	1.744E-08	2.140E-04	2.317	7.900E-06	0.14	1.760E-03
	7	9.768E-09	1.074E-03	1.298	1.660E-08	2.140E-04	2.206	5.200E-06	0.16	1.700E-03
	8	8.936E-09	1.065E-03	1.187	1.818E-08	2.140E-04	2.416	4.000E-06	0.20	2.550E-03
	10	9.214E-09	1.232E-03	1.225	1.662E-08	2.140E-04	2.209	6.100E-06	0.15	2.890E-03
	11	9.983E-09	9.781E-04	1.327	1.712E-08	2.140E-04	2.275	7.600E-06	0.13	2.230E-03
	14	1.045E-08	8.926E-04	1.389	1.570E-08	2.140E-04	2.086	5.400E-06	0.16	2.610E-03
	15	1.001E-08	9.687E-04	1.330	1.546E-08	2.140E-04	2.054	5.800E-06	0.14	2.430E-03
	16	1.049E-08	1.015E-03	1.394	1.753E-08	2.140E-04	2.330	6.800E-06	0.17	1.300E-03
	20	8.990E-09	1.040E-03	1.195	1.759E-08	2.140E-04	2.337	3.200E-06	0.19	1.840E-03
	23	8.973E-09	1.128E-03	1.192	1.778E-08	2.140E-04	2.363	2.500E-06	0.20	2.410E-03
	24	1.119E-08	8.803E-04	1.487	1.544E-08	2.140E-04	2.052	4.400E-06	0.17	3.030E-03
	26	1.028E-08	9.810E-04	1.366	1.642E-08	2.140E-04	2.182	3.300E-06	0.18	2.130E-03
	27	1.007E-08	1.047E-03	1.339	1.726E-08	2.140E-04	2.294	4.300E-06	0.18	1.680E-03
	29	9.370E-09	1.006E-03	1.245	1.791E-08	2.140E-04	2.380	4.100E-06	0.17	2.350E-03
	30	1.127E-08	8.478E-04	1.497	1.581E-08	2.140E-04	2.101	6.000E-06	0.17	2.410E-03
	31	9.954E-09	1.103E-03	1.323	1.721E-08	2.140E-04	2.287	5.100E-06	0.15	2.400E-03
	32	1.012E-08	1.189E-03	1.344	1.688E-08	2.140E-04	2.243	4.900E-06	0.18	2.140E-03
	33	1.055E-08	8.307E-04	1.403	1.607E-08	2.140E-04	2.135	9.800E-06	0.15	1.770E-03
	38	9.597E-09	1.020E-03	1.275	1.763E-08	2.140E-04	2.343	4.800E-06	0.19	2.610E-03
	39	1.040E-08	9.850E-04	1.382	1.585E-08	2.140E-04	2.106	7.500E-06	0.13	3.740E-03
	$\bar{x}$	**9.983E-09**	1.145E-03	1.327						
	$\bar{x} \pm$	**5.546E-10**	1.500E-04	0.074						

Tab.6.19: 2-component fit for calculating ACTH response to 10nM CRH (1 h) after 114 h

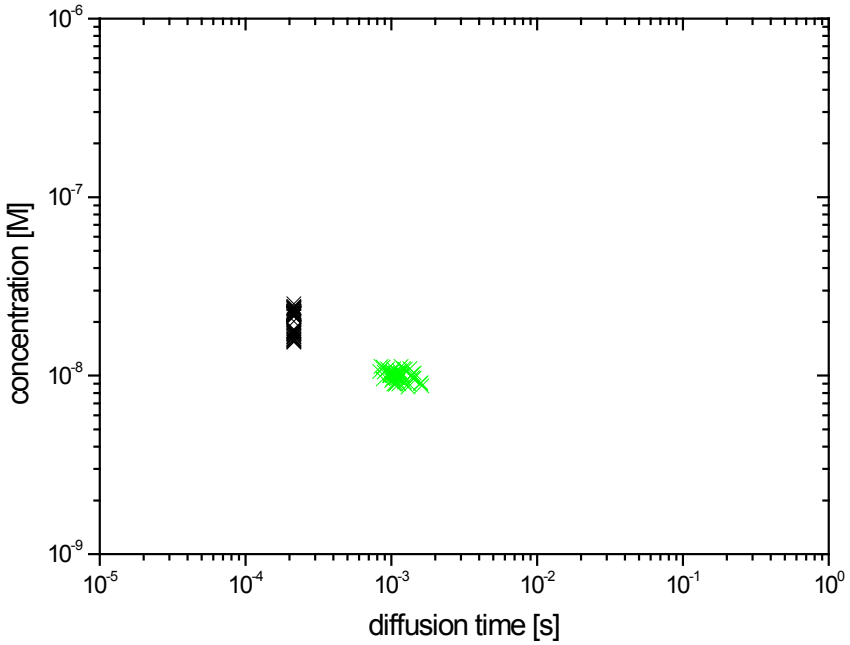

Fig. 6.15: Concdiff-plot of 2-component fit to 10nM CRH (1 h) after 114 h

	2fit	c_2	t_2	p_2	c_1	t_1	p_1	tauT	Triplet	chi²
167	#	[M]	[s]		[M]	[s]		[s]		
	2	1.046E-08	1.148E-03	1.391	2.099E-08	2.140E-04	2.789	4.100E-06	0.21	2.070E-03
	3	1.005E-08	1.195E-03	1.336	2.002E-08	2.140E-04	2.660	5.200E-06	0.2	1.590E-03
	4	1.064E-08	8.904E-04	1.413	1.863E-08	2.140E-04	2.476	4.300E-06	0.19	1.940E-03
	7	1.208E-08	8.577E-04	1.606	1.777E-08	2.140E-04	2.361	9.200E-06	0.16	1.930E-03
	8	1.080E-08	1.053E-03	1.436	1.911E-08	2.140E-04	2.540	1.000E-05	0.15	2.010E-03
	11	1.157E-08	8.220E-04	1.537	1.869E-08	2.140E-04	2.483	9.700E-06	0.16	2.170E-03
	12	1.154E-08	1.011E-03	1.533	1.876E-08	2.140E-04	2.493	7.200E-06	0.19	2.210E-03
	13	1.034E-08	1.129E-03	1.374	1.930E-08	2.140E-04	2.564	5.600E-06	0.17	1.820E-03
	15	1.186E-08	9.359E-04	1.576	1.746E-08	2.140E-04	2.321	7.800E-06	0.15	2.210E-03
	18	1.006E-08	9.147E-04	1.337	1.950E-08	2.140E-04	2.591	5.800E-06	0.18	2.120E-03
	24	1.050E-08	9.755E-04	1.396	1.988E-08	2.140E-04	2.642	4.800E-06	0.2	2.720E-03
	26	1.110E-08	8.901E-04	1.475	1.806E-08	2.140E-04	2.400	7.000E-06	0.18	2.320E-03
	27	9.768E-09	1.012E-03	1.298	2.017E-08	2.140E-04	2.680	4.900E-06	0.18	2.330E-03
	28	1.205E-08	1.045E-03	1.601	1.845E-08	2.140E-04	2.451	7.600E-06	0.19	2.330E-03
	30	9.684E-09	1.044E-03	1.287	2.027E-08	2.140E-04	2.694	5.100E-06	0.2	1.720E-03
	31	1.251E-08	8.370E-04	1.662	1.719E-08	2.140E-04	2.284	7.000E-06	0.17	2.960E-03
	32	1.020E-08	1.113E-03	1.356	1.870E-08	2.140E-04	2.484	3.800E-06	0.2	2.440E-03
	36	9.662E-09	1.293E-03	1.284	1.978E-08	2.140E-04	2.628	5.900E-06	0.18	1.480E-03
	37	1.142E-08	9.395E-04	1.518	1.843E-08	2.140E-04	2.450	9.000E-06	0.16	2.240E-03
	38	1.269E-08	8.372E-04	1.686	1.721E-08	2.140E-04	2.287	7.700E-06	0.18	1.600E-03

	40	1.051E-08	9.146E-04	1.396	1.905E-08	2.140E-04	2.531	5.400E-06	0.19	2.000E-03
195	2	1.152E-08	8.491E-04	1.530	1.547E-08	2.140E-04	2.056	4.400E-06	0.17	2.490E-03
	3	1.101E-08	8.000E-04	1.463	1.443E-08	2.140E-04	1.918	7.300E-06	0.1	2.380E-03
	5	9.632E-09	8.000E-04	1.280	1.532E-08	2.140E-04	2.036	6.300E-06	0.12	2.390E-03
	6	9.618E-09	8.000E-04	1.278	1.429E-08	2.140E-04	1.899	3.500E-06	0.15	2.720E-03
	7	1.131E-08	8.187E-04	1.503	1.395E-08	2.140E-04	1.854	6.700E-06	0.15	3.120E-03
	8	1.011E-08	8.000E-04	1.344	1.491E-08	2.140E-04	1.982	4.600E-06	0.14	2.000E-03
	11	1.156E-08	8.000E-04	1.536	1.349E-08	2.140E-04	1.793	4.300E-06	0.17	3.780E-03
	12	1.008E-08	8.000E-04	1.340	1.496E-08	2.140E-04	1.987	4.800E-06	0.16	3.260E-03
	19	1.067E-08	9.056E-04	1.418	1.488E-08	2.140E-04	1.978	5.300E-06	0.17	2.670E-03
	21	1.076E-08	8.485E-04	1.431	1.398E-08	2.140E-04	1.857	5.000E-06	0.15	2.530E-03
	22	9.975E-09	9.528E-04	1.326	1.495E-08	2.140E-04	1.987	5.300E-06	0.16	2.530E-03
	25	1.021E-08	8.000E-04	1.357	1.611E-08	2.140E-04	2.141	4.400E-06	0.18	2.220E-03
	30	1.100E-08	8.000E-04	1.461	1.413E-08	2.140E-04	1.878	4.000E-06	0.19	3.280E-03
	32	1.008E-08	9.325E-04	1.340	1.525E-08	2.140E-04	2.026	5.500E-06	0.15	3.120E-03
	35	1.146E-08	8.071E-04	1.524	1.419E-08	2.140E-04	1.886	6.400E-06	0.15	2.560E-03
	39	1.056E-08	8.784E-04	1.403	1.487E-08	2.140E-04	1.976	7.000E-06	0.14	2.180E-03
	$\bar{x}$	**1.079E-08**	9.257E-04	1.433						
	$\bar{x} \pm$	**6.983E-10**	1.024E-04	0.092						

Tab.6.20: 2-component fit for calculating ACTH response to 10nM CRH (2 h) after 114 h

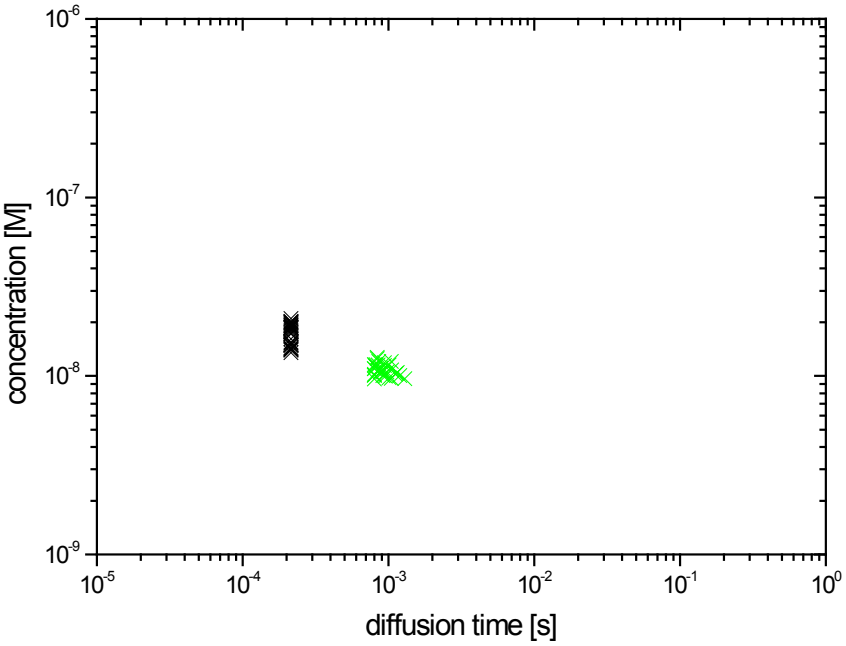

Fig. 6.16: Concdiff-plot of 2-component fit to 10nM CRH (2 h) after 114 h

172	2fit	c_2	t_2	p_2	c_1	t_1	p_1	tauT	Triplet	chi²
	#	[M]	[s]		[M]	[s]		[s]		
	3	1.102E-08	9.367E-04	1.464	2.204E-08	2.370E-04	2.930	6.200E-06	0.16	1.930E-03
	9	1.053E-08	1.109E-03	1.399	2.184E-08	2.370E-04	2.902	6.100E-06	0.18	2.230E-03
	11	1.131E-08	1.164E-03	1.503	2.035E-08	2.370E-04	2.704	8.600E-06	0.15	2.570E-03
	19	1.206E-08	9.679E-04	1.603	1.876E-08	2.370E-04	2.493	7.100E-06	0.14	2.030E-03
	27	1.115E-08	1.018E-03	1.482	2.162E-08	2.370E-04	2.874	5.300E-06	0.15	2.360E-03
	28	1.047E-08	1.138E-03	1.392	2.247E-08	2.370E-04	2.986	6.600E-06	0.17	1.610E-03
	30	1.212E-08	9.425E-04	1.611	1.996E-08	2.370E-04	2.652	6.700E-06	0.14	1.940E-03
	31	1.191E-08	1.025E-03	1.583	2.175E-08	2.370E-04	2.890	5.900E-06	0.17	1.670E-03
	38	1.140E-08	1.105E-03	1.515	2.175E-08	2.370E-04	2.891	5.300E-06	0.16	2.150E-03
	$\bar{x}$	**1.138E-08**	1.033E-03	1.512						
	$\bar{x} \pm$	**4.800E-10**	7.687E-05	0.064						

Tab.6.21: 2-component fit for calculating ACTH response to 10nM CRH (22 h) after 136 h

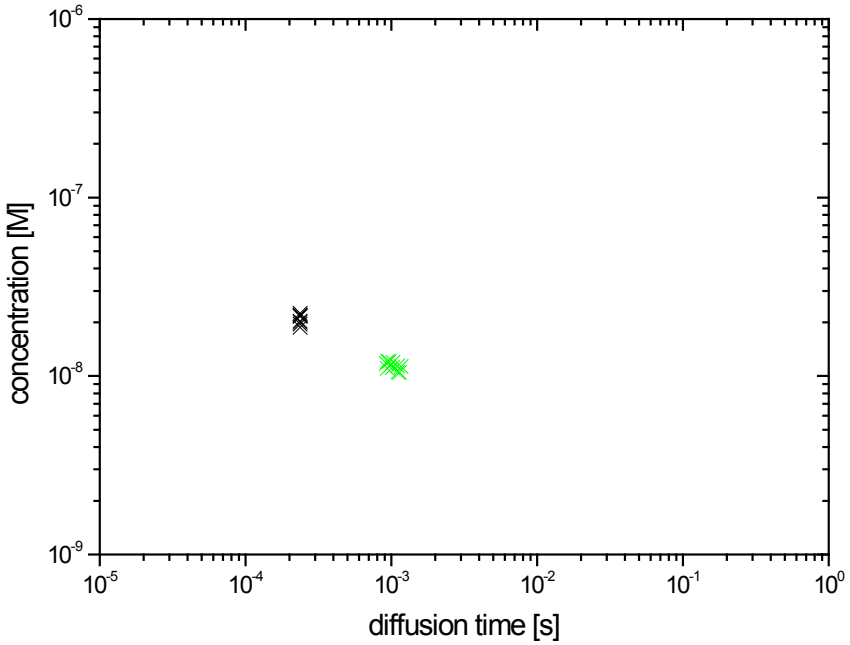

Fig. 6.17: Concdiff-plot of 2-component fit to 10nM CRH (22 h) after 136 h

206	2fit	c_2	t_2	p_2	c_1	t_1	p_1	tauT	Triplet	chi²
	#	[M]	[s]		[M]	[s]		[s]		
	5	1.116E-08	8.865E-04	1.483	1.793E-08	2.140E-04	2.382	4.500E-06	0.17	2.240E-03
	6	1.082E-08	1.164E-03	1.438	1.769E-08	2.140E-04	2.351	8.600E-06	0.16	1.770E-03
	7	1.006E-08	1.054E-03	1.337	1.811E-08	2.140E-04	2.406	4.200E-06	0.2	1.680E-03
	8	1.005E-08	9.367E-04	1.336	1.812E-08	2.140E-04	2.408	2.900E-06	0.2	2.650E-03

10	1.000E-08	1.084E-03	1.330	1.861E-08	2.140E-04	2.473	3.800E-06	0.19	2.200E-03
11	1.129E-08	1.007E-03	1.500	1.771E-08	2.140E-04	2.353	6.800E-06	0.18	2.650E-03
13	1.072E-08	9.169E-04	1.424	1.782E-08	2.140E-04	2.368	5.400E-06	0.15	2.010E-03
16	1.003E-08	1.099E-03	1.332	1.867E-08	2.140E-04	2.482	5.900E-06	0.14	1.600E-03
17	1.126E-08	9.278E-04	1.496	1.806E-08	2.140E-04	2.400	5.600E-06	0.16	2.550E-03
19	1.141E-08	8.735E-04	1.517	1.780E-08	2.140E-04	2.366	6.100E-06	0.16	1.620E-03
21	1.119E-08	1.032E-03	1.487	1.715E-08	2.140E-04	2.279	5.500E-06	0.18	2.370E-03
22	9.423E-09	1.029E-03	1.252	1.994E-08	2.140E-04	2.649	5.100E-06	0.16	2.160E-03
27	9.976E-09	9.782E-04	1.326	1.971E-08	2.140E-04	2.620	3.700E-06	0.2	3.140E-03
36	1.025E-08	1.187E-03	1.362	1.927E-08	2.140E-04	2.561	5.700E-06	0.14	2.250E-03
$\bar{x}$	**1.055E-08**	1.013E-03	1.401						
$\bar{x} \pm$	**5.758E-10**	8.017E-05	0.076						

Tab.6.22: 2-component fit for calculating ACTH response to 5nM CRH (22 h) after 114 h

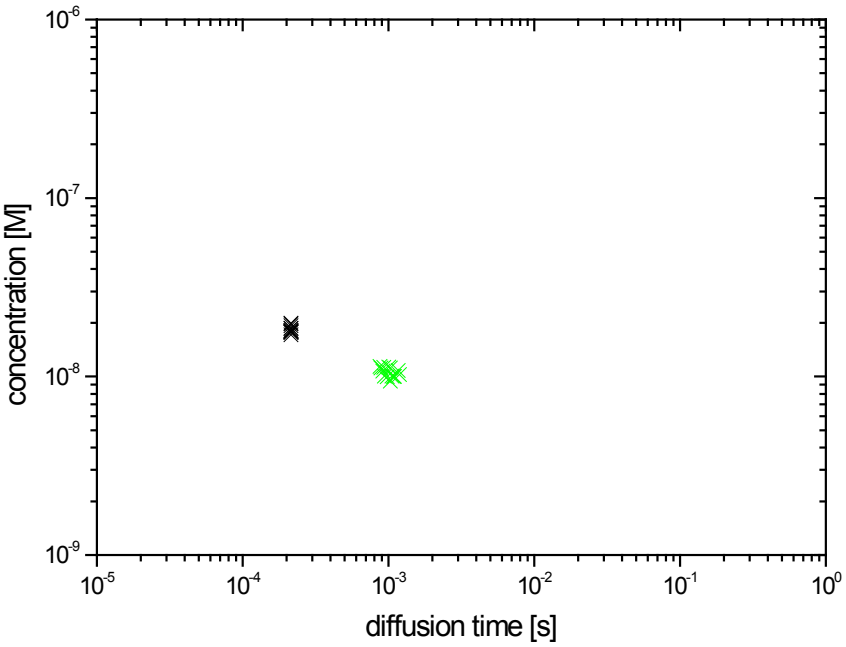

Fig. 6.18: Concdiff-plot of 2-component fit to 5nM CRH (22 h) after 114 h

2fit	c_2	t_2	p_2	c_1	t_1	p_1	tauT	Triplet	chi²
#	[M]	[s]		[M]	[s]		[s]		
3	1.166E-08	9.757E-04	1.549	1.785E-08	2.140E-04	2.372	8.300E-06	0.18	1.70E-03
4	1.130E-08	9.769E-04	1.502	1.765E-08	2.140E-04	2.346	7.400E-06	0.16	1.68E-03
9	1.019E-08	1.135E-03	1.354	1.782E-08	2.140E-04	2.368	4.900E-06	0.17	1.77E-03
11	1.053E-08	9.105E-04	1.399	1.811E-08	2.140E-04	2.407	6.000E-06	0.17	2.51E-03
13	9.982E-09	1.211E-03	1.327	1.743E-08	2.140E-04	2.317	6.100E-06	0.16	2.16E-03

21	9.308E-09	1.084E-03	1.237	1.843E-08	2.140E-04	2.449	3.700E-06	0.18	3.37E-03
24	1.029E-08	1.017E-03	1.367	1.774E-08	2.140E-04	2.358	8.100E-06	0.16	1.99E-03
25	1.165E-08	8.731E-04	1.549	1.717E-08	2.140E-04	2.281	7.200E-06	0.16	1.78E-03
35	1.116E-08	8.477E-04	1.484	1.860E-08	2.140E-04	2.471	6.000E-06	0.17	1.74E-03
37	1.109E-08	9.920E-04	1.473	1.769E-08	2.140E-04	2.351	8.400E-06	0.16	1.87E-03
39	9.824E-09	9.266E-04	1.305	1.841E-08	2.140E-04	2.447	4.800E-06	0.18	3.84E-03
$\bar{x}$	**1.063E-08**	9.954E-04	1.413						
$\bar{x} \pm$	**6.701E-10**	8.461E-05	0.089						

Tab.6.23: 2-component fit for calculating ACTH response to 10nM CRH (22 h) after 114 h

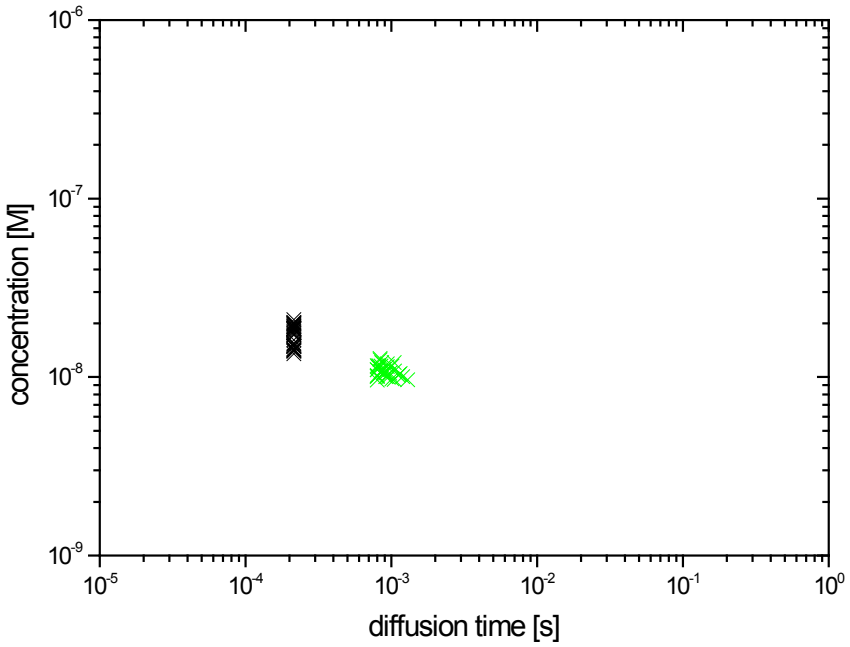

Fig. 6.19: Concdiff-plot of 2-component fit to 10nM CRH (22 h) after 114 h

2fit	c_2	t_2	p_2	c_1	t_1	p_1	tauT	Triplet	chi²
#	[M]	[s]		[M]	[s]		[s]		
3	9.141E-09	1.403E-03	1.215	2.000E-08	2.140E-04	2.658	3.800E-06	0.14	2.640E-03
4	1.088E-08	9.243E-04	1.446	1.777E-08	2.140E-04	2.362	4.500E-06	0.17	2.500E-03
5	1.007E-08	1.105E-03	1.338	1.875E-08	2.140E-04	2.492	5.800E-06	0.15	1.890E-03
14	9.368E-09	1.095E-03	1.245	2.060E-08	2.140E-04	2.738	5.400E-06	0.15	2.090E-03
15	1.025E-08	1.002E-03	1.362	1.886E-08	2.140E-04	2.506	4.200E-06	0.18	2.140E-03
17	1.093E-08	1.021E-03	1.453	1.831E-08	2.140E-04	2.434	4.400E-06	0.17	2.020E-03
20	1.050E-08	1.177E-03	1.396	1.902E-08	2.140E-04	2.528	4.400E-06	0.17	2.930E-03
21	1.079E-08	1.290E-03	1.434	1.829E-08	2.140E-04	2.431	6.600E-06	0.14	2.440E-03
22	9.971E-09	1.428E-03	1.325	1.985E-08	2.140E-04	2.637	6.600E-06	0.15	2.460E-03

204

24	9.987E-09	1.022E-03	1.327	1.799E-08	2.140E-04	2.391	4.200E-06	0.17	2.240E-03
27	9.444E-09	1.195E-03	1.255	1.907E-08	2.140E-04	2.534	4.500E-06	0.15	1.770E-03
29	1.135E-08	1.013E-03	1.508	1.780E-08	2.140E-04	2.366	7.300E-06	0.15	1.900E-03
31	9.183E-09	1.177E-03	1.220	1.983E-08	2.140E-04	2.635	5.600E-06	0.14	1.860E-03
32	1.105E-08	1.179E-03	1.468	1.795E-08	2.140E-04	2.385	5.500E-06	0.15	2.010E-03
34	1.034E-08	9.087E-04	1.373	1.915E-08	2.140E-04	2.545	5.100E-06	0.17	2.370E-03
37	9.438E-09	1.352E-03	1.254	2.004E-08	2.140E-04	2.663	7.600E-06	0.13	2.200E-03
39	9.981E-09	1.333E-03	1.326	1.859E-08	2.140E-04	2.470	6.200E-06	0.17	1.830E-03
$\bar{x}$	**1.016E-08**	1.154E-03	1.350						
$\bar{x} \pm$	**5.685E-10**	1.346E-04	0.076						

Tab.6.24: 2-component fit for calculating ACTH response to 36nM CRH (22 h) after 114 h

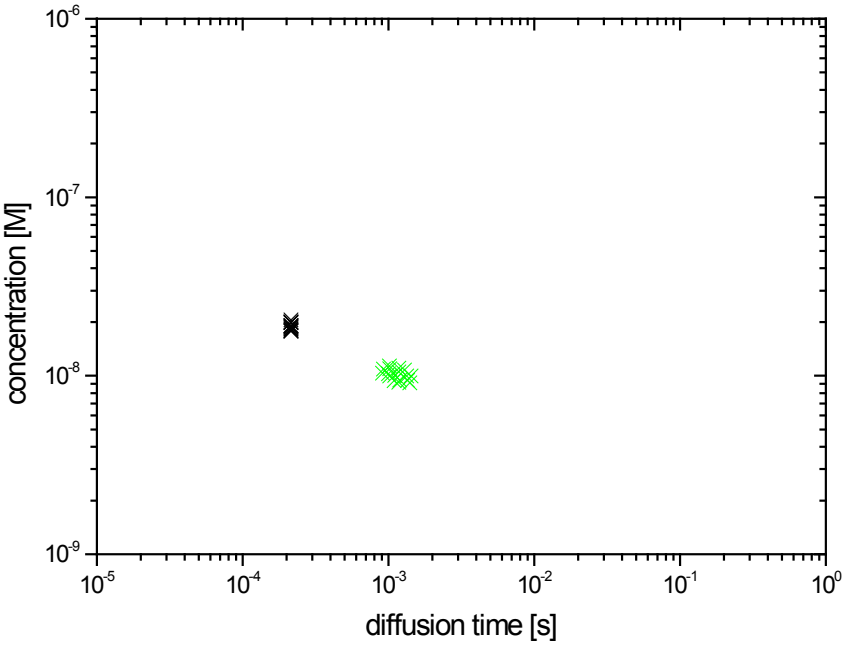

Fig. 6.20: Concdiff-plot of 2-component fit to 36nM CRH (22 h) after 114 h

2fit	c_2	t_2	p_2	c_1	t_1	p_1	tauT	Triplet	chi²
#	[M]	[s]		[M]	[s]		[s]		
1	9.823E-09	1.088E-03	1.305	1.987E-08	2.140E-04	2.641	4.300E-06	0.17	1.590E-03
2	1.030E-08	1.149E-03	1.369	1.930E-08	2.140E-04	2.564	6.200E-06	0.17	1.560E-03
3	8.729E-09	1.107E-03	1.160	1.937E-08	2.140E-04	2.574	4.400E-06	0.17	1.870E-03
5	9.222E-09	1.139E-03	1.225	1.836E-08	2.140E-04	2.441	3.900E-06	0.18	2.730E-03
6	1.034E-08	1.150E-03	1.375	1.735E-08	2.140E-04	2.305	6.400E-06	0.15	1.960E-03
13	8.777E-09	1.095E-03	1.166	1.849E-08	2.140E-04	2.457	4.300E-06	0.17	1.920E-03
15	9.742E-09	9.149E-04	1.295	1.696E-08	2.140E-04	2.254	3.400E-06	0.16	2.160E-03

17	9.174E-09	1.038E-03	1.219	1.886E-08	2.140E-04	2.507	4.100E-06	0.18	2.610E-03
18	8.349E-09	1.277E-03	1.109	2.027E-08	2.140E-04	2.693	4.100E-06	0.18	1.750E-03
19	1.203E-08	8.636E-04	1.598	1.702E-08	2.140E-04	2.261	7.700E-06	0.15	1.590E-03
20	8.078E-09	1.328E-03	1.073	1.942E-08	2.140E-04	2.581	3.300E-06	0.18	2.340E-03
21	1.167E-08	8.000E-04	1.550	1.673E-08	2.140E-04	2.223	6.200E-06	0.16	2.120E-03
24	9.977E-09	1.006E-03	1.326	1.781E-08	2.140E-04	2.366	7.400E-06	0.14	2.160E-03
26	8.726E-09	1.316E-03	1.160	1.960E-08	2.140E-04	2.605	3.200E-06	0.2	2.510E-03
27	9.253E-09	1.089E-03	1.230	1.897E-08	2.140E-04	2.522	5.800E-06	0.16	2.040E-03
28	1.048E-08	8.882E-04	1.392	1.916E-08	2.140E-04	2.547	3.300E-06	0.21	2.670E-03
29	1.067E-08	9.263E-04	1.418	1.745E-08	2.140E-04	2.319	6.500E-06	0.16	2.030E-03
31	8.657E-09	1.272E-03	1.150	1.953E-08	2.140E-04	2.595	4.000E-06	0.2	2.020E-03
33	9.765E-09	1.015E-03	1.298	1.870E-08	2.140E-04	2.485	6.400E-06	0.15	2.270E-03
36	9.668E-09	1.187E-03	1.285	1.898E-08	2.140E-04	2.523	4.900E-06	0.17	3.010E-03
37	8.074E-09	1.507E-03	1.073	1.847E-08	2.140E-04	2.454	3.200E-06	0.18	2.180E-03
38	1.113E-08	8.494E-04	1.479	1.670E-08	2.140E-04	2.220	4.200E-06	0.19	2.690E-03
$\bar{x}$	**9.665E-09**	1.091E-03	1.284						
$\bar{x} \pm$	**8.739E-10**	1.386E-04	0.116						

Tab.6.25: 2-component fit for calculating ACTH response to 54nM CRH (22 h) after 114 h

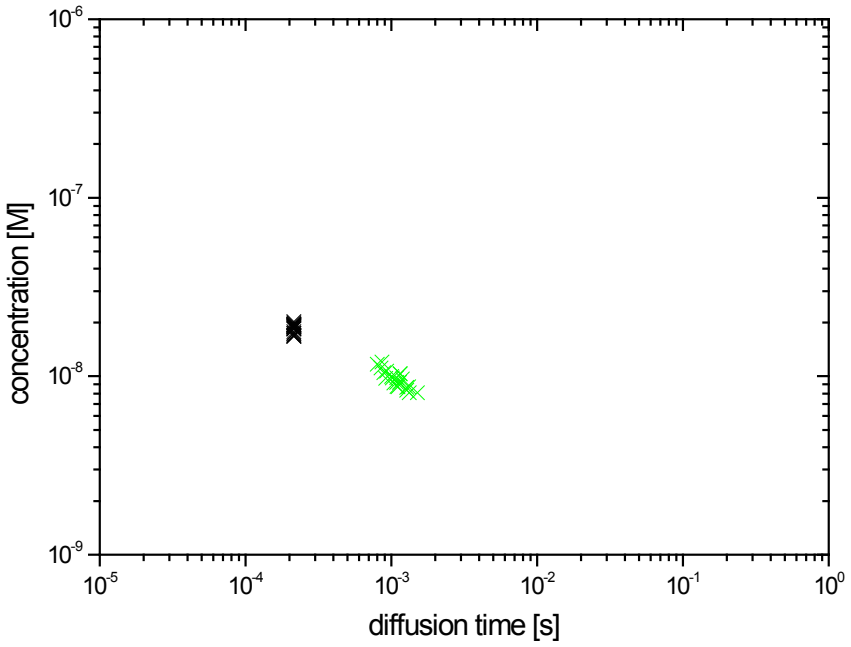

Fig. 6.21: Concdiff-plot of 2-component fit to 54nM CRH (22 h) after 114 h

7 References

HPA-axis

[1] Antoni MH, Lutgendorf SK, Cole SW, Dhabhar FS, Sephton SE, McDonald PG, Stefanek M, and Sood AK (2006): The influence of bio-behavioural factors on tumour biology: pathways and mechanisms. *Nat Rev Cancer*, 6:240-248

[2] Arbiser JL, Morton CC, Bruns GA, and Majzoub JA (1988): Human corticotropin releasing hormone gene is located on the long arm of chromosome 8. *Cytogenet Cell Genet*, 47(3):113-6

[3] Bloomquist BT, Eipper BA, Mains RE (1991): Prohormone-converting enzymes: regulation and evaluation of function using anti-sense RNA. *Mol Endocrinol*, 5:2014–2024

[4] Buckingham JC (2006): Glucocorticoids: exemplars of multi-tasking. *Br J Pharmacol*, 147:258-268

[5] Buckingham JC, Christian HC, Gillies GE, Philip JG, and Taylor AD (1996): The hypothalamo-pituitary-adrenocortical immune axis. *Published in: The Physiology of Immunity,* eds. Kendall MD, and Marsh JA, p 331-354, *CRC Press Inc*, ISBN 0-8493-8033-2

[6] Carter AM, Homan J, Fraser M, Richardson BS, and Challis JR (1995): Inhibition of ACTH secretion blocks hypoxia-induced increase of adrenal cortical blood flow in fetal sheep. *Am J Physiol Endocrinol Metab*, 269(3):598-604

[7] Chrousos GP (2009): Stress and disorders of the stress system. *Nat Rev Endocrinol*, 5:374-381

[8] Crine P, Gianoulakis C, Seidah NG, Grossand F, Pezalla PD, Lis M, Chretien M (1978): Biosynthesis of β-endorphin from β-lipotropin and a larger molecular weight precursor in rat pars intermedia. *Proc Natl Acad Sci USA*, 75:4719–4722

[9] Giordano R, Picu A, Broglio F, Bonelli L, Baldi M, Berardelli R, Ghigo E, and Arvat E (2004): Ghrelin, hypothalamus-pituitary-adrenal (HPA) axis and Cushing's syndrome. *Pituitary*, 7(4):243-248

[10] Guillemin R, and Rosenberg B (1955): Humoral hypothalamic control of anterior pituitary: a study with combined tissue cultures. *J Endocrinol*, 57:599-607

[11] Habib KE, Gold PW, and Chrousos GP (2001): Neuroendocrinology of stress. *Endocrinol Metab Clin North Am*, 30:695-728

[12] Heaney AP, Melmed S (2004): Molecular targets in pituitary tumours. *Nat Rev Cancer*, 4:285-295

[13] Henley DE, Russell GM, Douthwaite JA, Wood SA, Buchanan F, Gibson R, Woltersdorf WW, Catterall JR, and Lightman SL (2009): Hypothalamic-Pituitary-Adrenal Axis Activation in Obstructive Sleep Apnea: The Effect of Continuous Positive Airway Pressure Therapy. *J Clin Endocrinol Metab*, 94(11):4234-4242

[14] Iwasaki Y, Aoki Y, Katahira M, Oiso Y, and Saito H (1997): Non-genomic Mechanisms of Glucocorticoid Inhibition of Adrenocorticotropin Secretion: Possible Involvement of GTP-Binding Protein. *Biochem Biophys Res Commun*, 235:295-299

[15] Kallen VL, Tulen JH, Utens EM, Treffers PD, De Jong FH, Ferdinand RF (2008): Associations between HPA axis functioning and level of anxiety in children and adolescents with an anxiety disorder. *Depress Anxiety*, 25(2):131-141

[16] Lowry PJ (1984): Pro-opiocortin: The multiple hormone precursor. *Biosci Rep*, 4:467

[17] Li CH, Geschwind II, Cole RD, Raacke ID, Harris JI, and Dickson JS (1955): Amino-Acid Sequence of Alpha-Corticotropin. *Nature*, 176:687-689

[18] Lupien SJ, McEwen BS, Gunnar MR, Heim C (2009): Effects of stress throughout the lifespan on the brain, behaviour and cognition. *Nature Rev Neuroscience*, 10:434-445

[19] Mains RE, Alam MR, Johnson RC, Darlington DN, Back N, Hand TA, and Eipper BA (1999): Kalirin, a multifunctional PAM COOH-terminal domain interactor protein, affects cytoskeletal organization and ACTH secretion from AtT-20 cells. *J Biol Chem*, 274:2929-2937

[20] Marsh JA, Kendall MD (1996): The Physiology of Immunity. *CRC Press*, ISBN 0-8493-8033-2

[21] Nobel Lectures: Physiology or Medicine 1942-1962, *Elsevier Publishing Company*, Amsterdam, 1964

[22] 1950 Nobel Prize for Medicine. *J Am Med Assoc*, 144(10):849, 1950

[23] Papadimitriou A, and Priftis KN (2009): Regulation of the Hypothalamic-Pituitary-Adrenal Axis. *Neuroimmuno Modul*, 16:265-271

[24] Park JJ, and Loh YP (2008): Minireview: How Peptide Hormone Vesicles Are Transported to the Secretion Site for Exocytosis. *Mol Endocrinol*, 22(12):2583-2595

[25] Peeters PJ, Göhlmann HW, Van den Wyngaert I, Swagemakers SM, Bijnens L, Kass SU, and Steckler T (2004): Transcriptional Response to Corticotropin-Releasing Factor in AtT-20 Cells. *Mol Pharmocol*, 66:1083-1092

[26] Raisman G (1997) An urge to explain the incomprehensible: Geoffrey Harris and the discovery of the neural control of the pituitary gland. *Ann Rev Neurosci*, 20:533-566

[27] Reeds DA, Hepburn PJ, McNicol AM, Francis K, Jasani B, Farrell WE, Lewis BM, Scanlon MF, and Ham J (2002): Loss of ACTH expression in cultured human corticotroph macroadenoma cells is consistent with loss of the POMC gene signal sequence. *Mol Cell Endocrinol*, 189:51-57

[28] Reisch N, Slawik M, Zwermann O, Beuschlein F, and Reinke M (2005): Genetic influence of an ACTH receptor promotor polymorphism on adrenal androgen secretion. *Eur J Endocrinol*, 153(5):711-715

[29] Saffran M, and Schally AV (1955): The release of corticotrophin by anterior pituitary tissue in vitro. *Can J Biochem Physiol*, 33:408-415

[30] Seasholtz A (2000): Regulation of adrenocorticotropic hormone secretion: lessions from mice deficient in corticotropin-releasing hormone. *J Clin Invest*, 105(9):1269-77

[31] Silva AP, Schoeffter P, Weckbecker G, Bruns C, and Schmid HA (2005): Regulation of CRH-induced secretion of ACTH and corticosterone by SOM230 in rats. *Eur J Enodcrinol*, 153:R7-R10

[32] Smith PE, and Smith IP (1922): The repair and activation of the thyroid in the hypophysectomised tadpole by the parenteral administration of fresh anterior lobe of the bovine hypophysis. *J Med Res*, 43(3):267-284

[33] Sternberg EM (2006): Neural regulation of innate immunity: a coordinated nonspecific host response to pathogens. *Nat Rev Immunol*, 6:318-328

[34] Swanwick GRJ, Kirby M, Bruce I, Buggy F, Coen RF, Coakley D, and Lawlor BA (1998): Hypothalamic-Pituitary-Adrenal Axis Dysfunction in Alzheimer's Disease: Lack of Association Between Longitudinal and Cross-Sectional Findings. *Am J Psychiatry*, 155:286-289

[35] Tangalakis K, Roberts FE, and Wintour EM (1991): The time-course of ACTH stimulation of cortisol synthesis by the immature ovine foetal adrenal gland. *J Steroid Biochem Mol Biol*, 42(5):527-532

[36] Tooze J, and Tooze SA (1986): Clathrin-coated Vesicular Transport of Secretory Proteins during the Formation of ACTH-containing Secretory Granules in AtT20 cells. *J Cell Biol*, 103:839-850

[37] Vale W, Spiess J, Rivier C, and Rivier J (1981): Characterization of a 41-residue ovine hypothalamic peptide that stimulates secretion of corticotropin and ß-endorphin. *Science*, 213:1394-1397

[38] Van den Bergh BRH, Van Calster B, Smits T, Van Huffel S, and Lagae L (2008): Antenatal Maternal Anxiety is Related to HPA-Axis Dysregulation and Self-Reported Depressive Symptoms in Adolescence: A Prospective Study on the Fetal Origins of Depressed Mood. *Neuropsychopharmacology*, 33:536-545

[39] Veldhuis JD, Iranmanesh A, Johnson ML, and Lizarralde G (1991): Amplitude, but not Frequency, Modulation of Adrenocorticotropin Secretory Bursts Gives Rise to the Nyctohemeral Rhythm of the Corticotropic Axis in Man. *J Clin Endocrinol Metab*, 71(2):452-463

[40] Woods MD, Shipston MJ, Mullens EL, and Antoni FA (1992): Pituitary Coricotrope Tumor (AtT20) Cells as a Model System for the Study of Early Inhibition by Glucocorticoids. *J Endocrinol*, 131:2873-2880.

[41] Yasamura Y (1968): Retention of differentiated function in clonal animal cell lines, particularly hormone-secreting cultures. *Am Zool*, 8:285-305

Applications of FCS

[42] Al-Soufi W, Reija B, Felekyan S, Seidel C, and Novo M (2008): Dynamics of Supramolecular Association Monitored by Fluorescence Correlation Spectroscopy. *ChemPhysChem*, 9:1819-1827

[43] Brandtzaeg P (1975): Rhodamine conjugates. Specific and non-specific binding properties in immunohistochemistry. *Ann. N.Y. Acad. Sci.*, 254:35-53

[44] Dong C, Zhang P, and Ren J (2008): Characterization of solution-phase DNA hybridization by fluorescence correlation spectroscopy: Rapid genotyping of C677T from methylenetetrahydrofolate reductase gene. *Talanta*, 71(3):1192-1197

[45] Haustein E, and Schwille P (2003): Ultrasensitive investigations of biological systems by fluorescence correlation spectroscopy. *Methods,* 29:153–166.

[46] Hess ST, Huang SH, Heikal AA, and Webb WW (2002): Biological and chemical applications of fluorescence correlation spectroscopy: A review. *Biochem,* 41:697–705.

[47] Magde D, Elson E, and Webb WW (1972): Thermodynamic Fluctuations in a Reacting System – Measurement by Fluorescence Correlation Spectroscopy. *Phys Rev Lett*, 29:705-708

[48] Maier C, Rünzler D, Schindelar J, Grabner G, Waldhäusl W, Köhler G, and Luger A (2005): G-protein-coupled glucocorticoid receptors on the pituitary cell membrane. *J Cell Sci*, 118(15):3353-3361.

[49] Maier C, Rünzler D, Wagner L, Grabner G, Köhler G, and Luger A (2002): Evidence of Specific Glucocorticoid Binding Sites on the Cell Membrane by Fluorescence Correlation Spectroscopy. *Single Mol*, 3(4):211-216.

[50] Maiti S, Haupts U, and Webb WW (1997): Fluorescence correlation spectroscopy: Diagnostics for sparse molecules. *Proc Natl Acad Sci USA*, 94:11753-11757.

[51] Politz JC, Browne ES, Wolf DE, and Pederson T (1998): Intranuclear diffusion and hybridization state of oligonucleotides measured by fluorescence correlation spectroscopy in living cells. *Proc Natl Acad Sci USA*, 95:6043-6048

[52] Schwille P, Haupts U, Maiti S, and Webb WW (1999): Molecular dynamics in living cells observed by fluorescence correlation spectroscopy with one- and two-photon excitation. *Biophys J*, 77:2251-2265.

[53] Schwille P, and Haustein E (2002): Fluorescence Correlation Spectroscopy: An Introduction to its Concepts and Applications. *A tutorial for the Biophysics Textbook*, http://www.biophysics.org/education/schwille.pdf

[54] Shahzad A, Köhler G, Knapp M, Gaubitzer E, Puchinger M, and Edetsberger M (2009): Emerging applications of fluorescence spectroscopy in medical microbiology field. *J Transl Med,* 7(1):99

Mathematical Modelling

[55] Gonzalez-Heydrich J, Steingard RJ, and Kohane I (1994): A computer simulation of the hypothalamic-pituitary-adrenal axis. *Proc Annu Symp Comput Appl Med Care*, p 1010

[56] Gupta S, Aslakson E, Gurbaxani BM, and Vernon SD (2007): Inclusion of the glucocorticoid receptor in a hypothalamic pituitary adrenal axis model reveals bistability. *Theor Biol Med Modell*, 4:8

[57] Lu J, Engl HW, and Schuster P (2006): Inverse bifurcation analysis: application to simple gene systems. *Algorithms for Molecular Biology*, 1(1):11.

[58] Savic D (2005): A mathematical model of the hypothalamo-pituitary-adrenocortical system and its stability analysis. *Chaos, solutions, and fractals*, 26:427-436

[59] Zarzer CA (2009): On Tikhonov regularization with non-convex sparsity constraints. *Inverse Prob*, 25:025006

Books

[60] Abbas AK, Lichtman AH, and Pillai S (2007): Cellular and Molecular Immunology. *Saunders*, 6th edition, ISBN 1-4160-3122-7

[61] Bear MF, Connors BW, and Paradiso MA (2006): Neuroscience: Exploring the Brain. *Lippincott Williams & Wilkins*, 3rd edition, ISBN 0-7817-6003-8

[62] Gell G, Brockwell D, and Smith A (2006): Handbook of Single Molecule Fluorescence Spectroscopy, *Oxford University Press*, 1st edition, ISBN 0-19-852942-2

[63] Hart H, Craine LE, and Hart DJ (1999): Organische Chemie. *Wiley-VCH*, 2nd edition, ISBN 3-527-30379-0

[64] Lakowicz JR (2006): Principles of Fluorescence Spectroscopy. *Springer*, 3rd edition, ISBN 0-387-31278-1

[65] Metzler DE (2001): Biochemistry – The Chemical Reactions of Living Cells, Volumes 1 and 2, *Academic Press*, 2nd edition, ISBN 0-12-492543-X

[66] Nussey S, Whitehead S, and Whitehead W (2001): Endocrinology: An Integrated Approach. *Informa Healthcare*, 1st edition, ISBN 1-85996-252-1

[67] Rigler R, Orrit M, and Basche T (2002): Single molecule spectroscopy, *Springer*, 1st edition, ISBN 3-54042453-9

[68] Rohatgi-Mukherjee KK (1986): Fundamentals of Photochemistry, *New Age International Publishers*, 2nd edition, ISBN 0-85226-784-3

[69] Widmaier EP, Raff H, and Strang KT (2005): Vander's Human Physiology: The Mechanisms of Body Function, *McGraw-Hill Science*, 10th edition, ISBN 0-07-312286-6

8 Abbreviations

A	absorbance
ACTH	adrenocorticotropic hormone, corticotrophin
Ar	argon
ATCC	American Type Culture Collection
AtT-20	mouse pituitary tumor cell line
c	concentration
C_H	constant domain of the heavy immunoglubulin chain
C_L	constant domain of the light immunoglobulin chain
C-term.	carboxyl terminal
CF	correction factor
CNS	central nervous system
CRH	corticotropin releasing hormone
°C	degree Celsius
d	distance, optical path length
DMEM	Dulbecco's Modified Eagle's Medium
Da	Dalton
e.g.	exempli gratia, for example
ELISA	Enzyme-linked Immunosorbent Assay
Em	emission
Ex	extinction
et al.	et alii, and others
ε	extinction coefficient [$M^{-1}cm^{-1}$]
FBS	fetal bovine serum
FCS	Fluorescence Correlation Spectroscopy
Fig.	figure
FSH	follicle-stimulating hormone
g	gram
x*g*	n times gravity
G (τ)	autocorrelation function

GH	growth hormone, somatotropin
h	hour
HAT	hypoxanthine and thymidine
HPA	hypothalamic-pituitary-adrenal
I	intensity of the absorbed light
I_0	intensity of the initial light beam
IgG	immunoglobulin G
k-	kilo [10^3]
l	litre
LAF_1	mouse cell line
LH	luteinizing hormone
µ-	micro [10^{-6}]
m	metre
m-	milli [10^{-3}]
min	minutes
M	molarity [mol l^{-1}]
MW	molecular weight
n-	nano [10^{-9}]
NHS	N-hydroxysuccinimide
N-term.	amino terminal
PBS	phosphate buffered saline
PCR	polymerase chain reaction
POMC	proopiomelanocortin
rER	rough endoplasmatic reticulum
rcf	relative centrifugal force
rpm	revolutions per minute, centrifuge rotor speed
s	second
Tab.	table
TSH	thyroid-stimulating hormone, thyrotropin
V	volume
V_H	variable domain of the heavy immunoglubulin chain
V_L	variable domain of the light immunoglubulin chain

9 Index of Figures

10 Index of Tables

11 Synopsis

Through important instrumental improvements in the last decades Fluorescence Correlation Spectroscopy (FCS) has become a powerful tool for studying supramolecular associations, DNA hybridization reactions, etc. However, monitoring and quantifying the real time release of a protein in a cellular reaction network by means of FCS opens a fundamentally new application of FCS, e.g. in the diagnostic field of medical science, and was the aim of our study. For this purpose the HPA axis network, which plays a key role in the endocrine system of humans, was chosen as a model for our studies. In support of this idea the stimulatory effect of CRH on corticotrophin (ACTH) release from adherent AtT-20 pituitaries was analysed. Following the idea of ELISA, a FCS Immunoassay was established for detecting ACTH molecules in solution. *In vitro* real-time release of ACTH into the extracellular space in the stationary phase has shown that CRH-induced stimulation of ACTH secretion run in two phases, an activation of a non-genomic pathway, appearing immediately in a few seconds and minutes after CRH binding to its membrane receptor, and a genomic one, requiring a longer exposure time of CRH. The latter, long-term effect is known to involve an increase in ACTH via the translation of the POMC mRNA, whereas the rapid exocytotic release within seconds and minutes of time is ascribed to a reservoir of ACTH vesicles, already existing directly beneath the cell surface from previous ACTH synthesis. These observations are consistent with previous reports showing the glucocorticoid-induced inhibition of ACTH secretion and thus indicating similar pathways for stimulating and inhibiting factors of ACTH secretion.

The obtained results and the conclusions that could be made demonstrated the single molecule sensitivity of this solution based technique. We have recently shown that FCS is a powerful spectroscopic tool for detecting even smallest amounts of molecules (in the nM and pM range) at a dynamic level and pointed out the advantages of FCS: quicker, more cost-efficient, and more sensitive than commercial fluorescent ELISAs.

12 Synopsis (in German)

Herausragende technische Errungenschaften der letzten Jahrzehnte machten Fluoreszenz Korrelations Spektroskopie (FCS) zu einer immer wichtigeren Analysetechnik für die Untersuchung supramolekularer Assoziationen, DNS Hybridisierungen, etc. Gerade die Sekretionsrate eines Proteins in einem zentralen Netzwerksystem des menschlichen Körpers live zu verfolgen, war Ziel dieser Arbeit und öffnet einen neuen Anwendungsbereich für FCS, beispielsweise in der medizinischen Diagnostik zur Detektion spezieller Tumor-Marker. Als zentrales Netzwerksystem wurde für diese Arbeit die Hypothalamus-Hypophyse-Nebennieren (HPA) Achse ausgewählt, der eine Schlüsselrolle im endokrinen Kreislaufsystem bzw. bei endokrinen Erkrankungen des Menschen zukommt. Es wurde der stressinduzierende, stimulierende Effekt von CRH auf die Corticotropin (ACTH) Abgabe von AtT-20 Hypophysenzellen analysiert. Mit einer eigens entwickelten und auf dem ELISA Prinzip basierten Methode, dem FCS Immunoassay, konnten mit extremer Genauigkeit ACTH Moleküle in einer Suspension detektiert werden. Die ACTH Ausstoßrate in der stationären Phase *in vitro* wurde in Echtzeit verfolgt und zeigte, dass die CRH-induzierte ACTH Sekretion in 2 Phasen verläuft: der Aktivierung eines non-genomischen Signalweges, welcher innerhalb von Sekunden bis Minuten nach Bindung des CRH Moleküls an dessen Membranrezeptor ausgelöst wird, und dem genomischen Weg, welcher wahrscheinlich erst nach Stunden zur ACTH Sekretion führt. Letzterer führt jedoch zu einer dauerhaften Erhöhung des ACTH Levels durch Translation der POMC mRNA, während die schnelle Exozytose von ACTH in den ersten Sekunden und Minuten auf ein sich direkt unter der Zellmembran befindliches Reservoir an ACTH-Vesikel früherer ACTH Synthesen zurückzuführen ist. Diese Beobachtungen bestätigen frühere Studien, die eine durch Glucocortciode hervorgerufene Hemmung der ACTH Sekretion zeigen und man daher beim ACTH Ausstoß von ähnlichen Signalwegen für stimulierende und inhibierende Faktoren ausgehen kann.

Die erhaltenen Resultate und die daraus abgeleiteten Aussagen zeigen die Sensitivität dieser Technik auf, die sogar kleinste Mengen an Molekülen (im nM- bis pM-Bereich) in einer Lösung nachweisen kann. FCS ist schneller, kostengünstiger und sensitiver als vergleichbare Fluoreszenz-ELISAs und stellt somit eine ernstzunehmende Alternative dar.

13 Curriculum vitae

Particulars

Surname:	**Puchinger**
Christian name:	**Martin Gerald**
Address:	Purkersdorferstraße 24
	A-3100 St. Pölten
e-mail:	martin.puchinger@univie.ac.at
Date of birth:	April 23rd, 1985
Place of birth:	St. Pölten, Austria
Nationality:	Austria
Confession:	Roman-Catholic

University education

01/2010 (intended)	Master of Science in Molecular Biology
09/2009	Participant of the *11th International Conference on Methods and Applications of Fluorescence*, Budapest, Hungary
11/2008 – 01/2010	Diploma Thesis entitled *'Investigation of ACTH response to various stress conditions of mouse AtT-20 pituitaries in vitro by means of Fluorescence Correlation Spectroscopy'* implemented at MFPL Vienna (research group of Prof. Dr. Gottfried Köhler)
07/2008	Participant of the *2nd Residential Summer School on Chemistry and Conservation Science*, Università degli Studi di Palermo, Palermo, Italy
07/2007	Participant of the *1st Residential Summer School on Chemistry and Conservation Science*, Αριστοτελείου Πανεπιστημίου Θεσσαλονίκης (Aristotle University of Thessaloniki), Thessaloniki, Greek
10/2004-01/2010	Molecular Biology at the University of Vienna (with main focus in Structural Biology, Immunology and Molecular Medicine)

Education

06/2003	Secondary school diploma with good success
09/1999 – 06/2003	Secondary school with main focus in scientific education, BORG St. Pölten, Schulring 16
09/1995 – 06/1999	Primary school with main focus in music education, BRG St. Pölten, Schulring 16
09/1991 – 06/1995	Elementary school, St. Pölten-Wagram

Military

10/2003 – 06/2004	Basic military service – as a military scientific expert at the ABC-defence school, Korneuburg, Austria

Publications

11/2009	Shahzad A, Köhler G, Knapp M, Gaubitzer E, Puchinger M, and Edetsberger M (2009): Emerging applications of fluorescence spectroscopy in medical microbiology field. *J Transl Med.* 7(1):99
2009	Puchinger M, Pilch E, and Puchinger L (2009): Investigation of historical seals by means of pyrolysis capillary gas chromatography. *Proceedings 2nd Residential Summer School – Chemistry and Conservation Science 2008. Chem Soc Ital.*, p 215-222, ISBN 978-88-86208-60-4
in press	Shahzad A, Knapp M, Edetsberger M, Puchinger M, Gaubitzer E, and Köhler G (2009): Diagnostic Application of Fluorescence Spectroscopy in Oncology Field: Hopes and challenges. *Appl Spectrosc Rev.*, (in press)

Posters

11/2009	Puchinger M, Zarzer C, and Koehler G (2009): Real time measurement of the release of ACTH from pituitary gland cells as a basis for mathematical signalling of the cellular reaction network. *SAB Meeting 2009*, MFPL, Vienna, Poster 25

08/2009	Lu J, Zarzer C, Kuegler P, Puchinger M, Shahzad A, Koehler G, Flamm C, and Machné R (2009): Data-Driven Inverse Analysis of a Negative Feedback Mechanism in Pituitary Gland Cells, *10th International Conference on Systems Biology*, Stanford, USA, Poster 1.037
07/2008	Puchinger M, Pilch E, and Puchinger L (2008): Investigation of historical seals by means of Pyrolysis Capillary Gas Chromatography. *2nd Residential Summer School – Chemistry and Conservation Science.*